SYSTEMS STUDIES ON SPATIOTEMPORAL DYNAMICS OF KINASE SIGNALING

by

Ambhighainath Ganesan

A dissertation submitted to Johns Hopkins University in conformity with the requirements for the degree of Doctor of Philosophy

Baltimore, Maryland

September, 2014

Abstract

Life is all about making the right decisions at the right time. Consequently, cells have evolved to "read" external signals, process this information and make decisions through a vast array of signaling molecules. Kinases are a key class of these signaling molecules that interact with other signaling molecules precisely in space and time to form exceedingly complex and dynamic signaling networks. As a result, these networks abound in non-linear connections leading to the emergence of interesting spatial and temporal changes in signaling activities such as oscillations. However, these are not just academically interesting emergent phenomena; cells have evolved to exploit such dynamics of signaling in space and time to process information efficiently and regulate crucial cellular processes ranging from insulin secretion to cellular adhesion. How kinase signaling networks help cells process information through such spatiotemporal dynamics is the central question of this dissertation.

We used a combination of modeling and experimentation to understand how kinases process information. In pancreatic beta-cells, information is conveniently encoded in the form of calcium oscillations. We found that the same input calcium signal may be decoded in different ways by distinct downstream pathways. This differential decoding may be optimized for regulating various cellular functions. Protein Kinase A (PKA) and calcium form a tightly integrated oscillatory circuit with the ability to tune temporal features of the oscillations. Such temporal modulation enables PKA to change its mode of action. The Extracellular-signal regulated kinase (ERK) cascade on the other hand employs sequential processing that integrates the calcium signals so as to produce sustained pathway

outputs. In neuroendocrine PC12 cells, ERK not only displays interesting temporal dynamics, but striking spatial differences as well. Such spatiotemporal differences manifest as a result of complex kinase-interaction networks, and these differences help to optimally regulate multiple cellular processes simultaneously.

Advisors:	Andre Levchenko, PhD; Jin Zhang, PhD
Readers:	Andre Levchenko, PhD; Jin Zhang, PhD; David T. Yue, MD, PhD
Thesis Committee:	Edward Lakatta, MD; Andre Levchenko, PhD; David T. Yue, MD, PhD; Jin Zhang, PhD

Acknowledgements

I would like to thank my advisors, Dr. Andre Levchenko and Dr. Jin Zhang for their mentoring and intellectual insights and inputs. I am particularly grateful for the confidence they reposed in me to explore the boundaries of Science freely. Most important of all, I am thankful to them for showing me how to ask the right questions in Science, and connect the dots and see the bigger picture.

I would like to thank Dr. David Yue especially for the generosity with his time as my thesis reader during an extremely busy time period, and for his guidance and advice on all my projects.

I would also like to thank my thesis committee members, Drs. Ed Lakatta and David Yue for their time, guidance, inputs and suggestions throughout my graduate years. I feel fortunate and gifted to have been guided by seminal experts and master scientists, who were ever-ready to comment and suggest ways to improve my projects, hone my critical thinking skills, and push me to better myself.

Next, I would like to thank Dr. Manoj Narayanan from IIT Madras, a teacher past compare who first induced the love for Biology in me. I would also like to thank my undergraduate mentor, Dr. Sathyanarayana Gummadi, for encouraging me to pursue scientific research.

I would also like to thank all the Zhang lab members for a fabulous time, professionally and personally. I am very grateful for all the help and training I received from fellow labmates (Drs. Charlene Depry, Sohum Mehta and Vedangi Sample) who

converted me into an experimentalist. I would also like to thank Qiang Ni and Dr. Nwe-Nwe Aye Han for their extensive collaborations in the pancreatic beta-cell project. I am also grateful to Archer Hamidzadeh who has been immensely helpful with and contributed significantly to my 'side projects.' Thanks are also due to Dr. Gary Mo for honing my argumentative skills, for general entertainment and for help with TIRF imaging. Finally, I would like to thank Jessica Yang, Dr. Sohum Mehta and Dr. Nwe-Nwe Aye Han for ensuring a consistent and steady supply of cells for me to work with.

I am also grateful for having had a chance to work with my collaborator, Dr. Yael Yaniv, whose curious mix of informative anecdotes about bunnies and latest scientific findings helped me pass long hours in dark imaging rooms easily.

I would like to thank all the administrative personnel from the Biomedical Engineering and Pharmacology Departments for their help in all the necessary administrative processes.

Finally, I would like to express my deepest gratitude to my family (especially my mom) and my numerous friends (special thanks to Aditya, DP, Harish, Krishna, Manu, Sathya and Raghu in no particular order) for being an amazing support structure for me - always ready to listen, offer suggestions and help me during trying times of exasperating experiments.

Table of Contents

List of Figures

List of Tables

Chapter 1 Introduction[1]

1.1 Cellular information processing through signaling dynamics

Cells use signaling cascades to make critical and complicated decisions in response to external stimuli in multiple contexts – apoptosis, metabolism and migration, to name a few. However, the process of cellular signaling in its most elemental form comprises nothing but a set of chemical reactions – perhaps, an old phenomenological remnant from the days of proto-cells which were likely little more than membranous bags of reacting molecules (*1*). Evidently there is a mismatch between the *complexity* of functional responses and the apparent *simplicity* of the underlying molecular mechanisms. During the course of evolution, life forms have bridged this gap primarily in two ways: a) by expanding the repertoire of signaling molecules (e.g., various posttranslationally modified forms and splice variants), and b) by exploiting temporal and spatial variations to diversify the portfolio of responses using the same set of signaling molecules.

Temporal changes in concentrations or activities of effector molecules in a signaling cascade occur commonly in response to external stimuli. Depending on the architecture of the signaling network, these temporal changes may be precisely controlled and coordinated to exhibit complex dynamics such as adaptation or oscillations. Oscillations, in fact, commonly occur in many organisms ranging from unicellular bacteria

[1] A version of this chapter has been published and appears in: Ganesan A and Zhang J. How cells process information: quantification of spatiotemporal signaling dynamics. *Protein Sci.* 2012, 21(7):918-928.

to complex mammalian cells. Temporal oscillations are thought to regulate metabolism (*2, 3*), cell cycle (*4*), circadian rhythms (*5, 6*), and rhythmic beating of the heart (*7*) among many other physiological processes. Alternately, signaling cascades could translate information about external stimuli to spatial dynamics of signaling molecules influencing a variety of cellular processes including cardiac function (*8*) and cell migration (*9*). Understanding the biophysical bases of spatiotemporal dynamics of signaling is therefore important in appreciating how cells process information from external cues to regulate cellular processes of biomedical importance. Researchers have been able to uncover mechanisms underlying signaling dynamics using a vast array of experimental tools and modeling approaches, some of which I briefly outline in the following sections.

1.2 Experimental tools for monitoring signaling dynamics

Monitoring most signaling molecules such as kinases, phosphatases and cytoskeletal proteins often requires cell lysis or fixation followed by immunoblotting and immunocytochemistry, where real time information is often lost (*10-14*). The advent of fluorescent protein (FP) technology combined with advancements in microscopy has however largely addressed these issues by making it possible to observe signaling dynamics in live-cell context with millisecond temporal resolution and tens of nanometer spatial resolution. An important frontier of this technology has been the development of suites of genetically encoded fluorescent biosensors for monitoring spatiotemporal dynamics of signaling molecules.

A popular class of single FP-biosensors like the GCaMP family of calcium indicators exploits changes in fluorescence of individual fluorophores to indicate

physiological events (*15, 16*). Single FP biosensors however are intensity based and are susceptible to motion artifacts, variations in intensity of excitation light and other optical parameters, and can therefore be complemented by ratiometric indicators, for instance exploiting Förster Resonance Energy Transfer (FRET) between a fluorophore pair. Many FRET-based biosensors have been developed for kinases and successfully employed to understand kinase biology (*17*). A typical FRET-based kinase activity reporter (KAR) (*18-21*) consists of a substrate peptide and a phospho-amino acid binding domain 'sandwiched' between two FPs. Phosphorylation of the substrate by the kinase of interest and the subsequent binding of the phosphorylated substrate to the phospho-amino acid binding domain results in a change in the distance and/or relative spatial orientation of the two FPs and hence a change in FRET between them (Figure 1.1). The KARs have become a valuable tool in elucidating mechanisms of kinase-mediated signaling regulation.

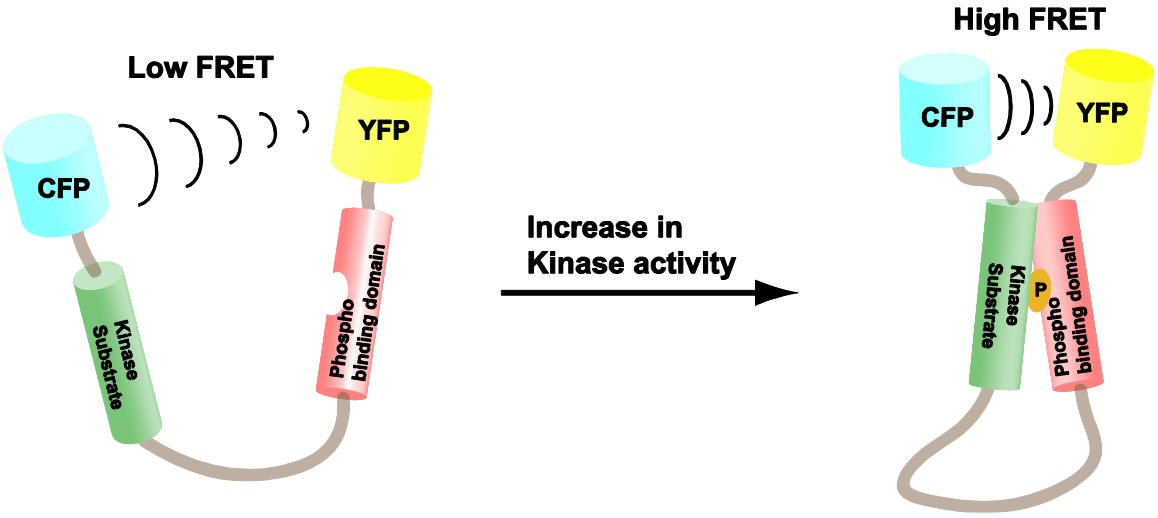

Figure 1.1: Schematic of FRET-based Kinase Activity Reporter.

Foremost among such kinases are the Protein Kinase A (PKA) and the Extracellular-signal Regulated Kinase (ERK) which have been implicated in virtually

every cell function. PKA activity dynamics, observed in real-time using the A Kinase Activity Reporter (AKAR) has helped us understand its role in cell migration (*22*), cardiac rhythm (*8*) and neuronal functions (*23*). The ERK activity dynamics measured using the ERK Activity Reporter (EKAR) has been used to uncover its role in long-term potentiation (*24*), neuronal development (*25*) and regulation of cell cycle (*26*). These biosensors have helped us in our attempts to understand how kinases process information through spatiotemporal dynamics to regulate pancreatic beta-cell and neuroendocrine cell functions, as explained in Chapters 2-4.

1.3 Computational modeling-aided approaches to discern signaling dynamics

Apart from a host of experimental tools detailed above, computational modeling is increasingly becoming an indispensable resource for researchers studying signaling dynamics. Quantitative models are especially helpful in the case of large signaling systems in which individual components interact in ways that may not be completely predictable based on the properties of these components studied separately, but may instead acquire emergent properties endowed by complex intermolecular interactions. Such, systems-level properties make it difficult to predict system responses intuitively (Figure 1.2).

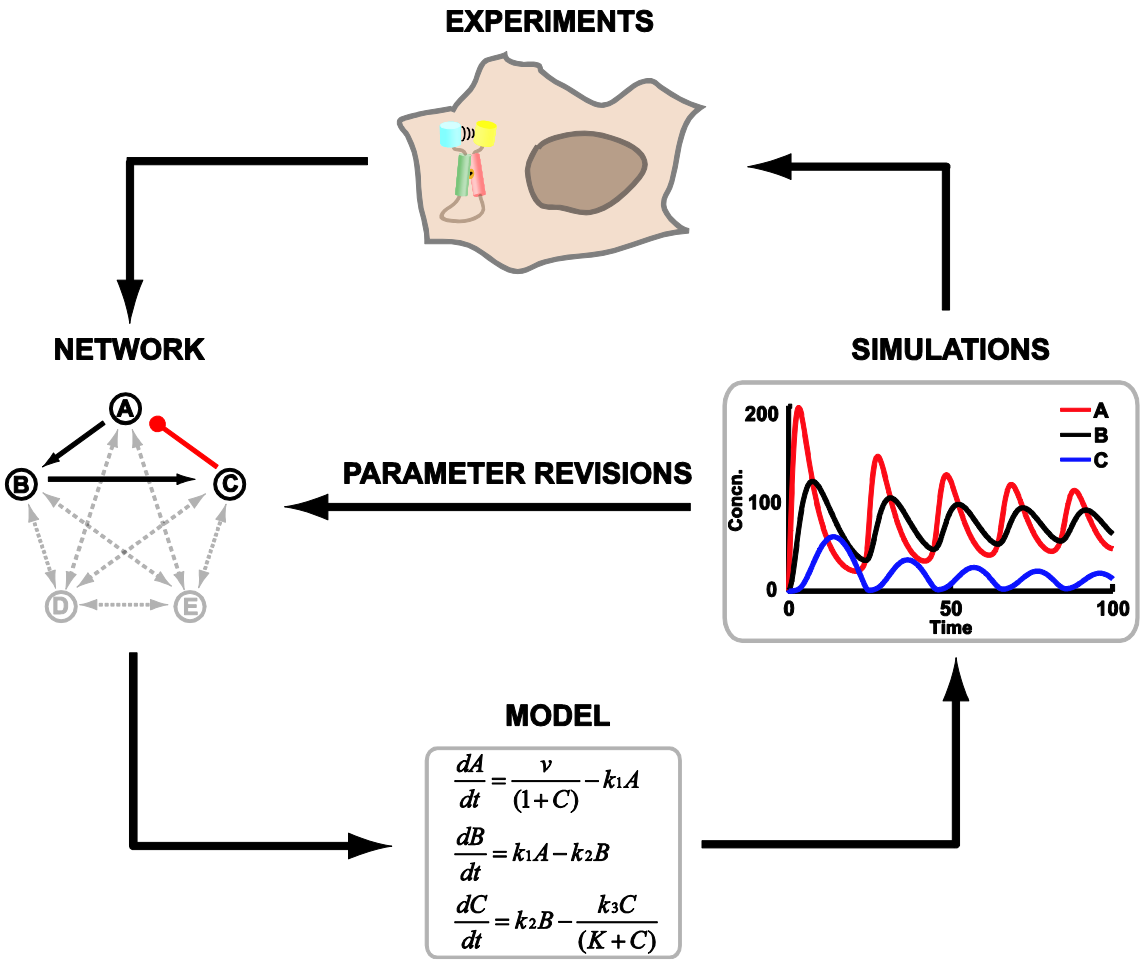

Figure 1.2: Modeling-driven dissection of signaling networks. Known non-linear connections (denoted by dark lines) in a network comprising three components A, B, and C are represented by a mathematical model. In this network, A activates B, B activates C, and C inhibits A in a negative feedback manner. Simulations of the model can then be matched with the experimental data. Any discrepancies between experiments and model can indicate the need for further improvements to the model, typically involving a revision of parameter values. Simulations can also reveal the presence of new connections (shown in dotted lines) leading to the formulation of a more complete network which can better explain experimental results.

In particular, the emergent properties can engender complex dynamical responses, including oscillations or multistability (*27, 28*), requiring modeling approaches for in depth understanding and analysis. Further, models can be powerful tools in generating and testing hypotheses quickly and inexpensively, leading to rational design of subsequent experiments. Models can also be powerful in generating quantitative paradigms integrating

diverse data into a single framework, and helping abstract the underlying evolutionary 'design' principles of signaling networks (*29, 30*), which may be subsequently used in reverse engineering of novel signaling networks (*31, 32*).

Biological signaling reactions, like their chemical counterparts, are subject to the laws of mass action and can therefore be mathematically represented in the form of ordinary differential equations (ODEs). An ODE, describing the rate of change of concentration of a molecular species, captures the balance (or imbalance) between the synthesis and degradation of a particular species, or its activation/inactivation through chemical modification. A system of ODEs can therefore theoretically predict the changes in the concentrations of the modeled species over various periods of time. ODE models have been widely used to describe temporal dynamics of signaling pathways. However, signaling molecules also exhibit spatial dynamics which can be important functionally. Arguably, the easiest approach to model spatial and temporal dynamics is to use ODE-based compartmentalized models. In such models, the cell is assumed to consist of different discrete compartments such as the plasma membrane, cytosol and nucleus. Temporal dynamics in each compartment is described by a separate set of ODEs, and a different set of ODEs is used to describe the flux of signaling molecules between compartments (Figure 1.3).

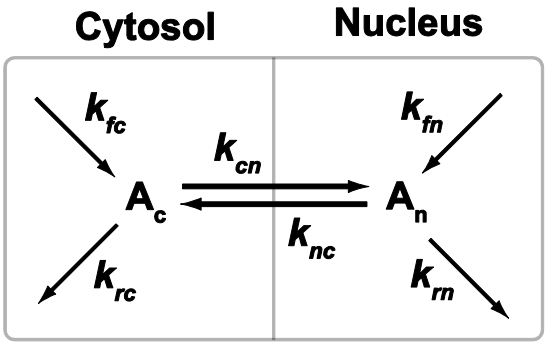

$$\textbf{Cytosol:}\ \frac{dA_c}{dt} = (k_{fc} - k_{rc}A_c) + (k_{nc}A_n - k_{cn}A_c)$$

$$\textbf{Nucleus:}\ \frac{dA_n}{dt} = (k_{fn} - k_{rn}A_n) + (k_{cn}A_c - k_{nc}A_n)$$

Figure 1.3: A representative compartmentalized model of spatial and temporal dynamics of the activity of a species, A. The cell is divided into two homogenous compartments: the cytosol and the nucleus. A is generated and degraded in the cytosol at rates k_{fc} and k_{rc}, respectively, and is generated and degraded in the nucleus at rates k_{fn} and k_{rn}, respectively. Further, A is assumed to shuttle between the two compartments at effective rates of k_{cn} and k_{nc}. Separate ODEs for each compartment are written by summing up the reaction and diffusion rates.

1.4 Temporal dynamics

Intracellular responses to an external stimulus often involve temporal changes in concentrations or activities of specific signaling molecules. Cells have therefore evolved to use variations in temporal dynamics as a means of inferring and reacting to external stimuli. Cellular signaling cascades are complex systems embedded with non-linearities in the form of feedback loops. Given the right conditions, a circuit with a negative feedback loop can produce diverse responses ranging from simple adaptation to complex oscillations (Figure 1.4).

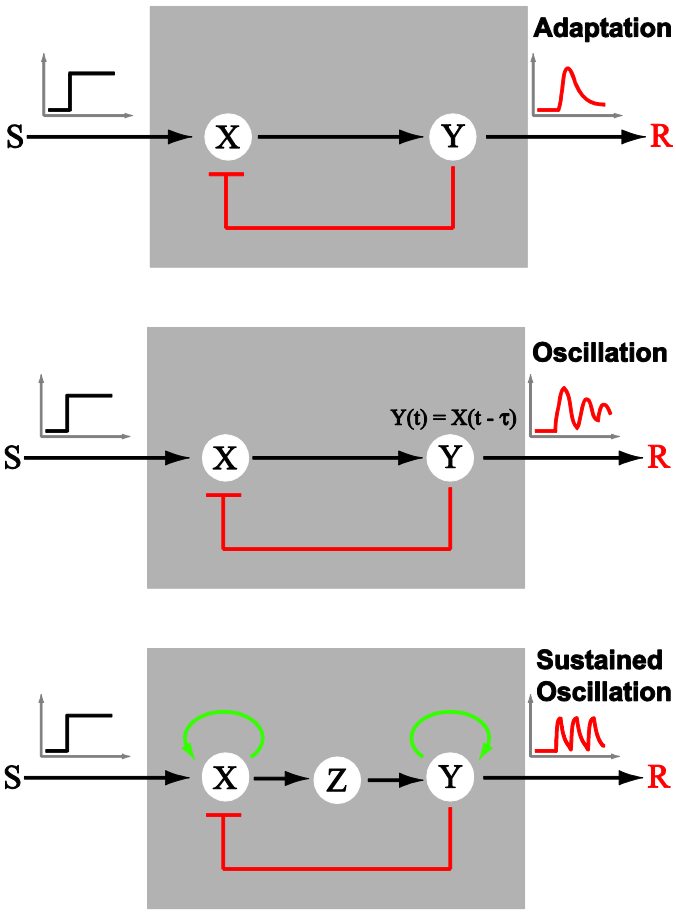

Figure 1.4: Temporal dynamics of signaling circuits with negative feedback loops in a representative system comprising two molecules, X and Y. (A) The presence of a negative feedback loop alone can produce a transient adaptive output signal in response to a "step-input" signal. (B) Negative feedback loop coupled with time-delay [represented explicitly as Y(t) = X(t-τ)] produces a damping oscillation in response to a ''step-input'' signal. (C) Negative feedback with time-delay (represented by the presence of an extra species, Z in the circuit) coupled with additional positive feedback loops results in sustained oscillations in response to a ''step-input'' signal. Positive feedback loops are denoted in green. Negative feedback loops are denoted in red.

Oscillations can be a rich means of communication within the cells. Cells may use the same oscillating signal to convey different outcomes through simple changes in the parameters of oscillations such as frequency and amplitude (*33, 34*). Calcium oscillations, have been linked to, among many other things, memory formation (*35, 36*), insulin secretion (*37, 38*) and cardiac rhythm (*39*). Oscillations in ERK activity have been posited

to influence cell cycle entry and hence cell proliferation (*26*). The transcription factor Nuclear Factor kappa B (NF-κB) exhibits complex oscillatory behavior which is thought to influence mammalian inflammatory immune responses (*40, 41*). Experimental monitoring of such temporal dynamics of signaling activities has been successfully used in conjunction with computational models to address fundamental questions pertaining to intracellular communication. In Chapters 2 and 3, I demonstrate how such approaches helped us understand how temporal signaling dynamics of PKA and ERK enable pancreatic beta-cells to process information.

1.5 Spatial dynamics

Simplistic models often assume cells to be homogeneous "bags" of molecules. While this first order of approximation may be sufficient to explain many temporal aspects of signaling, a cell, in reality, is made up of spatially restricted organelles and compartments that perform pre-defined sets of functions. To achieve spatially distinct signals, the cell employs different mechanisms ranging from use of organelle-specific signaling molecules and pathways to modulation of different pools of spatially universal signaling molecules such as calcium. Precise spatial dynamics of signaling is achieved by a combination of physical processes (diffusion), chemical factors (balance between the rates of synthesis and degradation of the signaling molecules) and structural factors (cellular structures, and scaffold or anchor proteins in the context of protein complexes) to sequester molecules in defined locations.

Spatial dynamics of second messenger molecules exemplified by calcium and cyclic adenosine monophosphate (cAMP) microdomains have been studied extensively.

Calcium 'sparks,' for instance are widely recognized to be the unitary events underlying the excitation-contraction coupling process and arise from spontaneous or evoked opening of a cluster of Ryanodine receptors (RyRs) resulting in local increases in calcium concentration (*42, 43*). The second messenger molecule, cAMP, also exhibits intricate spatial dynamics influencing cardiomyocyte contractility. Compartmentation of cAMP signaling and the resulting gradients in the activity of the effector, PKA have been directly observed using fluorescent reporters (*41, 43-45*). Combining such experimental approaches with modeling, Saucerman et al. (*8*) identified potential signaling mechanisms for regulating spatial PKA activity dynamics. Both PKA mediated buffering of cAMP and restricted cAMP diffusion mediated by cAMP-degrading phosphodiesterases (PDEs) help establish the phosphorylation gradients.

1.6 Aims and significance

Cells are complex dynamic entities that register, react and respond to changing external conditions. This processing of the external information and subsequent decision making processes are carried out by signaling molecules, in significant part through the temporal and spatial dynamics of signaling as detailed in the preceding sections. A major class of such signaling molecules are kinases which are thought to regulate about 30 % of the human proteome (*46*). However, how the spatiotemporal dynamics of kinase signaling activities influences cellular decision making capacity is still largely unclear. Therefore, in this thesis I set out to answer three major questions, each of which is addressed in a separate aim as detailed below:

1. How do cells use temporal kinase activity dynamics to modulate the capacity of signaling output?
2. How are temporally complex signals decoded by kinases?
3. How do spatial dynamics of kinase activity influence cellular function?

1.6.1 Specific Aim 1: To study effects of temporal PKA dynamics in pancreatic beta-cells

The cAMP-dependent Protein Kinase (PKA) is a prototypical kinase that influences action potential propagation via modulation of calcium channels and cardiomyocyte contractility (*47, 48*). The cAMP signaling pathway modulates glucose-dependent insulin secretion; however the molecular details are beginning to emerge only recently. We hypothesized that cAMP actions in pancreatic beta-cells may be effected through PKA. In this aim, we discovered oscillations in PKA activity and built a mathematical model to help us predict the role of PKA in modulating calcium dynamics. Our model simulations predicted that PKA not only initiates but also frequency-modulates intracellular calcium oscillations via a feedback loop which was subsequently confirmed through experiments. Furthermore, our results suggest that decoding of intracellular calcium oscillations by PKA can result in flexible spatiotemporal modulation of target substrate activities.

1.6.2 Specific Aim 2: To investigate the temporal ERK dynamics in pancreatic beta-cells

The extracellular signal-regulated protein kinase 1/2 (ERK1/2) is a central signaling molecule that has been shown to influence cell survival and proliferation in many systems including beta-cells (*49, 50*). Upon glucose stimulation, ERK1/2 is activated in a calcium-dependent manner, and activated ERK phosphorylates and modifies the function of transcription factors that regulate insulin gene transcription and cell survival (*51-53*). Characterization of ERK-calcium crosstalk and dissecting the molecular mechanisms that underlie this crosstalk are essential to ultimately understanding how pancreatic beta-cell health including survival and proliferation is affected. In this aim, we uncovered the mechanisms of calcium-dependent ERK1/2 activation and discovered that information transfer down the ERK cascade has a direct bearing on the signaling versatility of the cascade.

1.6.3 Specific Aim 3: To understand the role of spatial ERK signaling dynamics on cell function

The ERK signaling system in the neuroendocrine pheochromocytoma PC12 cells is a classical model that highlights how temporal signaling dynamics influences cell fate. An EGF stimulus results in transient ERK activity which leads to cell proliferation. On the other hand, exposing the cells to NGF causes them to differentiate due to sustained ERK activity. While the temporal aspects of ERK signaling have been studied in detail, the spatial dynamics of ERK signaling is largely unknown. Using genetically encoded biosensors specifically targeted to different sub-cellular organelles of PC12 cells, we

discovered that distinct spatial activity patterns are evoked for the same stimulus. In this aim, we investigated the mechanisms that result in this differential spatial pattern and uncovered the resulting functional implications.

Chapter 2 Signaling diversity of PKA achieved via a calcium-cAMP-PKA oscillatory circuit[2]

2.1 Introduction

Protein kinases serve as major information transducers in cells and are responsible for regulating diverse cellular functions (*54, 55*). However, the molecular mechanisms underlying this signaling diversity are not well understood, particularly with regard to the role of the spatiotemporal regulation of kinases. Although important progress has been made towards understanding of the spatial compartmentalization of kinases (*56, 57*), much less is known about how temporal regulation of kinase action can be exploited to encode diverse signals and control different functional outcomes (*58*).

PKA, a prototypical protein kinase (*59*), plays a host of important roles in a variety of cellular locations. Among these is the regulation of calcium-triggered exocytosis at the cell membrane, a process critical to many cellular functions (*60*). In pancreatic beta cells, exocytosis is critical for the pulsatile insulin secretion that is regulated by a variety of stimuli, including electrical, metabolic and hormonal signals (*61, 62*). Calcium influx is stimulated when glucose metabolism produces an increase in the [ATP]/[ADP] ratio that inhibits K-ATP channels and induces membrane depolarization, leading to the opening of voltage-gated calcium channels. When activated either by glucose (*63*) via calcium or by

[2] A version of this chapter has been published and appears in: Ni Q*, Ganesan A*, Aye-Han NN*,Gao X, Allen MD, Levchenko A, Zhang J. Signaling diversity of PKA achieved via a Ca^{2+}-cAMP-PKA oscillatory circuit. *Nat Chem Biol.* 2011, 7(1):34-40.
* denotes co-first authorship

hormones such as glucagon-like peptide 1 via classical G protein–coupled receptor signaling (*62*), PKA can in turn modulate the calcium signal (*64, 65*) and also directly influence exocytotic insulin release (*60*). For instance, a PKA-dependent mechanism operates during the initial phase of glucose-induced exocytosis (*66*), and impairment of this process has been implicated in the pathogenesis of type 2 diabetes (*67*).

Here, we investigated the role of the temporal regulation of PKA in integrating and transducing a variety of signals. By combining fluorescent biosensor-based live-cell tracking of signaling activities with mechanistic modeling, we demonstrate that PKA exhibits oscillatory activity and, together with calcium and cAMP, forms a highly integrated oscillatory circuit in MIN6 beta cells. The organization of this oscillatory circuit allows PKA to modulate the frequency of oscillation, to integrate input signals and to exert spatiotemporal control of substrate phosphorylation. This demonstration of a functional role for the temporal regulation of a protein kinase in achieving signaling diversity helps to establish a new model for encoding signaling information within temporal patterns, such as the frequency of oscillation of an enzymatic activity.

2.2 Results

2.2.1 Oscillatory PKA activity

We first set out to monitor the time profile of PKA activity changes in MIN6 pancreatic beta-cells in response to the K^+ channel blocker, tetraethyl ammonium chloride, TEA which mimics glucose action. Calcium and cyclic adenosine monophosphate (cAMP) are both known to oscillate in beta-cells in response to glucose or TEA stimulation (*68*). However, the dynamics of the primary effector of cAMP, PKA was unknown. The PKA

activity dynamics are governed by the activation and deactivation kinetics of PKA. As a result, a wide range of PKA activity responses are possible, in theory at least, ranging from oscillatory to integrated responses (**Figure 2.1A**) with different implications for regulating cellular processes.

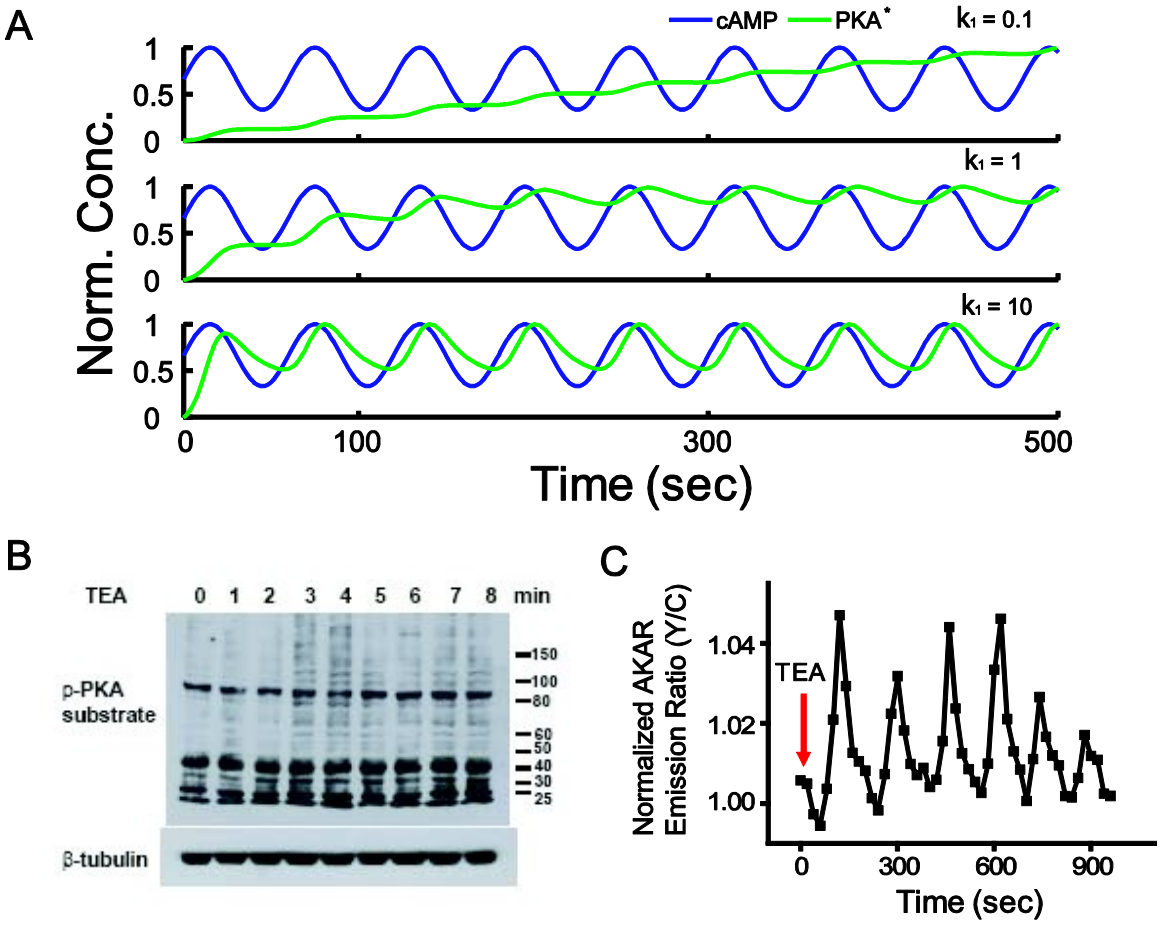

Figure 2.1: Oscillatory changes in PKA activity in single MIN6 beta cells. A. Simulation of PKA activity in the presence of oscillatory cAMP, showing different activity patterns depending on the characteristics of the oscillations and parameters of PKA activation and deactivation. A parameter reflecting the binding of cAMP to PKA homodimer was varied in this simulation. k_1 is the ratio of the new value to the nominal value of this parameter. Norm. conc., normalized concentration; PKA, active PKA. B. Phospho-immunoblot analysis using an anti-phospho PKA substrate antibody showed sustained increases in substrate phosphorylation by PKA upon TEA treatment of MIN6 β-cells. C. A representative time course of yellow/cyan emission ratio changes in single MIN6 beta cells expressing AKAR, a FRET-based PKA activity reporter, revealed single-cell PKA activity oscillations (n = 21).*

Therefore, we decided to experimentally determine the PKA activity dynamics. Accordingly, MIN6 cells were treated with TEA (20 mM), lysed at different time points and the PKA activity probed through the phospho-PKA substrate antibody. We observed a sustained and elevated PKA activity response to TEA (Figure 2.1B), suggesting that PKA activity might not conform to cAMP oscillations or that the oscillatory PKA activity is masked at the cell-population level. To analyze the temporal dynamics of PKA at the single-cell level, we performed fluorescence imaging of endogenous PKA activity using a genetically encoded A-kinase activity reporter (AKAR) (*69, 70*). In contrast to the population level experiments, this analysis revealed oscillatory PKA activity (Figure 2.1C), suggesting a repetitive shifting of the balance between the actions of PKA and counteracting phosphatases in single cells. These oscillations occurred with a period of 1–6 min in >60% of AKAR-expressing MIN6 cells (n = 21), matching the frequency of the calcium oscillation patterns previously reported in these cells (*68*). Therefore, PKA activity exhibits oscillatory changes in single MIN6 cells, which were likely masked in cell population studies because the observed oscillations in PKA activities were asynchronous, varying in phase and frequency among individual cells.

2.2.2 Synchronized oscillations of PKA, calcium and cAMP

Given that calcium is known to oscillate under the same conditions and to serve as an important signal in beta cells, we characterized the temporal correlation between PKA activity and calcium dynamics by performing coimaging experiments using AKAR in conjunction with the calcium dye Fura-2 (*71*) in single MIN6 cells. For these experiments, we engineered a red-shifted AKAR, AKAR-GR (Figure 2.2), based on enhanced GFP and

the red fluorescent protein mCherry (referred to here as RFP), to allow better signal separation from Fura-2.

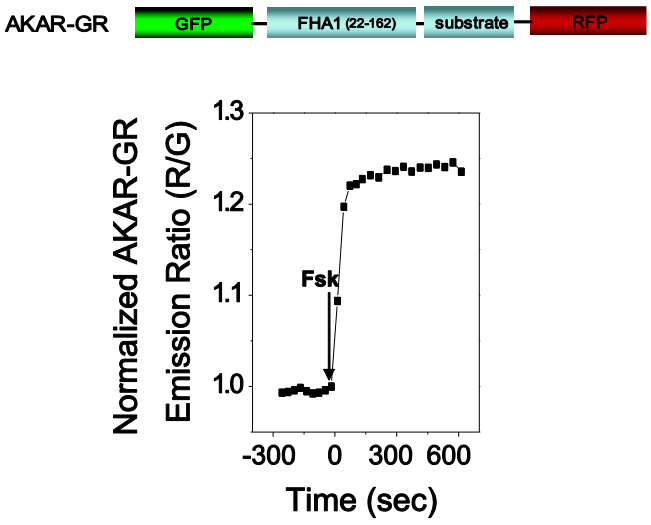

Figure 2.2: Schematic and representative time course of AKAR-GR upon Fsk stimulation in HEK-293 cells.

We found that the PKA oscillations and calcium oscillations were 'in register' with each other (Figure 2.3B). Notably, during each cycle of oscillation, the rise in the calcium transient appeared to follow, with a noticeable lag, the accumulation of PKA activity. This pattern likely reflected the PKA-mediated potentiation of calcium influx via voltage-gated calcium channels and/or inositol trisphosphate receptors (IP3R) (*72, 73*). Moreover, the decrease in PKA activity in each cycle was surprisingly rapid when compared to the transient PKA activities observed in other cell types (Figure 2.4A) (*74*), and it was precisely correlated with the declining phase of the calcium spike, suggesting that there is a calcium-dependent mechanism in place to ensure the rapid downregulation of and/or counterbalancing of PKA activity.

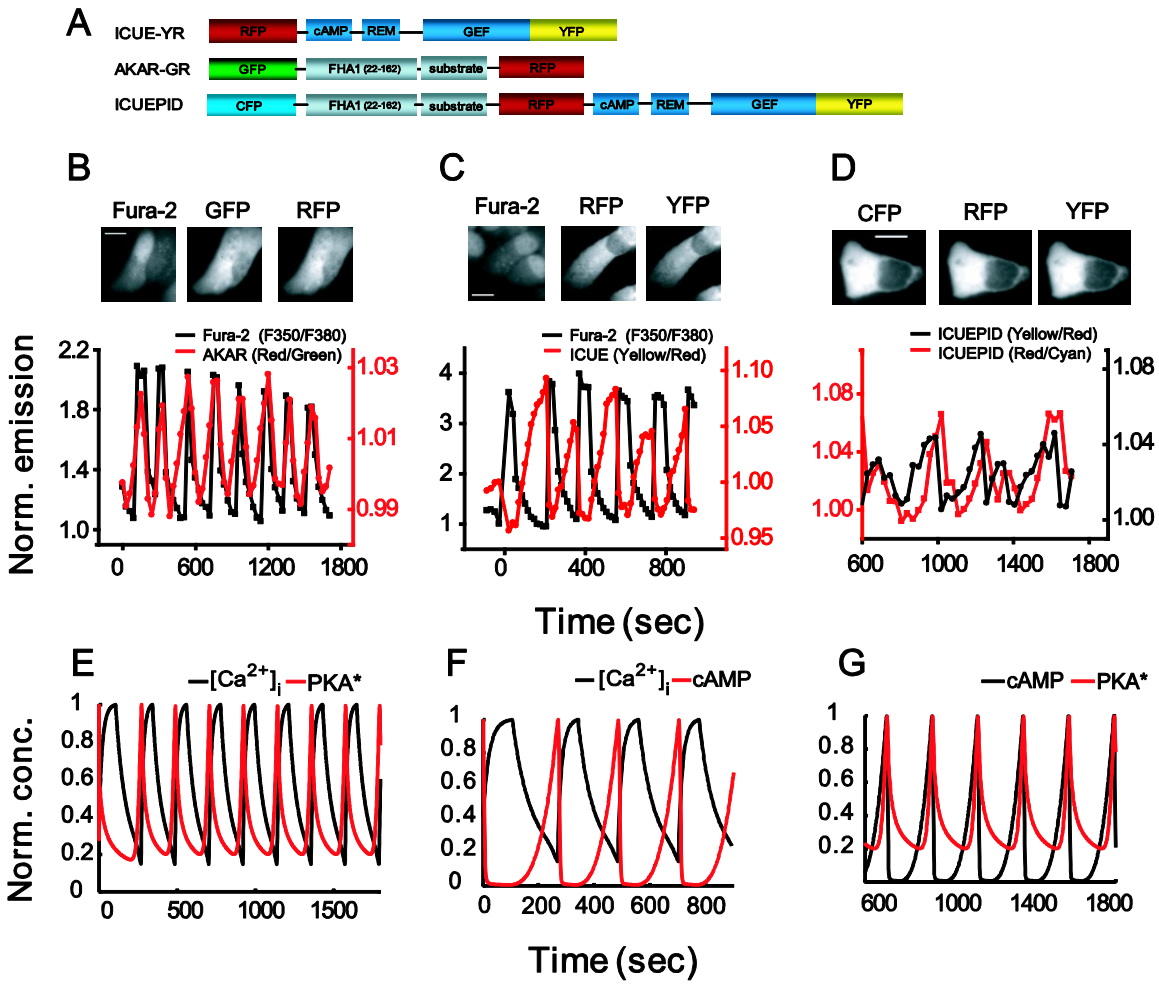

Figure 2.3: Oscillatory changes in PKA activity, cAMP and calcium dynamics are highly coordinated in MIN6 cells. A. Domain structures of ICUE-YR, AKAR-GR and a single-chain dual-specificity biosensor, ICUEPID, for PKA activity and cAMP dynamics. B. (Top) Fluorescence images of MIN6 cells expressing AKAR-GR loaded with Fura-2. (Bottom) Representative time courses showing coordinated oscillations in PKA activity (monitored by AKAR-GR, red) and calcium (monitored by Fura-2, black) in single MIN6 cells. Scale bar, 10 µm. C. (Top) Fluorescence images of a MIN6 cell expressing ICUE-YR loaded with Fura-2. (Bottom) Representative time courses showing coordinated oscillations in cAMP (monitored by ICUE-YR, red) and calcium (monitored by Fura-2, black) in single MIN6 cells. Scale bar, 10 µm. D. (Top) Fluorescence images of a MIN6 cell expressing ICUEPID. (Bottom) Representative time courses showing coordinated oscillations in PKA activity (red) and cAMP (black) monitored by ICUEPID in single MIN6 cells. Scale bar, 10 µm. E. Simulation of the model showing calcium (black) and active PKA (PKA, red) oscillations. F. Simulation of the mathematical model showing calcium (black) and cAMP (red) oscillations. G. Simulation of the model showing cAMP (black) and active PKA (PKA*, red) oscillations. Norm. emission, normalized emission; norm. conc., normalized concentration. Normalization in simulations made with respect to the maximal value in the corresponding time course.*

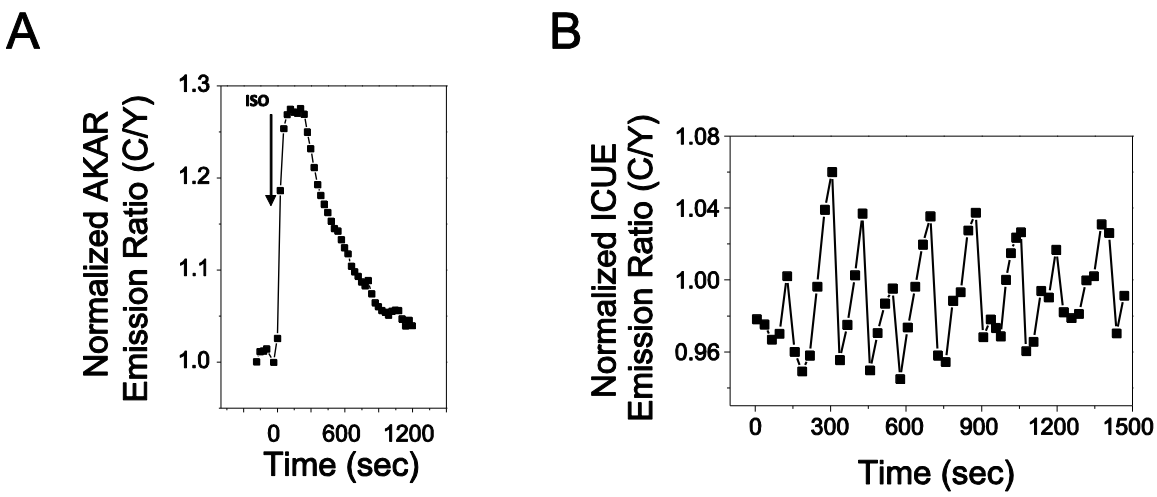

Figure 2.4: AKAR and ICUE responses. A. Representative time course of AKAR response upon isoproterenol stimulation in HEK293 cells B. Representative cAMP response to TEA in MIN6 cells measured using the cAMP biosensor, ICUE.

In MIN6 cells, calcium-dependent regulation of PKA can occur through calcium-dependent adenylate cyclases and phosphodiesterases (PDEs) (*74*), the enzymes that produce and degrade cAMP, respectively. Indeed, as previously observed (*68*), cAMP was found to oscillate under the same conditions when visualized with a fluorescent cAMP indicator, ICUE (*75, 76*) (Figure 2.4B). Simultaneous imaging using a red-shifted ICUE, ICUE-YR (Figure 2.3A) and Fura-2 in single MIN6 cells confirmed that these cAMP oscillations are highly synchronized with the calcium oscillations (Figure 2.3C).

The high degree of synchronization between PKA and calcium and between cAMP and calcium suggested that all three components were regulated in a temporally coordinated fashion. As PKA activity is often compartmentalized in various systems, we asked whether the cAMP and PKA oscillations were also correlated in the local cellular context. To answer this question, we took advantage of a new single-chain dual-specificity biosensor for parallel detection of PKA activity and cAMP dynamics (Figure 2.3A). This biosensor contains both cAMP-sensitive and PKA-dependent molecular switches and can

simultaneously capture the dynamics of two signaling events in the same local environment, thereby facilitating quantification and correlation of these signaling activities. In MIN6 cells expressing this single-chain dual-specificity biosensor, TEA treatment elicited oscillatory signals from both reporting units (Figure 2.3D). These oscillations were highly temporally coordinated, with cAMP rises always preceding increases in PKA activity, suggesting that oscillations in PKA activities are indeed locally driven by oscillatory changes in cAMP levels.

2.2.3 Analysis of the calcium-cAMP-PKA oscillatory circuit

The precise temporal correlation between the oscillatory activities of calcium, cAMP and PKA suggests a complex underlying mechanism involving multiple feedback interactions. To better understand this signaling circuit, we constructed a mathematical model (See Section 2.4 for complete details) by incorporating a detailed description of the biochemical events involving these three key molecular components (*77*). In our model, the interplay between the membrane-potential regulation and calcium forms the first feedback loop, consistent with the Chay-Keizer model (*78*). A second feedback loop, centered around calcium, cAMP and PKA, was incorporated by explicitly introducing putative regulation of both voltage-gated L-type calcium channels and IP3R by active PKA (*72, 73*). Additional links needed to complete the model were introduced on the basis of a network topology analysis determining the minimal model sufficient to account for several qualitative features of our experimental findings (*77*). When operating under assumptions about parameter values consistent with literature data, the model was able to capture the detailed dynamic relationships between various molecular components observed in our

experiments (Figure 2.3). Our combined experimental and modeling data therefore suggest the existence of a functional signaling circuit consisting of calcium, cAMP and PKA. In this circuit, the activities of all the components are temporally regulated in the form of synchronized oscillations, as a result of a tight coupling between these components through feedback interactions.

2.2.4 Role of PKA in the oscillatory circuit

To dissect the role of PKA in this oscillatory circuit, we examined the effects of altered PKA activity on the oscillatory patterns of the calcium-cAMP-PKA system. The model predicted that the oscillatory behavior of the system, as indicated by the calcium signal, would strongly depend on the level of PKA activity, although oscillation of PKA activity was not required for maintaining calcium oscillations (Figure 2.5). Inhibition of PKA activity was predicted to have strong abolishing effects on calcium oscillations (Figure 2.6A). Indeed, addition of the PKA inhibitor H89 to MIN6 cells rapidly terminated calcium oscillations, indicating that PKA activity was required (Figure 2.6B). Consistent with this observation, no TEA-induced calcium oscillations were observed in 17 of 24 cells in the presence of a specific PKA inhibitor, RFP-tagged PKI. This result represents a three-fold reduction in oscillatory behavior compared to control cells, over 87% of which showed calcium oscillations (Figure 2.7). In contrast, the model predicted that increasing PKA activity would modulate the frequency of the calcium oscillations (Figure 2.8A). This prediction was tested by monitoring calcium dynamics when a general phosphodiesterase inhibitor, 3-isobutyl-1-methylxanthine (IBMX), was added to MIN6 cells after TEA-induced calcium oscillations were established. We found that every cell showing regular

oscillations both before and after IBMX addition exhibited an increase in oscillation frequency (n = 15) (Figure 2.8B), demonstrating that cAMP-PKA activity can modulate the calcium oscillation frequency.

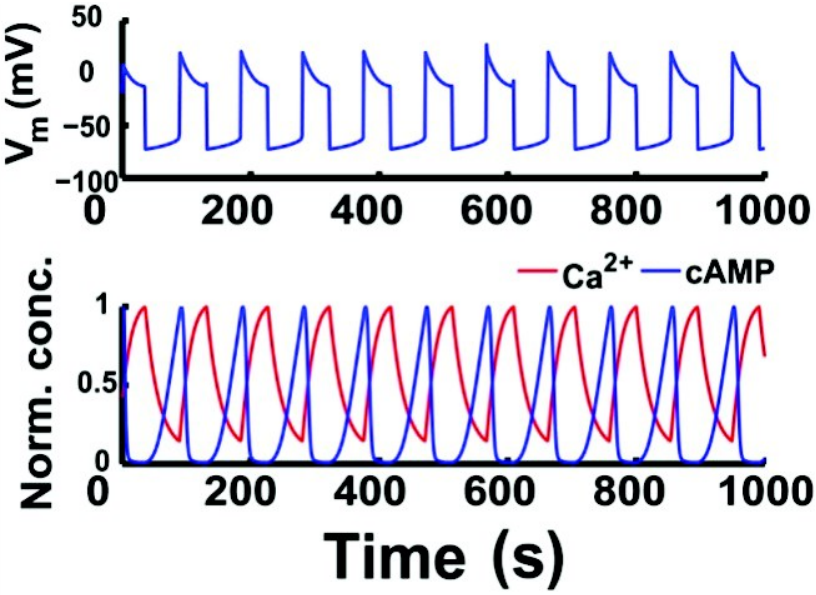

Figure 2.5: Model simulation of membrane potential (V_m), calcium (Ca^{2+}) and cAMP responses under constant PKA activity conditions.

On the other hand, PKA-mediated phosphorylation is continuously counter-balanced by phosphatase activity. For instance, PKA and phosphatase PP2B are known to have opposing effects on L-type calcium channels via phosphorylation and dephosphorylation of the channels, respectively (*79*). Our model predicted that changes in PP2B activity would have an effect opposite to that of PKA activity in terms of modulating the frequency of calcium oscillations (Figure 2.9A). Consistent with this prediction, treatment of MIN6 cells with 3 μM cyclosporine A, a PP2B inhibitor, increased the frequency of TEA-induced calcium oscillations (n = 7) (Figure 2.9B), indicating that the ability of PKA to modulate calcium oscillation is under the influence of opposing phosphatase activities.

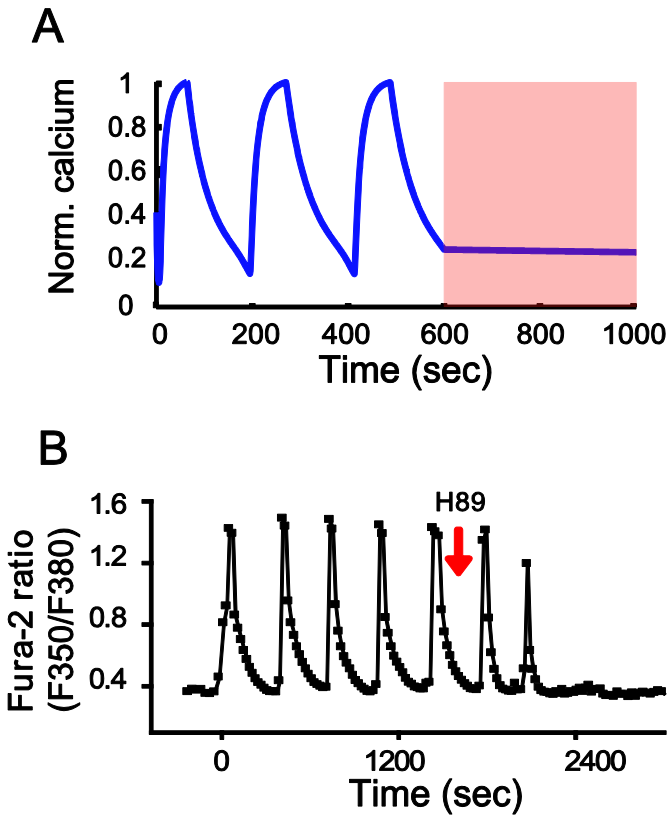

Figure 2.6: PKA activity is required for calcium oscillation and tunes its frequency. A. Simulation of the model in the presence or absence of PKA (shaded region). B. The effect of inhibiting PKA by H89 (10 μM) on calcium oscillations.

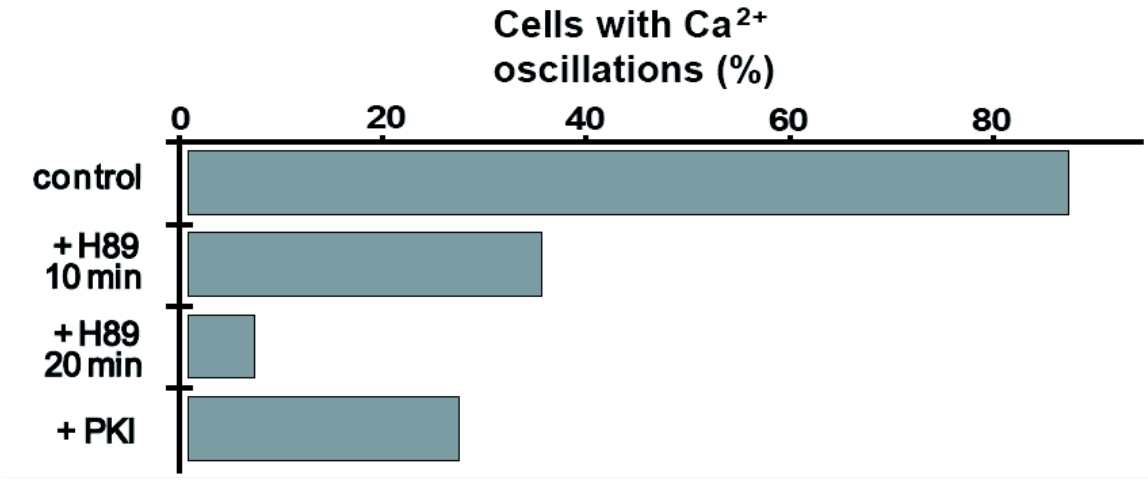

Figure 2.7: PKA inhibition affects calcium oscillations. Percentages with calcium oscillation for control cells, cells treated with H89 for 10 min or 20 min, and cells expressing PKI, a specific PKA inhibitor.

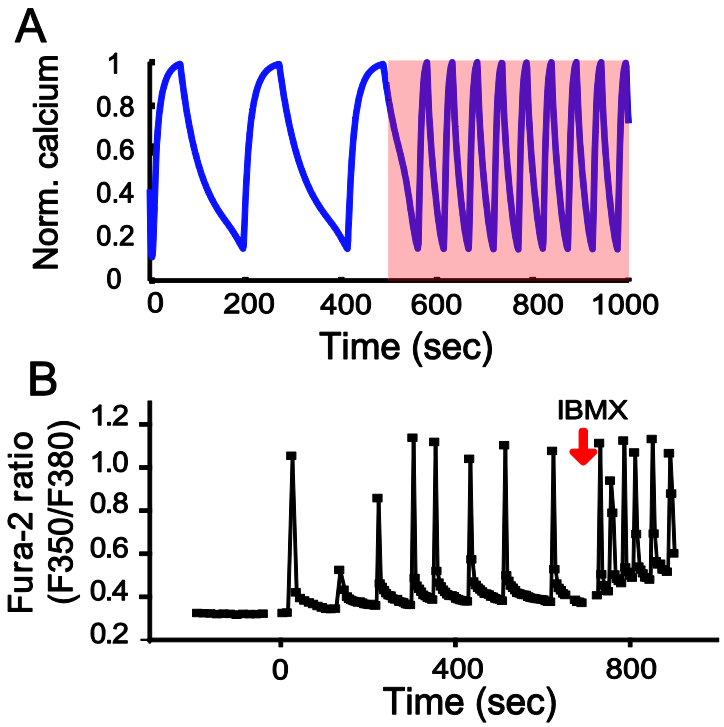

Figure 2.8: PDE inhibition modulates calcium oscillation frequency. A. Simulation of the model with increased feedback achieved when PDE activity is decreased (shaded region). B. The effect of adding a PDE inhibitor IBMX (100 μM) on calcium oscillations (n = 15).

Notably, model simulations also showed that when compared to the calcium oscillation amplitude, the oscillation frequency was considerably more sensitive to changes in PKA activity (Figure 2.10). This finding suggests a role for PKA as a frequency modulator. Taken together, these data suggest that PKA activity can directly modulate the oscillatory patterns of the calcium-cAMP-PKA signaling circuit, thereby affecting cellular processes under the control of calcium.

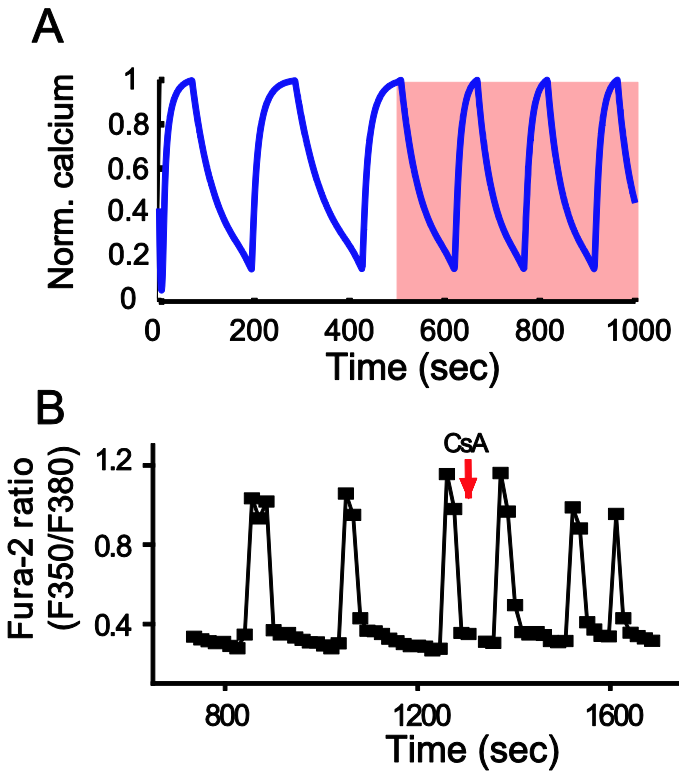

Figure 2.9: PP2B inhibition modulates calcium oscillation frequency. A. Simulation of the model with increased feedback achieved when PP2B activity is decreased (shaded region). B. The effect of adding a PP2B inhibitor cyclosporine A (CsA) (3 μM) on calcium oscillations (n = 7).

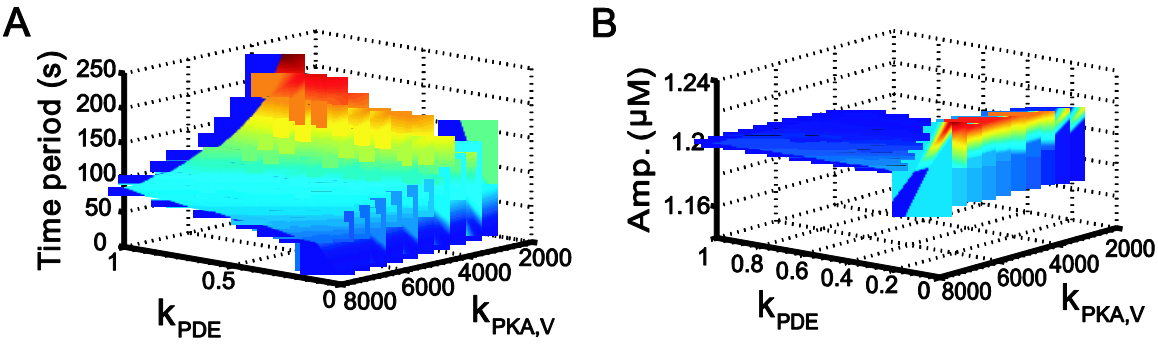

Figure 2.10: Simulations predict calcium oscillation frequency modulation. A. Effect of PKA activation and activity parameters on the frequency of oscillations, simulated by the simultaneous variation of a parameter relating to the extent of PKA phosphorylation of channels ($k_{PKA,V}$) and a parameter controlling the maximal activity of PDE (k_{PDE}). B. Effect of PKA activation and activity parameters on the amplitude of oscillations, simulated by the simultaneous variation of $k_{PKA,V}$ and k_{PDE}. Amp., amplitude of oscillations.

2.2.5 Direct activation of PKA triggers the oscillatory circuit

Beta cells are constantly subject to regulation by a broad range of distinct signals, including electrical, metabolic and hormonal signals (*61, 62*). Given the tunability of this signaling circuit and the capacity of its major components to connect to different signal-sensing networks (*80, 81*), one of its important functions may be to integrate multiple input signals that can independently activate the circuit's components. Thus, it is possible that various signals, via direct activation of different components, can trigger the oscillations of this signaling system. To test this hypothesis, 1–3 μM of 8-bromoadenosine-3′,5′-cyclic monophosphate-acetoxymethylester, a cAMP analog that preferentially activates PKA, was added to MIN6 cells expressing AKAR. In over 40% of the cells (n = 16), the addition of this cAMP analog alone triggered oscillatory changes in PKA activity (Figure 2.11), similar to the TEA-induced oscillations. Furthermore, different strengths of the input signals could apparently be encoded into different activity patterns, because higher doses (10–20 μM) of the same cAMP analog triggered a gradual increase in PKA activity with a small-amplitude higher-frequency oscillatory change superimposed on the monotonic activation rise (Figure 2.11A) (n = 13). Our mathematical model captured the basic characteristics of the oscillations induced by direct activation of PKA (Figure 2.11B) and suggested that sufficiently strong PKA feedback can initiate oscillations even when the feedback loop involving calcium and membrane potential is initially inactive. Furthermore, the distinct PKA activity patterns induced by low doses and high doses of cAMP (Figure 2.11) showed an elaborate transition of behaviors that is indicative of the frequency change of the oscillatory circuit. Thus, PKA is an integral component of the oscillatory circuit and

is capable of not only tuning but also enabling the oscillatory circuit behaviors in response to specific input signals.

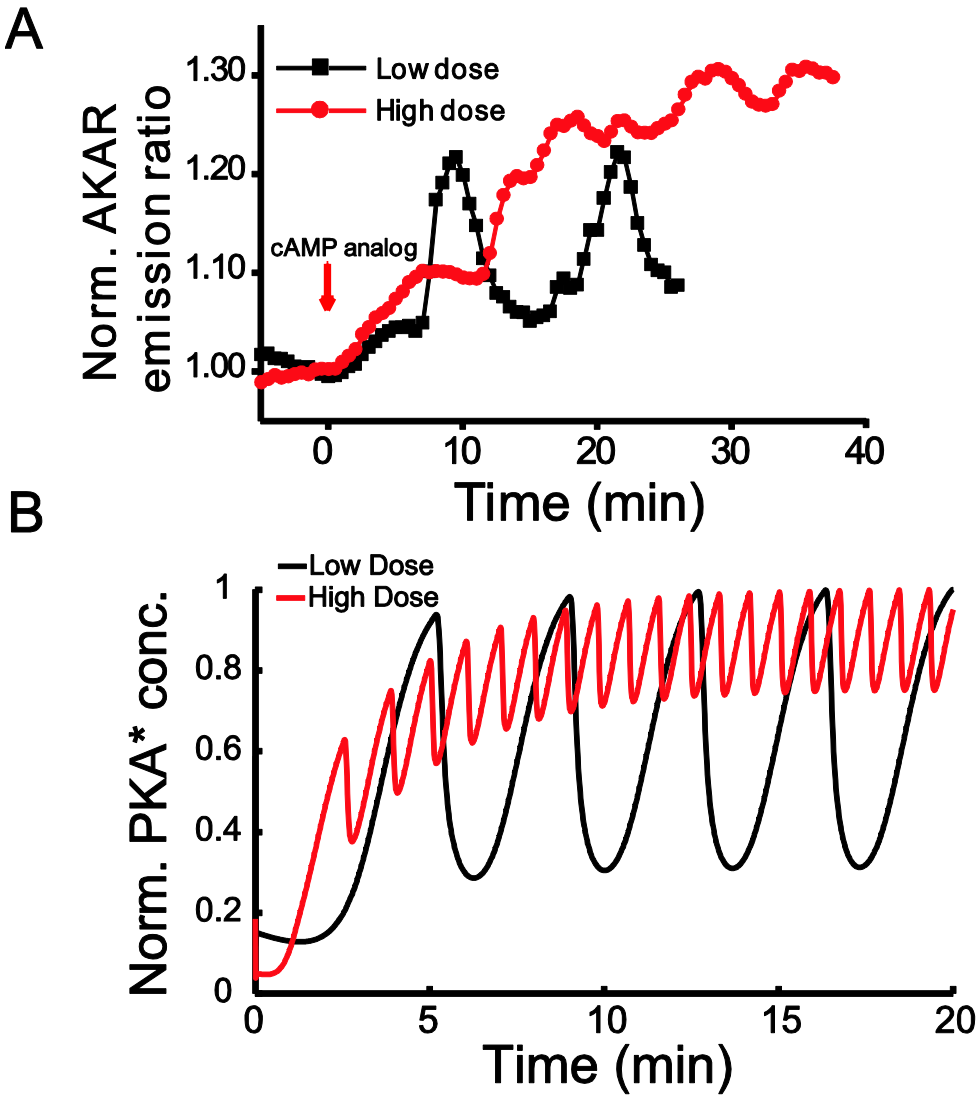

Figure 2.11: Direct activation of PKA triggers the oscillation of the circuit. A. Representative time courses showing different oscillatory PKA behaviors upon stimulation with low (1–3 μM) and high (10–20 μM) doses of a PKA-specific cAMP analog (n = 16 and 13, respectively). B. Simulation of the model showing the different oscillatory PKA activities upon stimulation with low and high levels of cAMP analog. PKA, active PKA.*

2.2.6 Spatiotemporal controls via oscillatory PKA activity

Each of the key components of the oscillatory circuit—calcium, cAMP and PKA—regulates a diverse set of cellular functions with high specificity. In the case of PKA, spatial compartmentalization of PKA-dependent signaling has been identified as an important mechanism underlying specific regulation of distinct functions (*57*). We propose that the oscillatory PKA activity enabled by the calcium-cAMP-PKA circuit can serve as a distinct mechanism for achieving signaling diversity.

At the level of temporal regulation, given an oscillatory PKA activity, both oscillatory and sustained phosphorylation of PKA substrates can be achieved, depending on the access of the substrate to phosphatases reversing PKA phosphorylation (Figure 2.12). For example, recruitment of PKA and phosphatase PP2B to L-type calcium channels can ensure efficient and rapid phosphorylation and dephosphorylation within this signaling complex (*79*). Repetitive phosphorylation of the channels, which has been suggested in previous studies to be critical for proper beta cell function (*82*), would in turn ensure that the activity of the channel reaches certain threshold level only periodically; this pattern would decrease the probability of spontaneous channel openings between insulin secretion phases. In contrast, PKA targets devoid of high local phosphatase activity can integrate multiple oscillation phases over time, thus enabling a distinct mode of regulation.

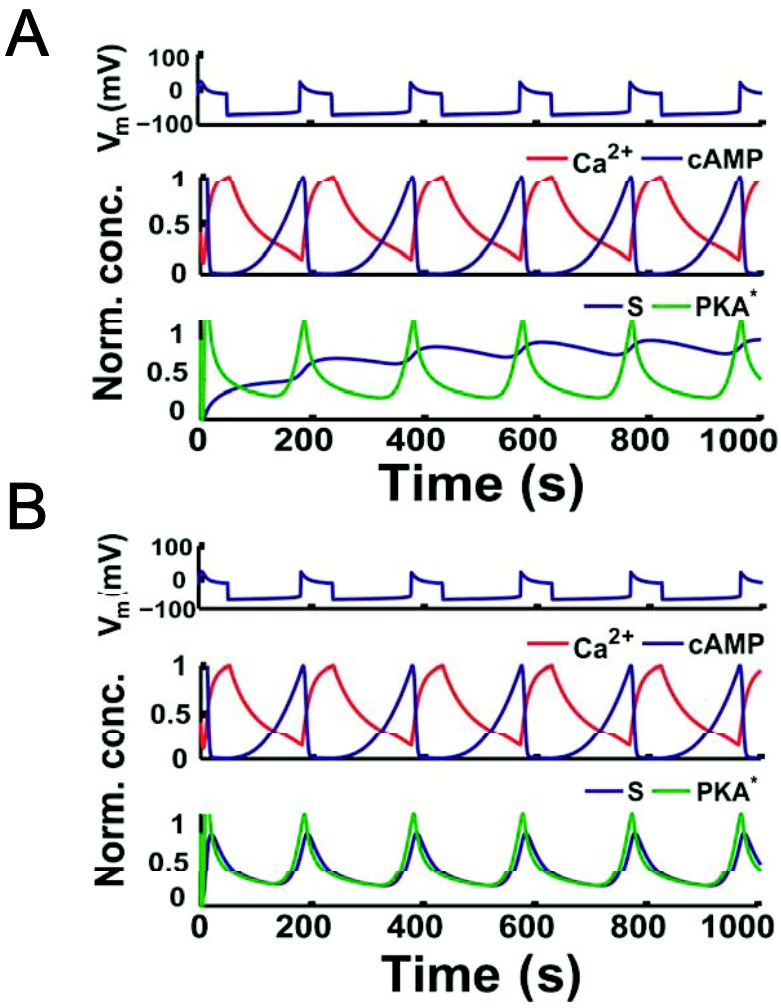

Figure 2.12: Simulation of effect of phosphatase activity on phosphorylation of generic target substrate, S. A. Low phosphatase activity. B. High phosphatase activity

More exquisite spatial control of PKA activity may also be achieved via oscillations. For instance, cAMP-PKA signaling microdomains, such as those defined by AKAP-assembled signaling complexes, may also depend on the kinetics of signaling reactions and the presence of regulatory feedback interactions (*44*). A local PKA signaling complex is typically assembled by A-kinase anchoring protein (AKAP) binding to the regulatory (R) but not the catalytic (C) subunit of PKA. This signaling compartmentalization can be lost if the unanchored C-subunit diffuses away after

dissociation from the R-subunit, rather than being recaptured when cAMP dissociates from the R-subunits. It is thus paradoxical that local PKA activity can be maintained for prolonged periods of time. Our model suggests that, under the experimental conditions analyzed above, this apparent paradox can be resolved, as the oscillatory circuit is capable of maintaining a relatively low time-averaged PKA activity, while having relatively high maximal peak PKA activity (Figure 2.13; local activation regime). The low average PKA activity implies a low average free concentration of the C-subunit in the signaling domain and thus a low escape rate of the subunit from the domain. Recapture of the C-subunit can help reset the local PKA activity cycle. At the same time, the peak PKA activity can periodically exceed the threshold levels needed for full activation of the target substrates and would be further enhanced if the substrates have limited access to the corresponding phosphatases (Figure 2.13). On the other hand, an enhanced input into PKA activation and the resulting high average PKA activity could lead to increased escape of the C-subunit from a local signaling domain (Figure 2.13; global activation regime). At the subcellular organelle level, increased escape of the C-subunit from a cytosolic signaling compartment could result in the C-subunit's translocation into the nucleus (Figure 2.14). We sought to experimentally validate this prediction. Indeed, we found that although low doses of a cAMP analog induced oscillations in the cytosol without affecting nuclear PKA activity or phosphorylation of an endogenous transcription factor CREB, the gradual increase in PKA activity with superimposed high-frequency oscillation induced by high doses of the analog led to an increase in nuclear PKA activity and CREB phosphorylation (Figure 2.13B-D). This effect on CREB phosphorylation was also observed with the cotreatment of CsA or IBMX with a low dose of the cAMP analog (Figure 2.15A) or with TEA (Figure 2.15B).

Thus, the oscillatory PKA activity can apparently encode context-dependent spatiotemporal information for controlling diverse output signals.

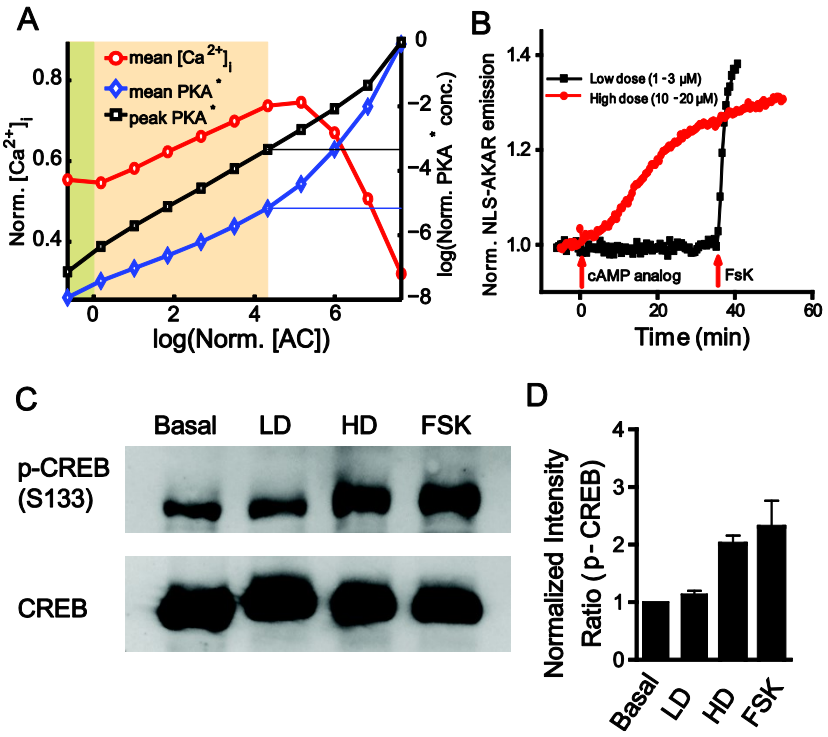

Figure 2.13: Oscillatory PKA activity confers spatial control of substrates. A. Simulation of the model showing the indirect activities of local (normalized mean intracellular calcium oscillations) and global (using normalized mean active PKA concentration as a proxy) targets of PKA activation upon increase in the input adenylate cyclase activity and hence frequency of oscillations. The expected "local activation" regime, defined by the adenylate cyclase activity at which the difference between log(normalized mean PKA activity) and log(normalized peak PKA activity) is maximal, is shaded in orange. The area shaded in green is bounded by the nominal adenylate cyclase activity, reflecting the expected physiological scenario. B. Representative time courses of nuclear-localized AKAR (NLS-AKAR) showing the absence and presence of nuclear PKA activity upon stimulation with low (1–3 µM) and high (10–20 µM) doses of a PKA-specific cAMP analog, respectively (n = 7 and 4, respectively). C. Phospho-immunoblot analysis using antiphospho-CREB (pSer133) shows no changes in CREB phosphorylation upon stimulation with a low dose (LD) of the cAMP analog (2 µM), whereas increased phosphorylation of CREB is observed upon stimulation with a high dose (HD) of the same cAMP analog (10 µM) or 50 µM forskolin (FsK). D. Densitometric analysis of phosphorylated CREB (pSer133) (n = 3) normalized to CREB expression shows a significant difference between the levels of CREB phosphorylation stimulated by the low and high doses of the cAMP analog.

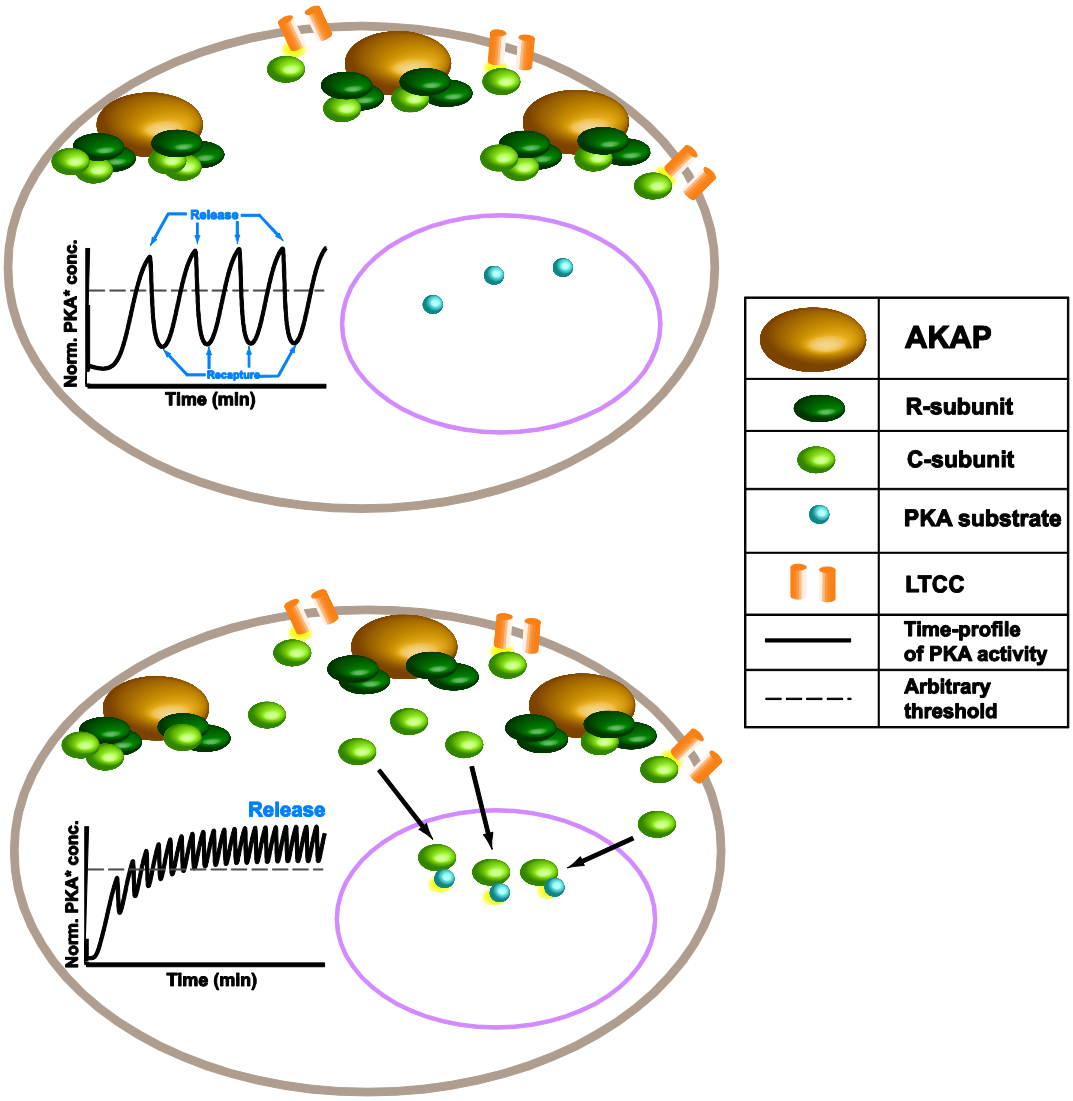

Figure 2.14: Schematic of spatial effects of PKA activity temporal dynamics. Under low frequency conditions, the mean PKA activity would be below a certain threshold for re-capture and so catalytic subunits would be periodically released and captured. However, under high frequency conditions, the mean PKA activity may cross the threshold leading to continued release of catalytic subunits which may then diffuse to a different compartment like the nucleus.

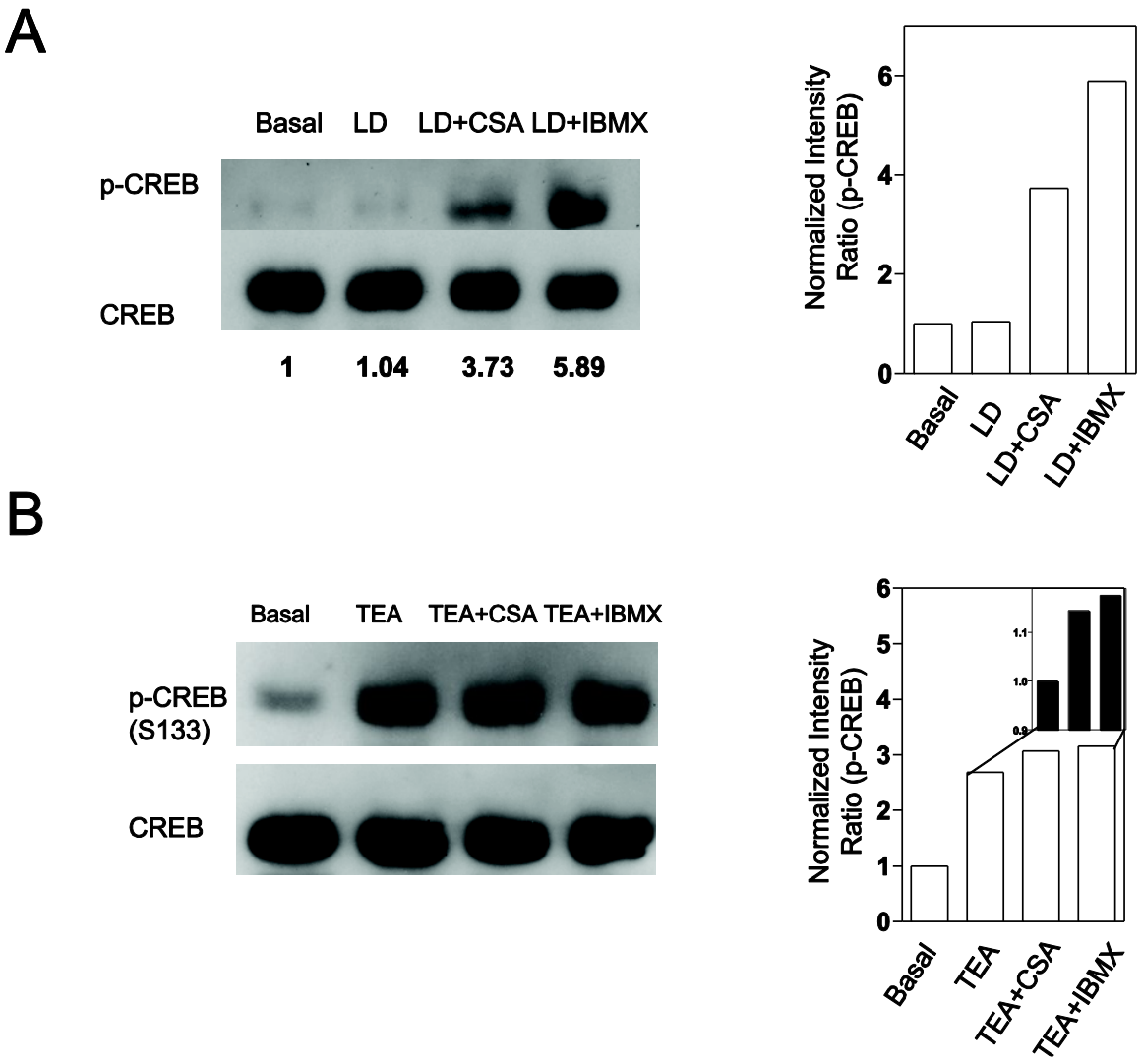

Figure 2.15: CREB activation in response to PP2B and PDE inhibition. Phospho-immunoblot analysis of CREB phosphorylation (pS133) in response to a low dose (LD) of the cAMP analog (2 μM), in the absence or presence of CsA (3 μM) or IBMX (100 μM), with densitometric analysis.

2.3 Discussion

Oscillation of signaling activity can be a versatile mechanism for achieving diversity and specificity. This notion was first demonstrated in the case of calcium oscillation, the frequencies of which are determined by the amount and type of extracellular signals (*83-85*) and can influence the efficiency and specificity of gene expression (*86, 87*).

Our analysis suggests that, as in the case of calcium oscillations, the frequency of PKA activity oscillation can be used as a signaling currency, integrating input signals according to their identities and doses and generating specific functional output (for example, local versus global signaling modes). In this way, the oscillatory PKA activity allows PKA to function as a versatile signaling transducer that can exert spatiotemporal controls over a variety of functional outcomes in response to specific signals. Future studies will directly evaluate the effects of changing the PKA oscillation frequency on cellular processes that are important to beta cell functions, such as gene expression and insulin secretion.

Our analysis further demonstrates that, in addition to transducing signals via activity oscillation, PKA in insulin-secreting cells also plays an active role in shaping the oscillatory patterns of other key components in the signaling circuit, such as calcium. This finding is in contrast to previous studies in which oscillations of several protein kinases (for example, PKA (*88*), PKC (*21*), mitogen-activated protein kinases (*89, 90*) and calmodulin-dependent protein kinase II (*91*)) were demonstrated, but the potential role of these kinases in shaping the oscillation patterns was not explored. It remains to be seen whether some of these kinases or other candidate kinases are also focal points of oscillatory activities.

Given that each of the key components in the calcium-cAMP-PKA circuit can regulate distinct functions, the synchronized oscillations ensure the coordinated activity of these key players, providing a mechanism for achieving efficient and specific control of cellular processes. Therefore, it is reasonable to suggest that complex cellular behaviors

may critically depend on such synchronization and coordination of various signaling molecules.

In summary, this current study provides a clear example of exquisite temporal control of a protein kinase within an oscillatory circuit. This signaling system could serve as a paradigm for understanding the spatiotemporal regulation of other signaling networks that control complex cellular processes. Furthermore, given the ubiquitous presence of the key components of the oscillatory calcium-cAMP-PKA circuit (*92, 93*), its effects are likely to be widespread, serving to regulate diverse processes in various cell types.

2.4 Computational model development

2.4.1 Introduction

Multiple signalling mechanisms are known to employ the second messenger calcium, with variable intracellular calcium levels ($[Ca^{2+}]_i$) used by divergent signalling cascades to elicit different responses, primarily mediated through protein kinases (*94*). The mathematical model for describing calcium oscillations in the pancreatic beta-cell system proposed here is built in a modular fashion, consistent with previous models, integrating them and incorporating new features. Particularly of note here is the role of PKA mediated feedback which serves to aid in calcium oscillations. The model is described below. First, we put it in the context of two related modeling studies.

Fridlyand et al. (*95*) described a model of calcium-cAMP oscillations in MIN6 cells, demonstrating in particular that the oscillations of cAMP linked to $[Ca^{2+}]_i$ changes due to glucose stimulation are anti-phasic. The calcium kinetics in this model are described

by calcium fluxes across the plasma membrane and ER membrane. The synthesis and degradation of cAMP are governed by the activities of calcium-calmodulin (CaM)-dependent Adenylate Cyclases (ACs) and Phosphodiesterases (PDEs) such as AC8 and PDE1C respectively. Simulations showed that a phase delay between calcium and cAMP oscillations could occur if CaM-dependent PDE activity was present but CaM-dependent AC activity was low. Increasing the CaM-dependent AC activity however resulted in calcium and cAMP oscillations that were in phase with each other. Consistent with this study, our own model topology analysis (see Section 2.4.3 below), and our experimental observations, the signaling circuit in our model involves calcium-activated PDE which leads to anti-phasic oscillations of calcium and cAMP. Overall, this model is focused on how the oscillations in cAMP may be 'enslaved' to calcium oscillations, without directly considering possible feedback from cAMP through Protein Kinase A (PKA), as considered in our model. Indeed, calcium levels in the pancreatic beta-cells have been shown to be modulated by cAMP-dependent mechanisms (*96, 97*). This likely occurs through direct or indirect modulation of channel conductances by a cAMP-dependent process. Simulations in the model by Fridlyand et al. illustrated this point by showing that calcium oscillations were affected when conductances of channels were varied directly. In contrast, our model incorporates an explicit feedback loop via PKA, in accordance with our experimental data, and focuses on the role of this feedback loop and its importance in defining the signal properties of this circuit.

The feedback from cAMP to calcium regulation has been modelled previously in Aplysia neurons by Gorbunova and Spitzer (*98*). The Gorbunova-Spitzer model comprises

3 states describing the kinetics of calcium, IP3R and cAMP. Calcium oscillations are generated by the interplay between calcium and IP3R in this model, which is based on a previous model by Tang and Othmer (*99*). Our model incorporates this interplay, while also detailing the contributions of potassium (K^+) and calcium currents across the plasma membrane in generating calcium oscillations. More importantly, the Gorbunova-Spitzer model describes the calcium dependence on cAMP using CaM dependent AC and the cAMP feedback on calcium in terms of cAMP levels directly. On the other hand, our model aims to expand on the role of this feedback by employing the dynamics of PKA activation and the subsequent phosphorylation of Voltage Dependent Calcium Channels (VDCCs) and Inositol trisphosphate Receptors (IP3Rs) by activated PKA. The basic circuitry of the components involved in this system and the different modules that make up this model are summarized in Figure 2.21.

In summary, the calcium oscillations in the pancreatic beta-cell system are modeled here to describe the interplay of membrane voltage (V_m), calcium, cAMP and PKA, each of which is developed and described as a semi-autonomous modeling module (Figure 2.21). The signal transduction cascade is initiated by depolarization of the plasma membrane (carried out experimentally by using K^+ channel blockers, such as TEA), which causes the opening of VDCCs resulting in an influx of calcium. An increase in intracellular calcium results in activation of CaM, which can modulate the activities of both AC and PDE. Consistent with the model presented here and previous findings by Fridlyand et al. (*95*), as mentioned before, we experimentally observed that calcium and cAMP follow an anti-phasic relationship which would necessitate the involvement of calcium inhibited ACs

and/or calcium activated PDEs. The binding of the second messenger, cAMP, to the regulatory subunits of PKA (R_2) releases the catalytic subunits (C_2), which in turn phosphorylate the VDCCs and IP3Rs that lead to a calcium influx and open up the internal calcium stores respectively, thereby setting up a negative feedback loop.

2.4.2 Voltage and Calcium modules of the model

The voltage module (Figure 2.21), comprising equations (1-9) below, describes the membrane potential dynamics and is based on the original set of equations employed in the Chay-Keizer model (*100*) and derived from a later version of the Chay-Keizer model detailed by Sherman, Li and Keizer (*101*). The values of the parameters for this and other model modules are detailed in Table 2.1. When the parameters present in the original model were used, we observed that the frequency of oscillations was much lower than the frequency of oscillations experimentally observed. Hence, some of the values were modified in order to corroborate the experimental data. Specifically, the conductance of VDCCs was reduced to 600 pS, as was similarly done in the model published by Fridlyand et al. (*95*) where the nominal value for VDCC conductance was chosen to be 670 pS. To match the change in VDCC activity owing to this reduced conductance and to match the experimentally observed frequency of oscillations, the conductance of the delayed rectifier K^+ channels also was reduced to 260 pS. We note that the conductance values are a function of the number of available channels, and can reflect the cell type-specific properties of the cells used in experiments. The value of the parameter f_i was chosen by Chay and Keizer on the basis of the timescale of the oscillations in their model, in the absence of any concrete experimental measurements for free calcium in pancreatic beta-cells. Since the frequency

of oscillations experimentally observed in our system was much lower than that in the study by Chay and Keizer, f_i was reduced accordingly to 1×10^{-4}. Apart from these frequency related parameters, the reversal potential for VDCCs, E_{Ca} was modified to 100 mV, since previous reports have consistently used this value (*100, 102*). The equations describing the voltage module are detailed below. The symbols have their usual meanings as described in Table 2.1, Table 2.2 and Table 2.3.

2.4.2.1 Voltage Module

$$m_\infty = 0.5\left(1+\tanh\left(\frac{V-v_1}{v_2}\right)\right) \quad \ldots 1$$

$$w_\infty = 0.5\left(1+\tanh\left(\frac{V-v_3}{v_4}\right)\right) \quad \ldots 2$$

$$\tau = \frac{1}{\cosh\left(\frac{V-v_3}{2v_4}\right)} \quad \ldots 3$$

$$I_K = g_K w(V-E_K) \quad \ldots 4$$

$$I_{Ca} = g_{ca} m_\infty (V-E_{Ca}) \quad \ldots 5$$

$$I_L = g_L(V-E_L) \quad \ldots 6$$

$$I_{K(Ca)} = g_{K(Ca)}\left(\frac{[Ca^{2+}]_i}{[Ca^{2+}]_i+K_{K(Ca)}}\right)(V-E_K) \quad \ldots 7$$

$$\frac{dV}{dt} = \frac{1}{C_m}\left(-I_{Ca}-I_K-I_L-I_{K(Ca)}\right) \quad \ldots 8$$

$$\frac{dw}{dt} = \phi\left(\frac{w_\infty - w}{\tau}\right) \quad \ldots 9$$

2.4.2.2 Calcium module

The calcium current through the VDCCs, and leak through other channels contribute to the calcium flux across the plasma membrane. For our initial model topology

analysis (see 2.4.3 below), we considered only the plasma membrane flux for the sake of simplicity and so described calcium dynamics as follows:

$$j_{Ca,V} = f_i(-\alpha I_{Ca} - v_{L,PM}[Ca^{2+}]_i) \quad \text{... 10}$$

2.4.3 Model Topology Analysis

2.4.3.1 Model Development

The main purpose of the modeling analysis in the present study was to develop a minimal yet sufficiently detailed model accounting for and constrained by the experimented observations, also presented here. The number of the molecular species considered and the accumulated prior research of possible chemical links between these species introduces considerable complexity into the initial model development, and potential for making it hard to manage and constrain sufficiently. We therefore initially considered several possible simplified versions of how the calcium and cAMP modules might interlink, in terms of their consistency with experimental data. Specifically, we focused on the experimental observations that calcium and cAMP oscillations are anti-phasic, suggesting the involvement of calcium-inhibited ACs and/or calcium-activated PDEs. We therefore explored different possible combinations in which the components of our circuit could be connected as shown in Figure 2.16.

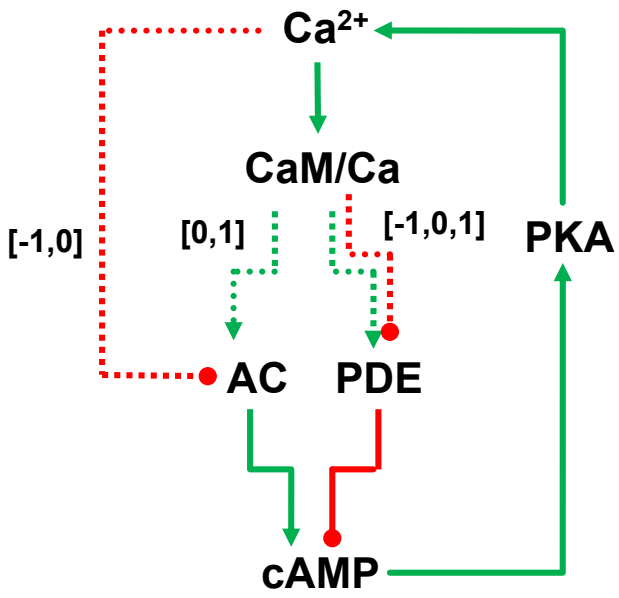

Figure 2.16: Possible topologies for the circuit with the components shown. Solid lines indicate fixed connections. Dotted lines indicate variable connections. The numbers -1, 0 and 1 indicate if the link is inhibitory, absent or activating respectively.

ACs can be activated by calcium-calmodulin ($CaM.Ca_4$) or inhibited by calcium. PDEs could also be $CaM.Ca_4$ dependent. The calcium-AC link may be present according to 2 possibilities – inactivation or no dependence – represented as -1 or 0. Similarly, ACs may or may not be activated by $CaM.Ca_4$ which is represented by 0 or 1. PDEs can be activated or inactivated by $CaM.Ca_4$ or can be independent of $CaM.Ca_4$ activity. So, this link can be represented as 1, -1 or 0, respectively. Accordingly, we have 2x2x3 = 12 possible circuits.

At this point, we chose to develop a heuristic model for cAMP and PKA kinetics incorporating these dependencies. Our experimental data shows a strong correlation between PKA and calcium dynamics with an increase in intracellular calcium following an increase in PKA activity (Figure 2.3E) indicating that the calcium flux could be modulated

by PKA likely through phosphorylation of calcium channels. We represent this PKA-calcium dependence as follows:

$$x_{PKA} = (1 + K_{PKACa}[PKA^*]) \quad \ldots 11$$

Therefore, the calcium flux can be modified as:

$$\frac{dCa}{dt} = j_{Ca,V}.x_{PKA} \quad \ldots 12$$

To model the dependence of ACs and PDEs on calcium-calmodulin ($CaM.Ca_4$), we assumed quick equilibration of calcium to calmodulin binding, and thus existence of quasi-steady-state levels of $CaM.Ca_4$, the concentration of which therefore is proportional to the concentration of calcium raised to the index of 4 (due to 4 Calcium binding sites). The factors describing these modulations are shown in equations 13 and 14. In these equations, K_{CacAMP} and $K_{CaMcAMP}$ are appropriate constants controlling these processes. While, in reality, the extent of Calmodulin mediated modulation of AC and PDE could be different, the goal of this preliminary model was to try to capture the essence of the experimental data qualitatively. Hence, we used the same x_{CaM} factor for both AC and PDE modulation.

$$x_{Ca} = (K_{CacAMP} + [Ca^{2+}]_i) \quad \ldots 13$$

$$x_{CaM} = (K_{CaMcAMP} + [Ca^{2+}]_i^4) \quad \ldots 14$$

The cAMP dynamics can therefore be described as:

$$\frac{d[cAMP]}{dt} = k_{f,CacAMP}.x_{Ca}^{g_{CacAMP}} + k_{f,CaMcAMP}.x_{CaM}^{g_{CaMcAMP}} - k_{d,cAMP}.x_{CaM}^{h_{cAMP}}.[cAMP] \quad \ldots 15$$

The indices g_{CacAMP}, $g_{CaMcAMP}$, h_{cAMP} reflect the presence or absence of the respective link in the chosen topology. For instance, in a circuit where AC is inhibited by calcium, not dependent on CaM, and PDE is activated by CaM, the appropriate indices would -1, 0 and 1, respectively.

Finally, the kinetics of PKA can be described by equation 16 below. The PKA homodimer consisting of 2 regulatory subunits (R_2) and 2 catalytic subunits (C_2) binds to 4 molecules of cAMP and gets activated, yielding the following time dependence:

$$\frac{d[PKA^*]}{dt} = k_{f,PKA}[cAMP]^4 - k_{d,PKA}[PKA^*] \quad \text{... 16}$$

Since, this is a representative model we initially assume that certain binding constants and the parameters pertaining to cAMP and PKA kinetics (K_{PKACa}, K_{CacAMP}, $K_{CaMcAMP}$, $k_{f,CacAMP}$, $k_{f,CaMcAMP}$, $k_{d,cAMP}$, $k_{f,PKA}$, $k_{d,PKA}$) have an arbitrary equal value of 0.5. To explore the sensitivity of the model to parameter variation, we varied 4 parameters defined below:

$$K_{PKAvar} = \log_{10}\left(\frac{K_{PKACa}}{K^o_{PKACa}}\right) where\ K^o_{PKACa} = 0.5\ \mu M^{-1}$$

$$\kappa = \log_2\left(\frac{K_{CacAMP}}{K_{CaMcAMP}}\right)$$

$$\lambda_c = \log_2\left(\frac{k_{f,cAMP}}{k_{d,cAMP}}\right), where\ k_{f,CacAMP} = k_{f,CaMcAMP} = k_{f,cAMP}(say)$$

$$\lambda_p = \log_{10}\left(\frac{k_{f,PKA}}{k_{d,PKA}}\right)$$

In each of the studied model variations, one of the chosen parameters is varied, while keeping the rest constant, thus yielding responses for all the 12 possible circuits. Based on experimental results, we further identified criteria that appropriate model topology should be able to satisfy:

1. The calcium and cAMP oscillations are anti-phasic.
2. Calcium rise phase and cAMP decay phase in each peak are coincident and very sharp.

To quantify the phase delay between the calcium and cAMP oscillations, we analysed the circular cross-correlation function (*C*) as a function of time of oscillations. If the oscillations are in phase, the maximum of *C* occurs at zero time lag. If the oscillations are out of phase, the maximum occurs at lags equalling multiples of the time period of the oscillation. We use the following metric to quantify the time delay:

$$Time\ delay\ metric = \frac{C(zero\ lag) - max(C)}{min(C) - max(C)} \quad \ldots 17$$

Therefore, for oscillations that are in-phase, we would have *C(zero lag)* near the maximum and so the metric has a small value. On the other hand, anti-phasic oscillations would result in larger metric values. To quantify the "sharpness" of the calcium rise and cAMP decay phases, we determined the $t_{1/2}$ of the respective phases as follows:

$$CaRise = mean\left(t_{\frac{A}{2}} - t_{Trough}\right) \quad \ldots 18$$

where $t_{A/2}$ is the time at which the calcium concentration level is half of its amplitude and t_{Trough} is the time at which the trough corresponding to a certain rise phase occurs. This $t_{1/2}$ is measured over multiple cycles and the mean is obtained.

Similarly, the cAMP decay phase is quantified as below:

$$cAMPDecay = mean\left(t_{Peak} - t_{\frac{A}{2}}\right) \quad \ldots 19$$

where, t_{Peak} is the time at which the peak occurs and $t_{A/2}$ is as defined above.

In each of the following simulations, where multiple circuits with different parameters are simultaneously compared, *CaRise* and *cAMPDecay* are normalized with respect to their corresponding maxima. Finally, a metric to quantify the coincidence of sharp rises in Ca and decays in cAMP is defined as:

$$RiseDecayMetric = \left(\frac{CaRise}{Max(CaRise)}\right).\left(\frac{cAMPDecay}{Max(cAMPDecay)}\right) \quad \ldots 20$$

2.4.3.2 Simulations

As described above, 4 parameters were varied to describe different possible circuits. In each such exercise, 3 different values for the parameter were chosen – represented by the set {-1,0,1} – a "low" value, a nominal value or a "high" value. The parameter value changes across the rows in the plots presented below (Figure 2.17-Figure 2.20). Therefore, each row corresponds to the full set of 12 circuits at a fixed parameter value. Conversely, each column corresponds to a particular circuit with the parameter value spanning the complete range. In the plots, the 'warmer' (red being the warmest) colours indicate a higher value for the corresponding metric and 'cooler' (blue being the coolest) colours correspond to lower values. White patches indicate that the corresponding circuits did not produce oscillations or produced complex oscillations with varying amplitude, a feature that we do not observe in our experimental results. The ordered set of numbers in the plots should be read as: [parameter value, Ca-AC link, CaM-AC link, CaM-PDE link]. As already mentioned, we looked for circuits that satisfied certain key criteria in accordance with our experimental results. So, we identified circuits that could produce anti-phasic oscillations (which correspond to warmer patches in the Time Delay Metric plots) and which had a simultaneously fast calcium rise phase and cAMP decay phase (which correspond to cooler patches in the Rise-Decay Metric plots).

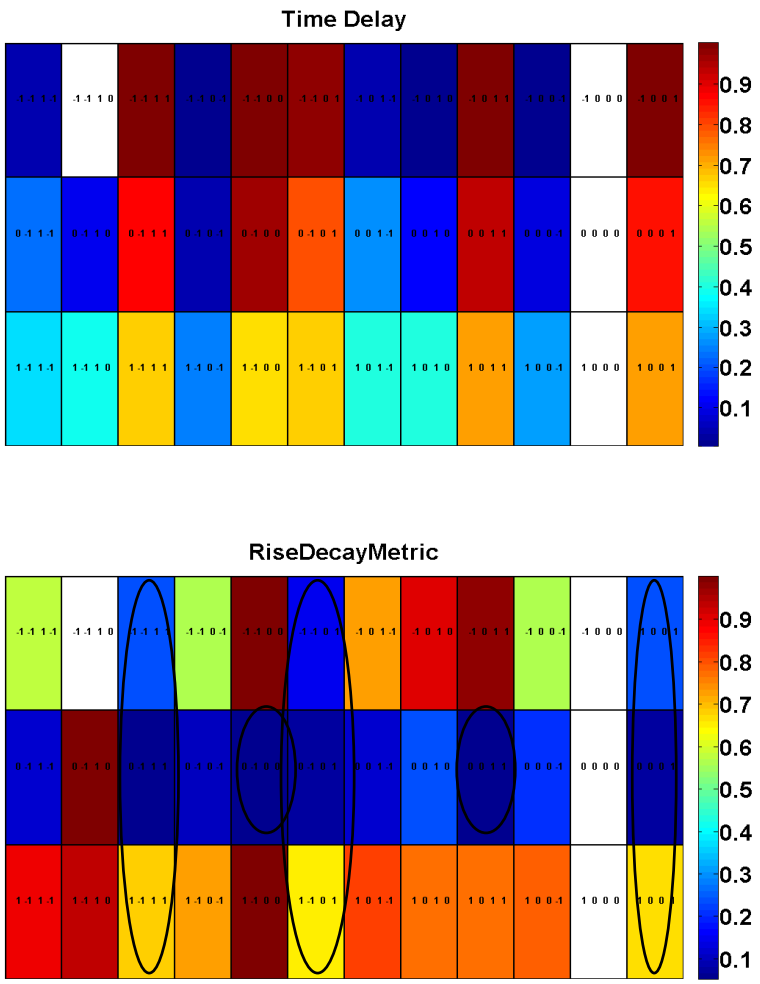

Figure 2.17: Topology analysis with changes in PKA feedback parameter. Changes in the time delay between Calcium and cAMP oscillations (top panel) and the coincidence of rapid calcium rise phase and a rapid cAMP decay phase (bottom panel) due to change in K_{PKAvar}. K_{PKAvar} takes one of the values {-1,0,1}.

First, we varied the parameter that relates to the PKA feedback to calcium. There appear to be 5 circuits that can produce anti-phasic oscillations and with sharp calcium rise and cAMP decay phases as shown by the black oval outlines in Figure 2.17. We also considered circuits with "yellow" patches in the 3rd row, because they have a shorter rise and decay phase compared to the other circuits at that parameter value.

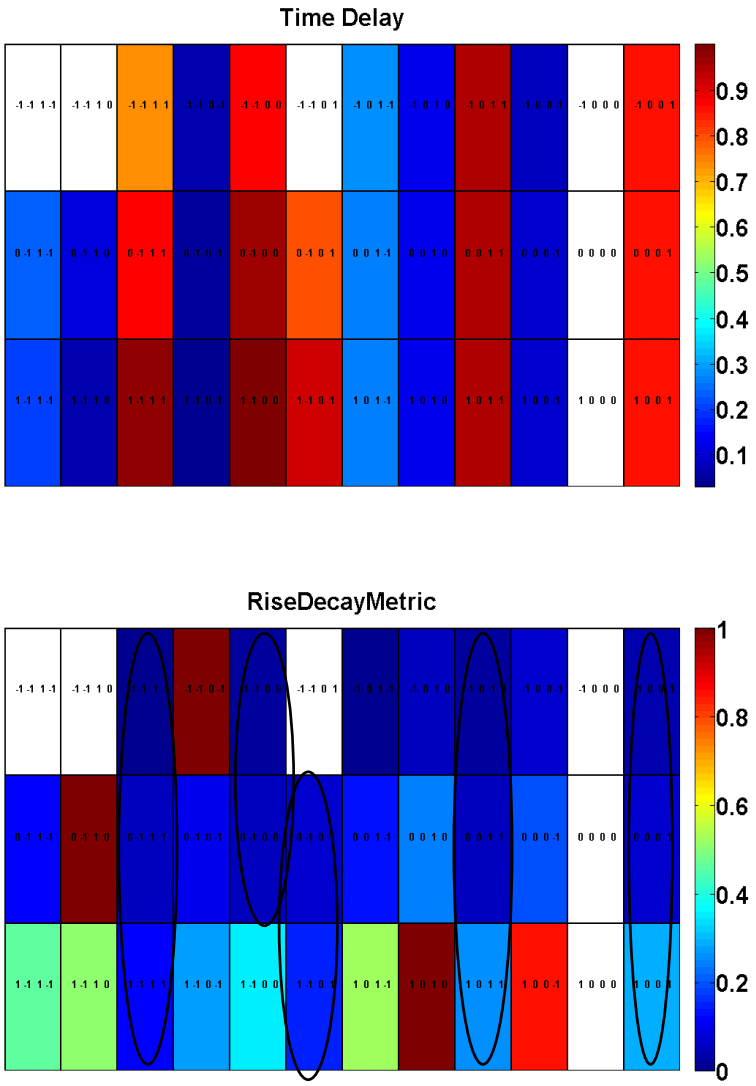

Figure 2.18: Topology analysis with changes in calcium and CaM binding parameters. Changes in the time delay between calcium and cAMP oscillations (top panel) and the coincidence of rapid calcium rise phase and a rapid cAMP decay phase (bottom panel) due to change in κ. κ takes takes one of the values {-1,0,1}.

We next examined the ratio of the parameters relating to calcium binding and CaM binding to the target protein (Figure 2.18). Again, we obtained 5 circuits that satisfied the required conditions. Three of them appeared to be robust in satisfying the criteria despite a change in parameter values.

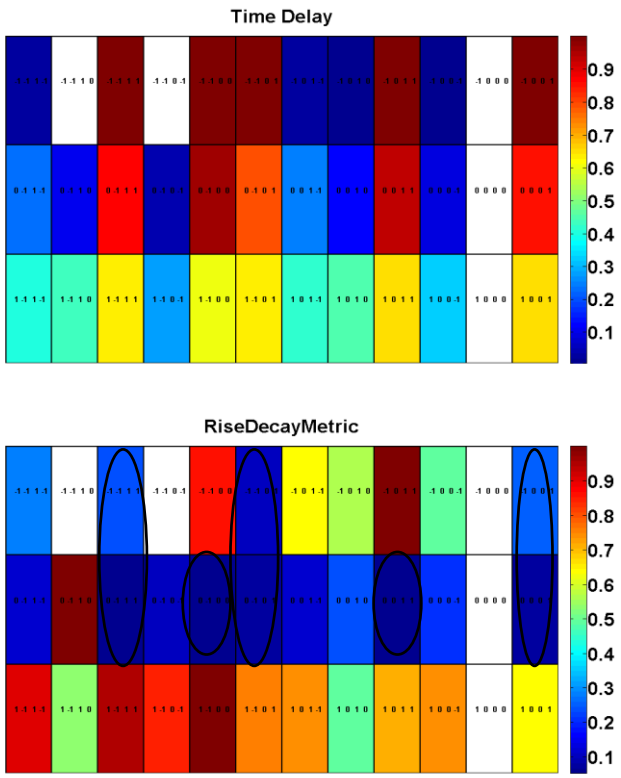

Figure 2.19: Topology analysis with changes in cAMP generation and degradation parameters. Changes in the time delay between calcium and cAMP oscillations (top panel) and the coincidence of rapid calcium rise phase and a rapid cAMP decay phase (bottom panel) due to change in λ_c. λ_c takes one of the values {-1,0,1}.

We next analyzed the ratio of the formation and degradation constants pertaining to cAMP dynamics (Figure 2.19). For the sake of convenience, we assumed the rate constant for formation to be same for both calcium dependent and CaM dependent ACs. This parameter was varied two-fold. A higher fold increase in the value of this parameter produced very high frequency oscillations with varying amplitude, a feature not consistent with our experimental results. Again, the same 5 circuits as in Figure 2.19 were found to satisfy the criteria, of which 3 circuits were relatively robust to parameter variation.

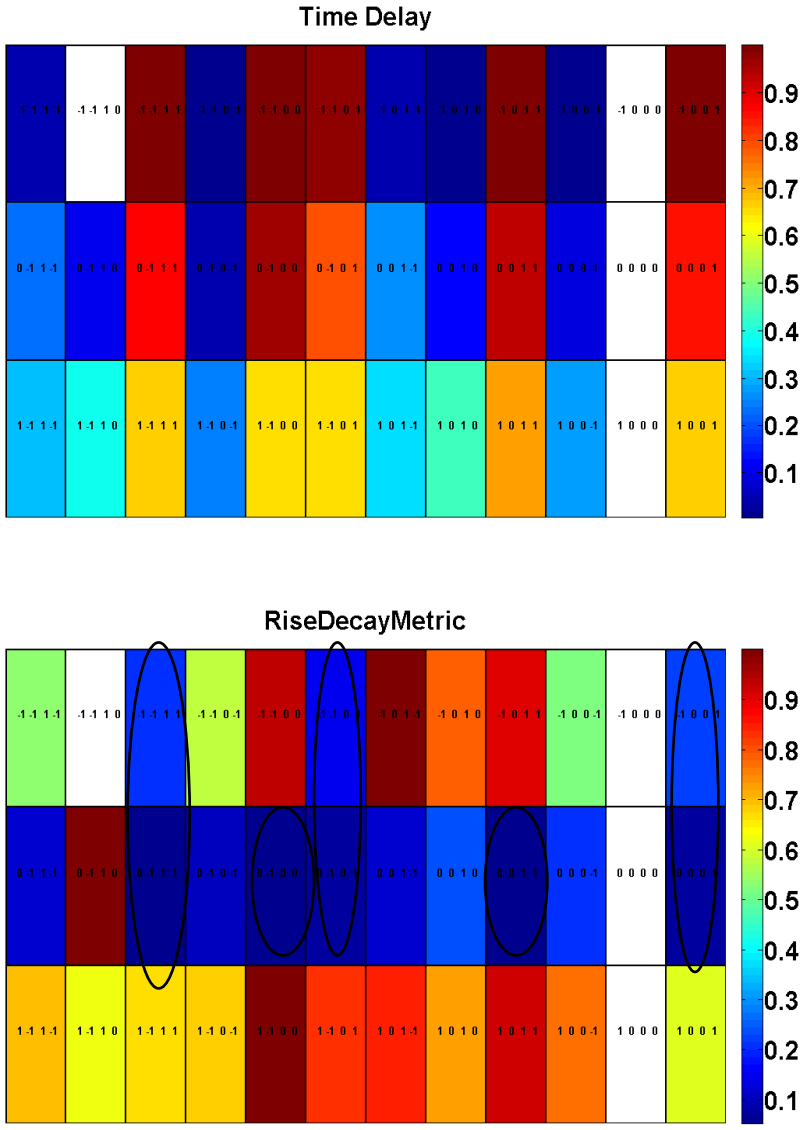

Figure 2.20: Topology analysis with changes in PKA formation and degradation parameters. Changes in the time delay between Calcium and cAMP oscillations (top panel) and the coincidence of rapid Calcium rise phase and a rapid cAMP decay phase (bottom panel) due to change in λ_p. λ_p takes one of the values {-1,0,1}.

We next studied the effect of the ratio of formation and degradation constants relating to PKA dynamics (Figure 2.20). As in Figure 2.19, we identified 3 relatively robust circuits of 5 possible candidates. Based on the above analyses, we identified the 5 following circuits that repeatedly satisfied the required criteria: (-1,1,1), (-1,0,0), (-1,0,1), (0,1,1) and

(0,0,1). Of these, the 3 following circuits appeared to be relatively robust to parameter variation in each case: (-1,1,1), (-1,0,1) and (0,0,1).

In all of the 3 circuits mentioned above, we found a common feature, namely that the 3rd number in the set is always 1. In other words, PDE activation by CaM is sufficient to produce Calcium and cAMP oscillations out of phase with each other, with Calcium having a sharp rise and cAMP having a sharp decay phase. We used this result in formulating our model for the Calcium-cAMP-PKA circuit as detailed in the following sections.

2.4.4 A Detailed Model of the Calcium-cAMP-PKA Signaling Circuit

Based on the results obtained by exploring different circuit combinations as described in Section 2.4.3, we identified the minimal topology that could explain our experimental results, as shown in Figure 2.21 below. Accordingly, we developed a mechanistic model for the calcium, cAMP and PKA modules for this circuit as detailed below. The Voltage module as mentioned previously is based on the Chay-Keizer model and was retained with the same modifications that were used in the model topology analysis detailed in Section 2.4.3. On the other hand, we developed a more comprehensive and mechanistic model to describe the dynamics of calcium, cAMP and PKA as is described in the following sub-sections.

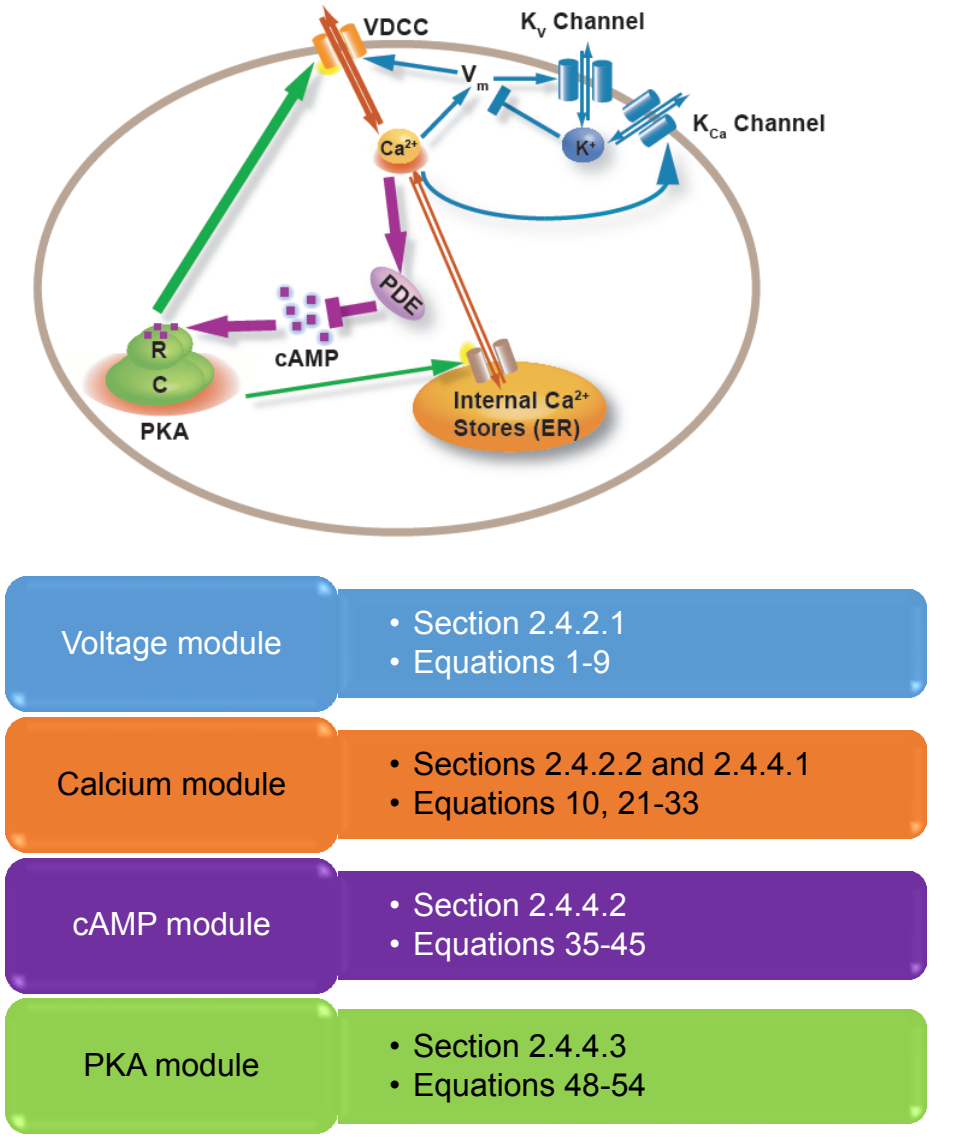

Figure 2.21: Circuitry of main molecular 'players' in the system. Note the two feedback circuits involving V_m and calcium, and calcium-cAMP-PKA. The latter is highlighted by thicker arrows. The different modules are represented by different colours per the legend shown on the right. VDCC, Voltage-Dependent Calcium Channel; V_m, Membrane potential; AC, Adenylate Cyclase; PDE, Phosphodiesterase; PKA, Protein Kinase A; R, Regulatory subunit of PKA; C, Catalytic subunit of PKA; ER, Endoplasmic Reticulum; cAMP, Cyclic adenosine monophosphate; K_v channel; Voltage-gated K^+ channel; K_{Ca} channel, Calcium-activated K^+ channel;IP3R, Inositol trisphoshphate receptor.

2.4.4.1 A more detailed model of the Calcium module

Apart from Calcium influx across the plasma membrane detailed in equation 10, calcium release from the internal stores is also assumed to play a major role in many processes that involve calcium oscillations, as evidenced by the glucose regulated expression of IP3Rs in rat pancreatic islets (*103*). Hence, equations were set up to describe the net calcium release from and uptake by internal stores mediated by IP3Rs and Smooth Endoplasmic Reticulum Calcium ATPases (SERCAs) respectively.

The driving force for the IP3R mediated flux was described in terms of the calcium gradient across the ER. The opening probability of IP3R was modelled as a bell-shaped function of $[Ca^{2+}]_i$ (equation 21) based on previous work (*104-106*). Further, IP3Rs have been shown to be regulated by phosphorylation by PKA (*107, 108*) as can also be deduced from our experimental results that indicate the presence of a PKA mediated feedback (which may occur via phosphorylation of channels that contribute to an increase in intracellular calcium levels). Hence, the effect of PKA on the flux through IP3R was incorporated by including a linear dependence on PKA, as shown below:

$$P_{open} = P_{maximum}\left(\frac{[Ca^{2+}]_i}{([Ca^{2+}]_i+K_a)([Ca^{2+}]_i+K_i)}\right) = P_{maximum}\left(\frac{B[Ca^{2+}]_i}{1+A[Ca^{2+}]_i+B[Ca^{2+}]_i{}^2}\right) \quad \dots 21$$

where, $A = (K_a + K_i)/(K_aK_i)$, $B = (1/K_aK_i)$.

$$\therefore \phi_{IP3R} = P_{open}.(C.[PKA^*]).([Ca^{2+}]_{stores} - [Ca^{2+}]_i) \quad \dots 22$$

To estimate the parameters governing the opening probability of the IP3R channel, previous models describing the IP3R gating of these channels were considered. While these models do not explicitly describe the mechanisms accounting for the bell-shaped curve

mentioned above, it is possible to derive the appropriate parameters by making certain assumptions and modifications as described below:

According to the Gorbunova-Spitzer Model (*98*), which is in turn based on a model by Tang and Othmer(*99*):

$$\frac{d[Ca^{2+}]_i}{dt} = \alpha_1(\beta - [Ca^{2+}]_i) + \left(\frac{\alpha_2[Ca^{2+}]_i(\beta-[Ca^{2+}]_i)(1-IP3R)}{\beta_0+[Ca^{2+}]_i}\right) - \beta_1\left(\frac{[Ca^{2+}]_i^2}{\alpha_3^2+[Ca^{2+}]_i^2}\right) \quad \dots 23$$

$$\frac{dIP3R}{dt} = -\epsilon(IP3R) + \frac{\beta_2[Ca]^2(1-IP3R)}{\beta_0+[Ca]} \quad \dots 24$$

where the Calcium fluxes in 23 are described in terms of the Voltage driven channels (1st term), IP3R mediated Calcium release (2nd term) and SERCA mediated Calcium uptake from the cytosol (3rd term).

For the sake of convenience, we assume in our model that the IP3R is at a quasi steady state. Therefore, the equation 24 modifies to:

$$1 - IP3R = \frac{\epsilon(\beta_0+[Ca^{2+}]_i)}{\beta_2[Ca^{2+}]_i^2+\epsilon(\beta_0+[Ca^{2+}]_i)} \quad \dots 25$$

$$\therefore \phi_{IP3R} = \left(\frac{\alpha_2[Ca^{2+}]_i(\beta-[Ca^{2+}]_i)}{\beta_0+[Ca^{2+}]_i}\right).\left(\frac{\epsilon(\beta_0+[Ca^{2+}]_i)}{\beta_2[Ca^{2+}]_i^2+\epsilon(\beta_0+[Ca^{2+}]_i)}\right) = \left(\frac{\alpha_2\epsilon[Ca^{2+}]_i(\beta-[Ca^{2+}]_i)}{\beta_2[Ca^{2+}]_i^2+\epsilon(\beta_0+[Ca^{2+}]_i)}\right) \dots 26$$

From (22) and (26) we obtain:

$$P_{open}.(C.[PKA^*]).([Ca^{2+}]_{stores} - [Ca^{2+}]_i) = \left(\frac{\alpha_2\epsilon[Ca^{2+}]_i(\beta-[Ca^{2+}]_i)}{\beta_2[Ca^{2+}]_i^2+\epsilon(\beta_0+[Ca^{2+}]_i)}\right) \quad \dots 27$$

Comparing LHS and RHS of the equation (27), we arrive at the following relations:

$$A = \frac{1}{\beta_0} \quad \dots 28$$

$$B = \frac{\beta_2}{\epsilon\beta_0} \quad \dots 29$$

$$C.[PKA^*] = \frac{\alpha_2}{B\beta_0} \quad \dots 30$$

Hence, from the Gorbunova-Spitzer model, one can estimate: A = 2.869 μM^{-1}, B = 28.69 μM^{-2}. Estimation of the parameter C, however, requires a complex iterative procedure, since it depends on [PKA^*], which in turn again depends on the above equations. Therefore, for the sake of convenience and to roughly estimate characteristic, order of magnitude value of this parameter, we assumed PKA^* to be in quasi steady state, in which case, one obtains the following relation as was shown by Gorbunova and Spitzer (refer to the Supplementary file accompanying the paper by Gorbunova and Spitzer (*98*) for more details):

$$[PKA^*] = k_{PKA-cAMP}[cAMP]^2 \quad \ldots 31$$

where, $k_{PKA\text{-}cAMP}$ = 2 μM^{-1}. Estimating an average cAMP concentration of about 0.3 μM, we get C = 2.133 μM^{-1}.

Finally, the SERCA activity was modeled as a function of $[Ca^{2+}]_i$ with a Hill's coefficient of 2, as was done by Gorbunova and Spitzer, and by Tang and Othmer.

Hence, the final equation for the calcium flux through the internal stores can be represented as:

$$j_{Ca,I} = C.k_{IP3R}.[PKA^*]\left(\frac{A[Ca^{2+}]_i}{1+A[Ca^{2+}]_i+B[Ca^{2+}]_i^2}\right)([Ca^{2+}]_{stores} - [Ca^{2+}]_i) - V_s\left(\frac{[Ca^{2+}]_i^2}{K_s^2+[Ca^{2+}]_i^2}\right) \quad \ldots 32$$

It should be noted that, while the equations of the voltage module employ parameters that are specifically suited for the pancreatic beta-cell system, the equations for flux across the internal stores employed by Gorbunova and Spitzer, and by Tang and Othmer were used in the context of Aplysia neurons and cardiac myocytes respectively. Hence, using the equations with the values derived above might lead to oscillations with

frequencies different from that observed in our experiments. In reality, parameters like IP3R density, for instance, that govern flux through internal stores would be expected to differ when used in the pancreatic beta-cell system. We are unaware of any measurements of the number or density of IP3Rs in these or other cell types. Nevertheless, the IP3R density on the pancreatic beta-cell ER would be expected to be quite different from that in other systems which necessitates the inclusion of another parameter, k_{IP3R}. The presence of this parameter is, in fact, necessary for the matching of experimental results and model simulations. Similarly, the parameters pertaining to SERCA activity were also refined so as to ensure robust oscillations of frequencies matching those in the initial experimental results. This process is a part of model 'training'. The trained model was then used to make further predictions as detailed earlier.

The values for the parameters were therefore, chosen in accordance with our experimental data: A = 0.2869 μM^{-1}, B = 2.869 μM^{-1}, C = 0.2133 μM^{-1}, k_{IP3R} = 0.05, V_s = 0.1 $\mu M.s^{-1}$, K_s = 10 μM.

The net calcium flux is the sum of calcium influx through the plasma membrane and calcium release by internal stores. As mentioned before, PKA phosphorylation of various channels that contributes to influx of calcium is most likely the manner of PKA mediated feedback that is indicated by our results. Hence, the PKA dependence of calcium flux across the plasma membrane was also incorporated semi-mechanistically. The net calcium flux can be therefore described as follows:

$$\frac{d[Ca^{2+}]_i}{dt} = j_{Ca,V}\left(1 + k_{PKA,V}[PKA^*]\right) + j_{Ca,I} \quad \ldots 33$$

2.4.5 cAMP Module:

A study by Leech et al. (*109*) indicated that adenylyl cyclases AC5 and AC6 were the predominant isoforms in human islets and rat islets, and in INS-1 and HIT-T15 cell lines. A study by Landa et al. (*110*) also indicated that AC5 and AC6 were present in MIN6 cells, the cells that constitute our experimental model. Both AC5 and AC6 are believed to be calcium-inhibitable isoforms (*111, 112*).

The kinetics for calcium inhibitable AC can be modelled as shown below:

$$j_{AC} = \frac{V_{AC,m}}{K_i + [Ca^{2+}]_i} \quad \ldots 34$$

Guillou, Nakata and Cooper (*113*) have previously analysed the kinetics of the AC6 isoform which served as the basis for the kinetic description of AC in our system. Although AC5 and AC6 may be the predominant isoforms, it is currently unknown which isoform(s) may be active in the calcium-cAMP-PKA circuit. Hence, we assumed the minimal model configuration that could corroborate our data. As shown in the Model Topology Analysis (Section 2.4.3), the key features of our experimental data could be replicated even with a Calcium and Calmodulin independent AC in the presence of Calmodulin activated PDEs. Accordingly, we modified the kinetics detailed by Guillou et al. to describe constant AC activity as explained below.

The value for K_i was estimated to be about 0.2 μM by Guillou et al. The maximal activity of calcium inhibited AC, $V_{AC,m}$, was also estimated from the same study, as follows:

From Figure 1 of the study mentioned above (*113*), the AC activity (per unit mass of the reaction volume) was estimated to be about 100 pmol.(min.mg)$^{-1}$. Further, the reaction volume was 100 μL and total protein content was about 0.5-2.5 mg/mL (as mentioned in the Methods section of the study by Guillou et al. (*113*)).

Assuming a fairly purified AC fraction, the AC concentration was taken to be approximately 1 mg/mL; then the *total* AC activity present in 100 μL of reaction volume (and hence, 100 μg of protein) can be expressed of the form:

100×10^{-12} mol $\times$100 μg/(60 s $\times$ 1 mg) = 0.167 pmol.s^{-1}.

Hence, the activity (per unit volume of reaction volume) can be written as:

0.167 pmol.s^{-1}/100 μL = 1.67×10^{-3} uM.s^{-1} ~ 0.002 μM.s^{-1}.

Therefore, the maximal activity (or $V_{AC,m}$) is of the order of 2×10^{-3} μM.s^{-1}. Assuming the mean $[Ca^{2+}]_i$ concentration of about 1 μM, one can estimate the order of the magnitude of the reaction flux:

$$j_{AC} = \frac{V_{AC,m}}{K_i+[Ca^{2+}]_i} \cong V_{AC,m} \quad \ldots 35$$

Therefore, j_{AC} is approximately equal to 0.002 μM.s^{-1}.

To derive the parameters for modelling the action of PDE, the kinetics described by Bhalla and Iyengar (*114*) were used. The PDE activity is believed to be dependent on Calmodulin molecules bound to 3 Ca^{2+} ions ($CaM.Ca_3$) and 4 Ca^{2+} ions ($CaM.Ca_4$). Additionally, it is also assumed that cAMP is degraded by Calcium-independent PDEs.

Referring to reaction C16 in Constants and Database of References section in the Supplementary material of the study by Bhalla and Iyengar (*114*), the kinetics of the activated form of PDE can be written as:

$$\frac{d[CaM.Ca_n.PDE]}{dt} = k_{16}[CaM.Ca_n].[PDE] - k_{-16}[CaM.Ca_n.PDE] \quad \ldots 36$$

As mentioned above, both CaM.Ca_3 and CaM.Ca_4 are believed to modulate PDE activity. Although reaction C16 mentioned in the Supplementary of the study by Bhalla and Iyengar deals with CaM.Ca_4, it is assumed here that the kinetics of the formation of the CaM.Ca_4 and CaM.Ca_3 complexes would not be drastically different. Hence, in the above equation 'n' would be either 3 or 4 depending on the complex being considered.

The steady state approximation for [CaM.Ca_n] complex can be written of the form:

$$[CaM.Ca_n] = \frac{[CaM_{tot}].[Ca^{2+}]_i^{\,n}}{[Ca^{2+}]_i^{\,n} + k_n[Ca^{2+}]_i^{\,n-1} + k_n k_{n-1}[Ca^{2+}]_i^{\,n-1} + \cdots + k_n k_{n-1} \ldots k_2[Ca^{2+}]_i^{\,1} + k_n k_{n-1} \ldots k_1} \quad \ldots 37$$

where, [CaM_{tot}] = 20 μM, n = 3 or 4, k_1=7.5 μM, k_2=2.7 μM, k_3=31 μM and k_4=31 μM. These parameter values are based on a study by Huang et al(*115*).

Assuming $[Ca^{2+}]_i$ is about 1 μM, the following approximation can be made, when n = 3 or 4:

$$[CaM.Ca_n] \cong a_c(n)[Ca^{2+}]_i^{\,n} \quad \ldots 38$$

$$a_c(n) = \frac{[CaM_{tot}]}{\prod_{i=1}^{n} k_i} = \begin{Bmatrix} 0.001\ for\ n = 4 \\ 0.03\ for\ n = 3 \end{Bmatrix} \quad \ldots 39$$

Since, both CaM.Ca_3 and CaM.Ca_4 are believed to play a major role in PDE kinetics (*116*), the cAMP kinetics was derived accordingly for both the complexes from the kinetics

detailed in reaction C18 in the Constants and Database of References section in the Supplementary material of the study by Bhalla and Iyengar.

$$\frac{d[cAMP]}{dt} = V_{AC,m} - \frac{V_{18}^{PDE}[cAMP]}{K_{18}^{PDE}+[cAMP]}[PDE^*] \quad \text{... 40}$$

Assuming that the PDE* complex is at steady state, equation (36) would lead to:

$$[PDE^*] = [PDE_t].(\frac{k_{16}}{k_{-16}})[CaM.Ca_n] \quad \text{... 41}$$

Therefore, from (40) and (41), the *degradation* flux of cAMP is given by:

$$\frac{d[cAMP]_{deg}}{dt} = \frac{V_{18}^{PDE}[cAMP]}{K_{18}^{PDE}+[cAMP]}\left(\frac{k_{16}}{k_{-16}}\right)[PDE_t].a_c(n).[Ca]^n = K_{n,c}[Ca]^n[cAMP] \quad \text{... 42}$$

The above modification is possible since, the usually assumed [cAMP] is much smaller than K_{18}^{PDE}.

Using these values, we get $K_{3,c} = 0.072\ \mu M^{-4}.s^{-1}$ and $K_{4,c} = 2.16\ \mu M^{-3}.s^{-1}$

$$j_{PDE} = \left(K_{3,c}[Ca^{2+}]_i^3 + K_{4,c}[Ca^{2+}]_i^4\right)[cAMP] \quad \text{... 43}$$

The synthesis of cAMP by AC, degradation by inhibitory and calcium independent PDEs and the net flux of cAMP can therefore, be represented by the following equations:

$$j_{AC} = \frac{V_{AC,m}}{K_i+[Ca^{2+}]_i} \cong V_{AC,m} \quad \text{... 35}$$

$$j_{PDE} = \left(K_{3,c}[Ca^{2+}]_i^3 + K_{4,c}[Ca^{2+}]_i^4\right)[cAMP] \quad \text{... 43}$$

$$j_{PDE,ind} = k_d[cAMP] \quad \text{... 44}$$

$$\frac{d[cAMP]}{dt} = j_{AC} - k_{PDE}(j_{PDE} + j_{PDE,ind}) \quad \text{... 45}$$

The parameter k_d for Calcium independent active fraction of PDE was assumed to be about $0.01\ s^{-1}$, as has been done by Fridlyand et al.

2.4.6 PKA Module:

To model PKA dynamics, we take into account the fact that it exists as a homodimer of its regulatory and catalytic subunits (R_2C_2). Upon binding of 4 molecules of cAMP to the regulatory subunits in serial fashion, the protein releases its catalytic subunits one-by-one. The reaction set J in the Constants and Database of References section in the Supplementary material of the study by Bhalla and Iyengar was used to model PKA dynamics. For the sake of convenience, it was assumed that the cAMP binding kinetics is relatively faster than the dissociation of catalytic subunit from the PKA complex. Consider, therefore, the kinetics when the 'i^{th}' molecule of cAMP (c) binds to the PKA dimer (R_2C_2) bound to '(i-1)' molecules of cAMP, which may be represented as below:

$$c_{i-1}R_2C_2 + c \underset{\mathbf{k_{if}},\ \mathbf{k_{ib}}}{\leftrightarrow} c_iR_2C_2$$

Assuming the cAMP-PKA complexes are at quasi steady state, we get:

$$\frac{d[c_iR_2C_2]}{dt} = k_{if}[c][c_{i-1}R_2C_2] - k_{ib}[c_iR_2C_2] = 0 \quad \text{... 46}$$

$$\therefore [c_iR_2C_2] = (k_{if}/k_{ib})[c][c_{i-1}R_2C_2] \quad \text{... 47}$$

In the above equations, 'c' is cAMP, R_2C_2 is the PKA homodimer and $c_iR_2C_2$ is the PKA homodimer bound to 'i' molecules of cAMP. Hence, we obtain:

$$[c_4R_2C_2] = K_1K_2K_3K_4[cAMP]^4[R_2C_2] \quad \text{... 48}$$

Hence, $K_i = k_{if}/k_{ib}$ (i = 1,2,3 or 4) in the equation (48).

Now, we consider the mass balances in this system. In a general case, where a complex is $[A_mB_n]$, 1 mol $[A_mB_n]$ would correspond to 'm' mol A and 'n' mol B. Using this for the following balances, we get:

Regulatory Subunit balance:

$$[R_2C_2]_0 = [R_2C_2] + [cR_2C_2] + [c_2R_2C_2] + [c_3R_2C_2] + [c_4R_2C_2] + [c_4R_2] + [c_4R_2C] \quad \dots 49$$

(all complexes have 2 regulatory subunits (*R*) each)

Catalytic subunit balance:

$$2[R_2C_2]_0 = 2[R_2C_2] + 2[cR_2C_2] + 2[c_2R_2C_2] + 2[c_3R_2C_2] + 2[c_4R_2C_2] + [c_4R_2C] + [PKA^*] \quad \dots 50$$

(all complexes have 2 catalytic subunits (*C*) each, except for c_4R_2C and PKA^*)

$$\therefore [R_2C_2]_0 = [R_2C_2] + [cR_2C_2] + [c_2R_2C_2] + [c_3R_2C_2] + [c_4R_2C_2] + \frac{[c_4R_2C]}{2} + \frac{[PKA^*]}{2} \quad \dots 51$$

Subtracting (49) from (51) we obtain:

$$[c_4R_2C] = [PKA^*] - 2[c_4R_2] \quad \dots 52$$

Further, the differential equations describing the dynamics of c_4R_2 and PKA^* were written based on the kinetics spelt out in reaction set J in the Constants and Database of References section in the Supplementary material of the study by Bhalla and Iyengar.

$$\frac{d[c_4R_2]}{dt} = k_{6f}[c_4R_2C] - k_{6b}[PKA^*][c_4R_2] \quad \dots 53$$

$$\frac{d[PKA^*]}{dt} = k_{5f}[c_4R_2C_2] - k_{5b}[PKA^*][c_4R_2C] + k_{6f}[c_4R_2C] - k_{6b}[PKA^*][c_4R_2] \quad \dots 54$$

Equations 48, 52, 53 and 54 thus comprise the PKA module.

2.4.7 List of main equations and parameters:

2.4.7.1 Equations:

Voltage Module:

$$m_\infty = 0.5\left(1 + \tanh\left(\frac{V - v_1}{v_2}\right)\right) \quad \dots 1$$

$$w_\infty = 0.5\left(1 + \tanh\left(\frac{V - v_3}{v_4}\right)\right) \quad \dots 2$$

$$\tau = \frac{1}{\cosh\left(\frac{V - v_3}{2v_4}\right)} \quad \dots 3$$

$$I_K = g_K w(V - E_K) \quad \text{... 4}$$

$$I_{Ca} = g_{ca} m_\infty (V - E_{Ca}) \quad \text{... 5}$$

$$I_L = g_L (V - E_L) \quad \text{... 6}$$

$$I_{K(Ca)} = g_{K(Ca)} \left(\frac{[Ca^{2+}]_i}{[Ca^{2+}]_i + K_{K(Ca)}} \right) (V - E_K) \quad \text{...7}$$

$$\frac{dV}{dt} = \frac{1}{C_m} \left(-I_{Ca} - I_K - I_L - I_{K(Ca)} \right) \quad \text{... 8}$$

$$\frac{dw}{dt} = \phi \left(\frac{w_\infty - w}{\tau} \right) \quad \text{... 9}$$

Calcium Module:

$$j_{Ca,V} = f_i(-\alpha I_{Ca} - v_{L,PM}[Ca^{2+}]_i) \quad \text{... 10}$$

$$j_{Ca,I} = C.k_{IP3R}.[PKA^*] \left(\frac{A[Ca^{2+}]_i}{1 + A[Ca^{2+}]_i + B[Ca^{2+}]_i^2} \right) ([Ca^{2+}]_{stores} - [Ca^{2+}]_i) - V_s \left(\frac{[Ca^{2+}]_i^2}{K_s^2 + [Ca^{2+}]_i^2} \right) \quad \text{... 32}$$

$$\frac{d[Ca^{2+}]_i}{dt} = j_{Ca,V} \left(1 + k_{PKA,V}[PKA^*] \right) + j_{Ca,I} \quad \text{... 33}$$

cAMP Module:

$$j_{AC} = \frac{V_{AC,m}}{K_i + [Ca^{2+}]_i} \cong V_{AC,m} \quad \text{... 35}$$

$$j_{PDE} = \left(K_{3,c}[Ca^{2+}]_i^3 + K_{4,c}[Ca^{2+}]_i^4 \right)[cAMP] \quad \text{... 43}$$

$$j_{PDE,ind} = k_d[cAMP] \quad \text{... 44}$$

$$\frac{d[cAMP]}{dt} = j_{AC} - k_{PDE}(j_{PDE} + j_{PDE,ind}) \quad \text{... 45}$$

PKA Module:

$$[c_4R_2C_2] = K_1K_2K_3K_4[cAMP]^4[R_2C_2] \quad \text{... 48}$$

$$[c_4R_2C] = [PKA^*] - 2[c_4R_2] \quad \text{... 52}$$

$$\frac{d[c_4R_2]}{dt} = k_{6f}[c_4R_2C] - k_{6b}[PKA^*][c_4R_2] \quad \text{... 53}$$

$$\frac{d[PKA^*]}{dt} = k_{5f}[c_4R_2C_2] - k_{5b}[PKA^*][c_4R_2C] + k_{6f}[c_4R_2C] - k_{6b}[PKA^*][c_4R_2] \quad \text{... 54}$$

2.4.7.2 Parameters

Table 2.1: Symbols, defintions, values and references for the parameters used in the model. * indicates these values have been modified. Refer text for details.

Symbol	Definition	Value (for parameters)	References for values
	Voltage Module		
v_1	Potential at which $m_\infty = 0.5$	-20 mV	[101]
v_2	Reciprocal of slope of voltage dependence of m_∞	24 mV	[101]
v_3	Potential at which $w_\infty = 0.5$	-16 mV	[101]
v_4	Reciprocal of slope of voltage dependence of w_∞	11.2 mV	[101]
g_K	Delayed rectifier K^+ channel conductance	260 pS	[101]*
g_{Ca}	VDCC conductance	600 pS	[101]*
g_L	Leak conductance	150 pS	[101]
$g_{K(Ca)}$	Calcium gated K^+ channel conductance	2000 pS	[101]
E_K	Delayed rectifier K^+ channel reversal potential	-75 mV	[101]
E_{Ca}	VDCC reversal potential	100 mV	[101]*
E_L	Reversal potential for membrane leak	-75 mV	[101]
$K_{K(Ca)}$	Binding constant of Calcium for K(Ca) channel	5 µM	[101]
C_m	Membrane capacitance	5.3 pF	[101]
ϕ	Temperature factor that can be used to change the relative time constants of V and w	35 s^{-1}	[101]
	Calcium Module		
f_i	Fraction of free intracellular Calcium (Note that this parameter was assumed to be 10^{-4} in the initial topology exploration analysis, but 10^{-6} in the current model)	1×10^{-4}-1x10^{-6}	[101]*
α	Factor to convert current in fA to µM.s^{-1}	4.5×10^{-3} µM.$(fA.s)^{-1}$	[101]
$v_{L,PM}$	Rate constant for Calcium leak through plasma membrane	150 s^{-1}	[101]
A	IP3R opening probability parameter, as defined in text	0.2869 μM^{-1}	Derived as mentioned in text
B	IP3R opening probability parameter, as defined in text	2.869 μM^{-2}	Derived as mentioned in text
C	IP3R opening probability parameter, as defined in text	0.2133	Derived as mentioned in text
$[Ca^{2+}]_{stores}$	Calcium concentration inside internal stores	1.56 µM	[99]

α_1	Rate constant for Calcium leak from ER to cytoplasm	2.96×10^{-3} s^{-1}	[98]
α_2	Rate constant for Calcium flux through IP3R	4.266 s^{-1}	[98]
α_3	Binding constant of Calcium to SERCA	0.03 μM	[98]
β	Volumetric average ER Calcium concentration	1.56 μM	[98]
β_0	Parameter controlling Calcium and IP3 binding to activating sites of IP3R	0.349 μM	[98]
β_1	Maximal activity of SERCA	0.999 $\mu M.s^{-1}$	[98]
β_2	Rate constant for Calcium binding to inhibitory site of IP3R with Calcium bound to activating site already	0.18 $(\mu M.s)^{-1}$	[98]
ε	Rate constant for Calcium dissociating from inhibitory site of IP3R with Calcium bound to activating and inhibiting sites	0.018 s^{-1}	[98]
$k_{PKA\text{-}cAMP}$	Parameter relating [PKA^*] and [cAMP] under quasi steady state conditions	2 μM^{-1}	[98]
k_{IP3R}	Parameter reflecting IP3R density in pancreatic beta-cells	0.05	Derived as mentioned in text
V_s	Maximal activity of SERCA	0.1 $\mu M.s^{-1}$	Derived as mentioned in text
K_s	Binding constant of Calcium to SERCA	10 μM	Derived as mentioned in text
	cAMP Module		
$V_{AC,m}$	Maximal activity of AC	0.002 $\mu M^2.s^{-1}$	Derived from [113]
K_i	Inhibitory constant for Calcium binding to AC	0.2 μM	Derived from [113]
k_{16}	Rate constant for $CaM.Ca_4$ binding to PDE	720 $(\mu M.s)^{-1}$	[114]
k_{-16}	Rate constant for $CaM.Ca_4$ dissociation from $CaM.Ca_4$.PDE complex	5 s^{-1}	[114]
CaM_{tot}	Total concentration of Calmodulin	20 μM	[114]
k_1	Equilibrium constant for Calcium binding to CaM	7.5 μM	[115]
k_2	Equilibrium constant for Calcium binding to CaM.Ca	2.7 μM	[115]
k_3	Equilibrium constant for Calcium binding to $CaM.Ca_2$	31 μM	[115]
k_4	Equilibrium constant for Calcium binding to $CaM.Ca_3$	31 μM	[115]
V_{18}^{PDE}	Maximal activity of activated PDE complex	10 s^{-1}	[114]

K_{18}^{PDE}	Michaelis-Menten constant for activated PDE complex	40 μM	[114]
PDE_t	Total PDE concentration	2 μM	[114]
$K_{3,c}$	Reduced rate constant of $CaM.Ca_3$ activated PDE degradation of cAMP	0.072 $(\mu M^4.s)^{-1}$	Derived as mentioned in text
$K_{4,c}$	Reduced rate constant of $CaM.Ca_4$ activated PDE degradation of cAMP	2.16 $(\mu M^3.s)^{-1}$	Derived as mentioned in text
k_d	Parameter controlling Calcium independent PDE degradation of cAMP	0.01 s^{-1}	[95]
	PKA Module		
K_1	Equilibrium constant for binding of cAMP to R_2C_2	1.64 μM^{-1}	Derived from [114]
K_2	Equilibrium constant for binding of cAMP to $c_1R_2C_2$	1.64 μM^{-1}	Derived from [114]
K_3	Equilibrium constant for binding of cAMP to $c_2R_2C_2$	0.68 μM^{-1}	Derived from [114]
K_4	Equilibrium constant for binding of cAMP to $c_3R_2C_2$	2.31 μM^{-1}	Derived from [114]
k_{5f}	Dissociation rate of 1 catalytic subunit from $c_4R_2C_2$	60 s^{-1}	[114]
k_{5b}	Association rate of 1 catalytic subunit to c_4R_2C	18 $(\mu M.s)^{-1}$	[114]
k_{6f}	Dissociation rate of catalytic subunit from c_4R_2C	60 s^{-1}	[114]
k_{6b}	Association rate of 1 catalytic subunit to c_4R_2	18 $(\mu M.s)^{-1}$	[114]

Table 2.2: Definitions for other symbols used in the model.

Symbol	Definition
m_∞	Steady state fraction of open voltage-dependent Calcium channels
w_∞	Steady state fraction of open voltage-dependent K^+ channels
τ	Time constant for the dynamics of opening probability of K^+ channel
I_K	Current through K^+ channel
I_{Ca}	Current through VDCC
I_L	Current through leak
$I_{K(Ca)}$	Current through Calcium gated K^+ channel
P_{open}	Open probability of IP3Rs
$P_{maximum}$	Maximum probability of opening IP3R
K_a	Binding constant for activation site of IP3R
K_i	Binding constant for inhibitory site of IP3R
Φ_{IP3R}	Calcium flux through IP3R
$j_{Ca,V}$	Calcium flux across plasma membrane
$j_{Ca,I}$	Ca flux through internal stores
j_{AC}	cAMP synthesis flux by AC
$CaM.Ca_n$	Calmodulin bound to 'n' Calcium ions
$CaM.Ca_n.PDE$	PDE bound to $CaM.Ca_n$, which is also activated PDE^* complex
$a_c(n)$	Parameter relating $[CaM.Ca_n]$ and $[Ca^{2+}]_i$
PDE^*	Activated PDE complex
j_{PDE}	cAMP degradation flux mediated by Calcium dependent PDEs
$j_{PDE,ind}$	cAMP degradation flux mediated by Calcium independent PDEs
$c_iR_2C_2$	PKA homodimer (R_2C_2) bound to 'i' molecules of cAMP
c_4R_2C	PKA complex (2 regulatory and 1 catalytic subunits) with 4 molecules of cAMP

Table 2.3: Initial conditions of various species and nominal values of other parameters used in the model.

Symbol	Definition	Values	Initial condition (I.C.)/Nominal value (N.V.)
V	Membrane potential	-20 mV	I.C.
w	Fraction of open voltage-dependent K^+ channels	0.2	I.C.
$[Ca^{2+}]_i$	Intracellular Calcium concentration	0.5 μM	I.C.
IP3R	Fraction of IP3R with Calcium bound to both activating and inhibiting sites	0.4	N.V.
cAMP	Intracellular concentration of 3'-5'-cyclic adenosine monophosphate	0.1 μM	I.C.
R_2C_2	PKA homodimer with 2 regulatory subunits (R) and 2 catalytic subunits (C)	1 μM	N.V.
c_4R_2	Complex of 4 molecules of cAMP bound to 2 regulatory subunits of PKA	0.5 μM	I.C.
PKA^*	Active PKA catalytic subunits	0.2 μM	I.C.
$k_{PKA,V}$	Coefficient of modulation of calcium fluxes by PKA	3×10^3	N.V.
k_{PDE}	Coefficient of modulation of the maximal PDE activity	1	N.V.
R_1	Coefficient of modulation of binding constant of cAMP to PKA	0	N.V.
R_2	Coefficient of modulation of dissociation of catalytic subunits of PKA	1	N.V.

2.5 Methods

2.5.1 Gene construction

EGFP and mCherry were PCR amplified to introduce appropriate restriction digest sites for subcloning into either AKAR or ICUE constructs. The genes of GR-AKAR and YR-ICUE were generated in pRSETB (Invitrogen) and then moved to pcDNA3 (Invitrogen) behind a Kozak sequence for mammalian expression. ICUEPID was generated from CRY-AKAR (*96*) in pcDNA3 by replacing mVenus with the molecular switch and mCitrine of ICUE2.

2.5.2 Cell Culture

MIN6 cells were plated onto sterilized glass coverslips in 35-mm dishes and grown to 50–90% confluency in DMEM (10% FBS) at 37°C with 5% CO_2. Cells were transfected using Lipofectamine 2000 (Invitrogen) and grown 20-48 h before imaging. For Calcium imaging experiments, cells were pre-incubated with 1 μM Fura-2/AM (Molecular Probes) for 10-20 min at 37 °C before imaging

2.5.3 Imaging

Cells were washed twice with Hanks' balanced salt solution buffer and maintained in the dark at room temperature. Cells were imaged on a Zeiss Axiovert 200M microscope with a cooled charge-coupled device camera (MicroMAX BFT512, Roper Scientific, Trenton, NJ) controlled by METAFLUOR 6.2 software (Universal Imaging, Downingtown, PA). Fura-2 dual excitation ratio imaging used two excitation filters [350DF10 for 350 nm excitation and 380DF10 for 380 nm excitation], a 450DRLP dichroic

mirror, and a 535DF45 emission filter. Dual red/green emission ratio imaging used a 480DF30 excitation filter, a 505DRLP dichroic mirror, and two emission filters [535DF45 for GFP and 653DF95 for RFP]. Dual red/cyan emission ratio imaging used a 420DF20 excitation filter, a 450DRLP dichroic mirror, and two emission filters [475DF40 for CFP and 653DF95 for RFP]. Dual yellow/red emission ratio imaging used a 495DF10 excitation filter, a 600DRLP dichroic mirror, and two emission filters [535DF25 for YFP and 653DF95 for RFP]. Dual cyan/yellow emission ratio imaging used a 420DF20 excitation filter, a 450DRLP dichroic mirror, and two emission filters [475DF40 for CFP and 535DF25 for YFP]. These filters were alternated by a filter-changer Lambda 10-2 (Sutter Instruments, Novato, CA). Exposure time was 50–500 ms, and images were taken every 10-30 s. Fluorescence images were background-corrected by subtracting the fluorescence intensity of background with no cells from the emission intensities of cells expressing fluorescent reporters. The ratios of 350/380, red/green, red/cyan, yellow/red, or yellow/cyan emissions were then calculated at different time points. The values of all time courses were normalized by dividing each by the average basal value before addition of drug.

2.5.4 Modeling

Model was built as detailed in Section 2.4. Simulations were carried out with custom written MATLAB programs. The system has 6 states: membrane potential (V_m), gating probability of K_+ channel (w), concentration of intracellular calcium ($[Ca^{2+}]_i$), [cAMP], concentration of cAMP bound regulatory subunits of PKA ($[c_4R_2]$), concentration of free catalytic subunit which is the active PKA ($[PKA^*]$). Kinetic equations for calcium flux through the plasma membrane were based on the Chay-Keizer model and the calcium release from internal stores was modeled as arising out of the coordinated activities of IP_3Rs and SERCAs.

Both the fluxes were dependent on PKA activity, thereby setting up a feedback loop. The increase in calcium modulates the activities of calcium-inhibitable AC6 and calcium activated PDE1, which in turn produce and degrade cAMP respectively. PKA is activated by the sequential binding of 4 molecules of cAMP and the catalytic subunit is released sequentially. Concentrations were normalized with respect to their respective maximal levels, for the ease of comparison. The programs were simulated for a sufficient time span (1000 s for traces) to produce sustained oscillatory patterns. Frequency of calcium oscillations was calculated using MATLAB's in-built FFT routine.

2.5.5 Western Blot Analysis

For analysis of oscillatory changes in PKA activity, MIN6 cells were stimulated with 20 mM TEA and washed with ice-cold phosphate-buffered saline at different time points (0, 1, 2, 3, 4, 5, 6, 7, 8 min). Cells were rapidly lysed in radioimmunoprecipitation assay lysis buffer containing protease inhibitor cocktail, 1 mM ethylenediaminetetraacetic acid (EDTA), 1 mM phenylmethylsulfonyl fluoride (PMSF), 1 mM $NaVO_4$, 1 mM NaF, and 25 nM Calyculin A. Cell lysates were incubated on ice for 30 min and centrifuged at 4°C for 20 min. Total protein was separated with 7.5 % SDS-polyacrylamide gel electrophoresis (PAGE) and transferred to nitrocellulose membranes, which were probed with phospho-PKA substrate or beta-tubulin antibody. Bands were visualized by enhanced chemiluminescence. The intensity of the bands was quantified, and the values were then normalized to beta-tubulin level by using UN-SCAN-IT (Silk Scientific, Orem, UT). For detection of nuclear PKA activity, MIN6 cells were stimulated with low dose (2 μM) or high dose (10 μM) of cAMP analog or 50 μM forskolin (FSK) and washed with ice-cold phosphate-buffered saline after 45 min incubation. Cells were then lysed as described

above. Total protein was separated with 7.5 % SDS-PAGE and transferred to nitrocellulose membranes, then probed with phospho-CREB (pS133) or CREB antibody. The intensity of the bands was quantified. The values of phospho-CREB level then were normalized to CREB expression level.

Chapter 3 Decoding of calcium oscillations by the ERK signaling cascade

3.1 Introduction

The extracellular-signal regulated kinases 1/2 (ERK1/2, referred to as ERK here for convenience) are central components of multiple signaling pathways controlling various cellular functions including cell proliferation, cell survival and migration (*117*). In excitable cells, the ERK signaling cascade also interfaces with calcium to achieve non-canonical cell type specific functions. Calcium-ERK crosstalk is deemed important for long term potentiation and memory formation in the brain (*118*), hypertrophy in the heart (*119*) and insulin production in the pancreas (*120*). In pancreatic beta-cells, ERK regulates insulin gene transcription (*51*) and secretory demand (*121*) thereby ensuring the overall health of the beta-cells for efficient insulin production. ERK is activated in beta-cells following stimulation with glucose, hormones and membrane-depolarizing agents in a calcium-dependent manner (*52, 122, 123*). However, how ERK decodes dynamically diverse calcium signals to regulate beta-cell functions is still unclear.

The canonical mode of activation of ERK which belongs to the mitogen activated protein kinase (MAPK) family begins with the activation of the small GTPase, Ras. Ras then activates the MAP Kinase Kinase Kinases, b-Raf and Raf-1 which in turn activate the MAP Kinase Kinase, MEK. Finally, activated MEK phosphorylates and activates ERK (*117*). Multiple candidate signaling molecules including PKA, PKC, CaMKII and PP2B have been suggested to activate one or more of the components of this cascade to facilitate

calcium-dependent ERK activation in beta-cells (*52, 123-125*). Here, we discovered that the ERK cascade in beta-cells can be activated through a calcium-dependent Ras Guanine Exchange Factor (RasGEF) called RasGRF2 which directly activates the canonical Ras-MEK-ERK cascade and influences temporal dynamics of ERK activity.

ERK activity temporal dynamics, especially oscillations (*26*) are thought to influence cell health and are mediated by complex feedback loops in other cells (*90, 126, 127*). In pancreatic beta-cells, depolarization-mediated ERK activity temporal dynamics is dictated by calcium dynamics. Importantly, kinetic differences at different steps of the ERK cascade are crucial for decoding of the input calcium signal by ERK. Sequential processing of the signal by different components of the ERK cascade enables the cell to selectively achieve robust ERK activity increase while still retaining crucial dynamical information for use in different contexts.

3.2 Results

3.2.1 Calcium-ERK crosstalk

We investigated the presence of a potential crosstalk between the calcium and ERK signaling pathways in MIN6 cells in two ways. First, we tested if calcium signals change in response to perturbation of ERK activity. To mimic the action of glucose, we treated the beta-cells with the potassium channel blocker, tetraethyl ammonium chloride (TEA) which depolarizes the plasma membrane and initiates calcium oscillations.

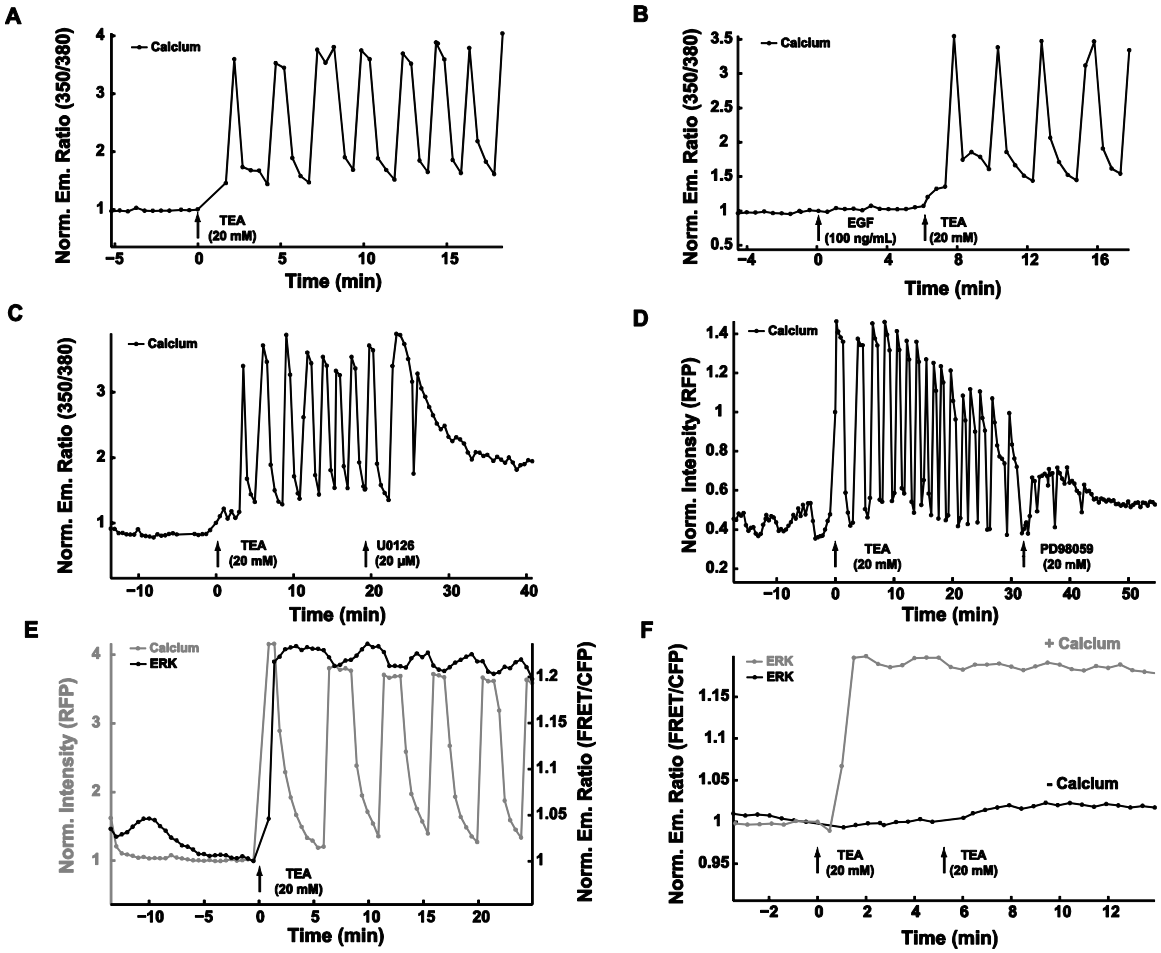

Figure 3.1: ERK-calcium crosstalk. A. Representative time course showing calcium oscillations (monitored by Fura2-AM) in response to TEA in single MIN6 cells (n=55). B. Representative time course showing calcium response to EGF (n=26). C. Representative time course showing calcium response to MEK inhibitor, U0126 (20 μM) following TEA stimulation (n=35). D. Representative time course showing calcium response (monitored by RCaMP) to MEK inhibitor, PD98059 (20 μM) following TEA stimulation (n=6). E. Representative time courses of calcium (grey, monitored by RCaMP) and ERK activity (black, monitored by $EKAR_{cyto}$) in response to TEA (n=31). F. Representative time courses of ERK activity in response to TEA in the presence of calcium (grey) and in the absence of calcium (black, n=3). Norm. Em. Ratio, Normalized Emission Ratio; Norm. Intensity, Normalized Intensity.

Expectedly, we observed intracellular calcium oscillations in 67 % of the cells (n = 55) using the calcium indicator Fura2-AM (Figure 3.1A). Pre-treatment of the cells with the epidermal growth factor (EGF), a known agonist of the ERK signaling cascade in MIN6 cells (*128*), failed to elicit any significant changes in dynamics of the calcium response

(Figure 3.1B) with calcium oscillations being observed in 58 % of the cells (n = 26). Surprisingly, however, inhibition of ERK signaling pathway achieved through the inhibitor, U0126 (*129*) disrupted the TEA-mediated oscillatory calcium signal (Figure 3.1C) in 83 % of the oscillating cells (n=35). Similarly, inhibition of the ERK pathway through another inhibitor, PD98059 (*130*) also resulted in disruption of calcium signals (Figure 3.1D**)** in all the cells that exhibited oscillations (n=6), as monitored by the red-fluorescent protein based calcium biosensor, RCaMP (*131*). This suggested a complex control mechanism of calcium by ERK; ERK is necessary for maintaining the TEA-mediated calcium oscillations but ERK activation alone is not sufficient to perturb calcium dynamics.

We then tested if the converse was true, i.e. if modulation of the calcium signal affects ERK activity. Particularly, given the rich dynamical nature of the calcium signal and the ability of ERK itself to exhibit varied temporal dynamics (*26, 58, 90, 132*), we wondered if ERK decodes the calcium oscillations and/or displays dynamical signaling behavior in MIN6 cells. Population level techniques such as immunoblotting can mask dynamical changes. We therefore employed the FRET-based biosensor, ERK Activity Reporter ($EKAR_{cyto}$) to track ERK activity dynamics in real-time in the cytosol of living cells (*20*). Significantly, this technique also enabled us to monitor both the calcium and ERK activity signals in the same cell and therefore directly correlate the two patterns in each cell. We achieved this through the use of the red-shifted calcium indicator, RCaMP (*131*) so as to ensure spectral separation from the cyan and yellow fluorescence of the $EKAR_{cyto}$ reporter.

Upon stimulation of beta-cells with TEA, ERK activity as monitored by $EKAR_{cyto}$ increased concomitantly with an increase in intracellular calcium (Figure 3.1E). Significantly, we observed that an overwhelming majority of the cells (90 %, n= 31) displayed sustained ERK activity response while the calcium levels in the same cells were found to be oscillatory. This is in stark contrast to the behavior of another kinase, PKA which consistently displays activity oscillations in response to the same oscillatory calcium signal (see Chapter 3). Interestingly, a minor fraction of the cells (16 %, n = 31) displayed small ERK activity oscillations overlaid on the sustained response (Figure 3.1E) suggesting that ERK activity dynamics is linked to calcium dynamics. Therefore, we tested if ERK activity increase is mediated by calcium increase. Accordingly, we stimulated the cells with TEA in low extracellular calcium conditions. This condition markedly diminished the ERK response in all the cells (n = 3, Figure 3.1F), suggesting that TEA-dependent increase in ERK activity is indeed mediated by an increase in intracellular calcium levels. Therefore, membrane-depolarization of MIN6 cells appears to setup a calcium-ERK feedback circuit. Such non-linear interactions can enrich signaling diversity through complex temporal and spatial dynamics. We therefore set out to dissect the mechanisms of calcium-ERK signaling crosstalk and investigate how ERK decodes calcium oscillations in beta-cells.

3.2.2 Mechanisms of depolarization-induced ERK activation

ERK is typically activated by a signaling cascade involving the small GTPase, Ras and the kinases Raf and MEK (*117*). To test if ERK activation in MIN6 cells is mediated by this cascade, we monitored ERK activity in cells expressing $EKAR_{cyto}$ and the dominant negative Ras mutant, HRasN17 (*133*). We observed markedly diminished ERK activity in

these cells (n=9) compared to control cells, in response to TEA confirming the role of Ras in depolarization-dependent ERK activation (Figure 3.2A). We then investigated if Ras itself is activated in response to intracellular calcium increase using the FRET-based biosensor, Raichu-EV-Ras (*134*) and RCaMP simultaneously. Interestingly, stimulation of cells with TEA resulted in calcium oscillations but an integrated Ras activity response (Figure 3.2B) in all the cells (n=5). On the other hand, cells incubated in low extracellular calcium did not elicit calcium or Ras activity increase in response to TEA (n = 16, Figure 3.2C) confirming that depolarization-mediated Ras activity increase is mediated by calcium.

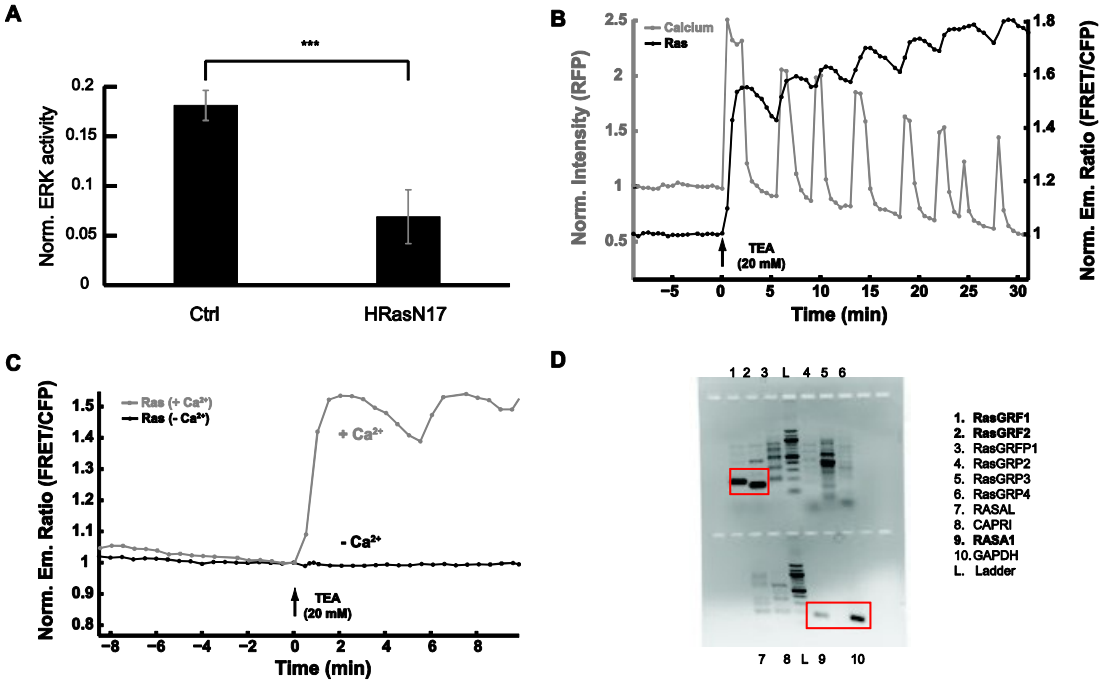

*Figure 3.2: Role of Ras in calcium-dependent ERK activation in MIN6 cells. A. Effect of Ras inhibition on ERK activity B. Representative time courses of calcium (gray, monitored by RCaMP) and Ras activity (black, monitored by Raichu-Ras) in response to TEA (n=5). C. Representative time courses of Ras activity in presence (black) or absence (gray) of calcium (n=16). D. Calcium-sensitive RasGEFs and RasGAPs in MIN6 cells. Norm. Em. Ratio, Normalized Emission Ratio; Norm. Intensity, Normalized Intensity. ***, P<0.005.*

One way by which calcium-mediated Ras activation and hence ERK activation could be achieved is through calcium-sensitive Ras Guanine Exchange Factors (cs-RasGEFs) and Ras GTPase Activating Proteins (cs-RasGAPs) which have been previously demonstrated to process calcium signals to activate Ras in HeLa cells (*135, 136*). We therefore probed for the expression of different cs-RasGEFs and cs-RasGAPs in MIN6 cells. We discovered that the cs-RasGEFs, RasGRF1 and RasGRF2, and the cs-RasGAP, RASA1 are expressed in MIN6 pancreatic beta-cells (Figure 3.2D).

RasGRF1 has been previously implicated in glucose intolerance and hypoinsulinemia (*137*). RasGRF2 which is homologous to RasGRF1 is an important player in the processing of calcium signals through the Ras/ERK signaling cascade in the context of long-term potentiation in the brain (*138*). We suspected that RasGRF2 may similarly be crucial to the ERK cascade mediated decoding of calcium signals in beta-cells. Therefore, we investigated the role of RasGRF2 by overexpressing a "Ras-dead" mutant of RasGRF2 (R1092A) which prevents Ras activation (*139, 140*) and subsequently measured ERK responses in these cells. Cells expressing the mutant RasGRF2 exhibited significantly decreased ERK activity in response to TEA as compared to control cells expressing wild type RasGRF2 (Figure 3.3A) indicating that RasGRF2 is indeed necessary for calcium-dependent ERK activation.

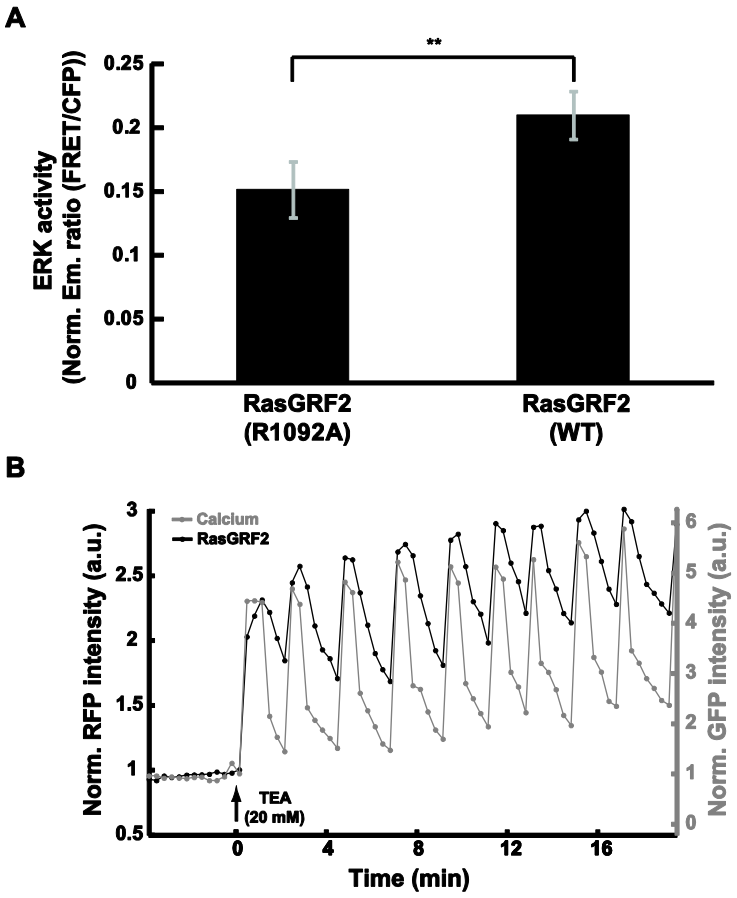

*Figure 3.3: Role of RasGRF2 in ERK activation in MIN6 cells. A. ERK activity in cells expressing the RasGRF2-R1092A mutant (n=9) compared to cells expressing wildtype (WT) RasGRF2 (n=6). B. Representative time courses of RasGRF2 activation (black, monitored by RasGRF2-mCherry) and calcium (grey, monitored by GCaMP-Kras) in response to TEA (n=7). Norm. Em. Ratio, Normalized Emission Ratio. **, P<0.05.*

Having established that calcium-dependent ERK activation is mediated by RasGRF2, we wondered if the latter is also activated in response to calcium increase. Again, we turned to live-cell imaging to answer this question. Ras-GRF2 has been shown to translocate to the membrane upon activation (*141*). Hence its activation can be easily and elegantly tracked by tagging RasGRF2 with a fluorescent protein and monitoring fluorescence intensity changes in the plasma membrane. We therefore simultaneously monitored RasGRF2 activation (using a RasGRF2-mCherry fusion construct) and

concomitant calcium changes (through the plasma membrane-specific green calcium indicator, GCaMP-Kras (*142*)) in TIRF mode. Expectedly, TEA stimulation resulted in calcium oscillations reflected by the changes in green intensity (Figure 3.3B). Strikingly however, we also observed concomitant oscillatory changes in the red fluorescent intensity in majority of the cells (86 %, n=7), likely driven by periodic translocation of the RasGRF2-mCherry molecules from the cytosol to the plasma membrane. This is in stark contrast to the activity profiles of the downstream molecules, Ras and ERK (Figure 3.1E and Figure 3.2B) suggesting a sequential processing of the input calcium signal in this signaling cascade. We therefore set out to investigate how the ERK cascade processes the calcium signal.

3.2.3 Decoding of oscillatory calcium signals by ERK pathway

Oscillations can be simply construed as a series of pulses. Understanding what happens in response to a simple pulse signal can therefore enable us to better comprehend how the ERK cascade processes a more complex oscillatory signal. Therefore, we subjected the cells to a pulse signal of depolarization using potassium chloride (KCl) and monitored the input signal (calcium) and the output signals at different steps in the ERK signaling cascade (RasGRF2, Ras and ERK) (Figure 3.4A-C). Expectedly, calcium levels rapidly rose upon application of KCl and rapidly decreased upon washing out of the stimulus. The red fluorescence intensity corresponding to the mCherry tagged to RasGRF2 also increased and decreased in tandem with calcium, detected by GCaMP-Kras (Figure 3.4A). This indicated that the Ras-GRF2 activation is reversible and that the deactivation

rates of calcium and RasGRF2 are closely matched. In contrast, the deactivation kinetics of Ras and ERK were considerably slower than calcium and RasGRF2 (Figure 3.4B-D).

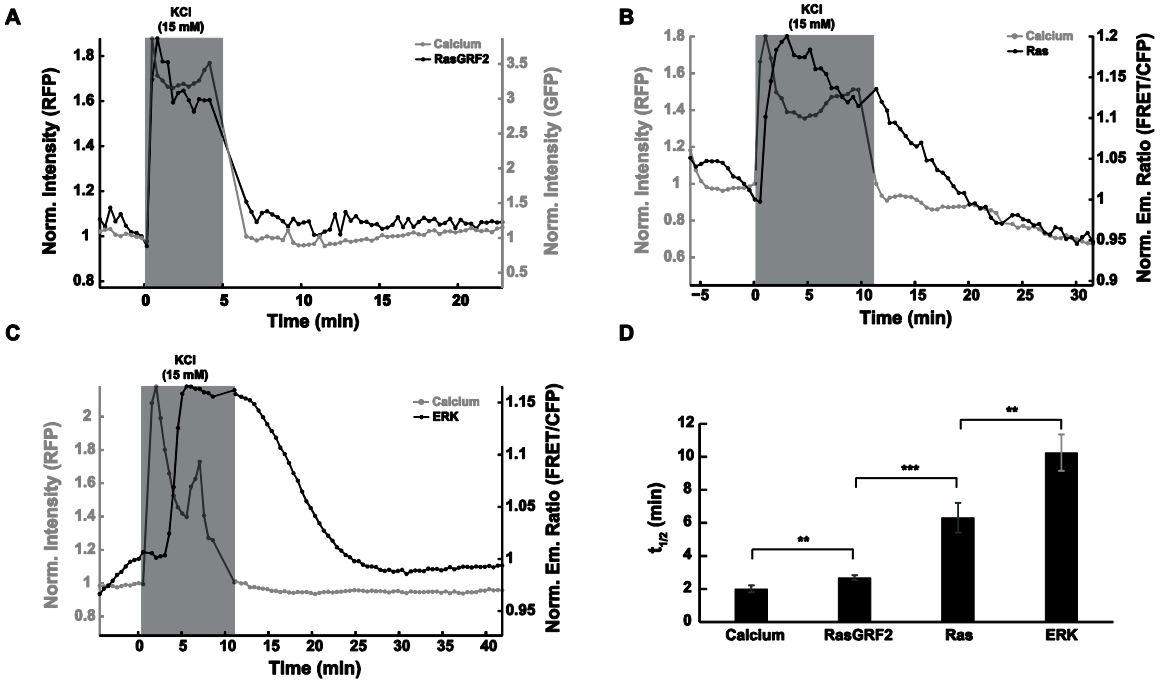

*Figure 3.4: Kinetics of different components of the ERK signaling cascade. A. Representative time course of RasGRF2 (black, monitored by RasGRF2-mCherry) and calcium (grey, monitored by GCaMP-Kras) to pulse of KCl stimulation (n=19). B. Representative time course of Ras (black, monitored by Raichu-Ras) and calcium (grey, monitored by RCaMP) to pulse of KCl stimulation (n=8). C. Representative time course of ERK activity (black, monitored by EKAR$_{cyto}$) and calcium (grey, monitored by RCaMP) to pulse of KCl stimulation (n=8). D. Deactivation kinetics ($t_{1/2}$ (min)) of calcium, RasGRF2, Ras and ERK. **, P<0.05. ***, P<0.005.*

Further, we confirmed that this is not an artifact of the biosensor. The deactivation kinetics of ERK can in fact be accelerated when the upstream kinase of ERK, MEK is inhibited in combination with the KCl washout (Figure 3.5). We hypothesized that the slow deactivation kinetics of ERK is responsible for the integration of the oscillatory calcium signal. Furthermore, the gradual change in the deactivation kinetics at different steps of the cascade suggests a sequential and gradual processing of the calcium signal. We set out to

test the hypothesis that the mismatch in deactivation kinetics of input and output signaling modules causes the integration of oscillatory input signals.

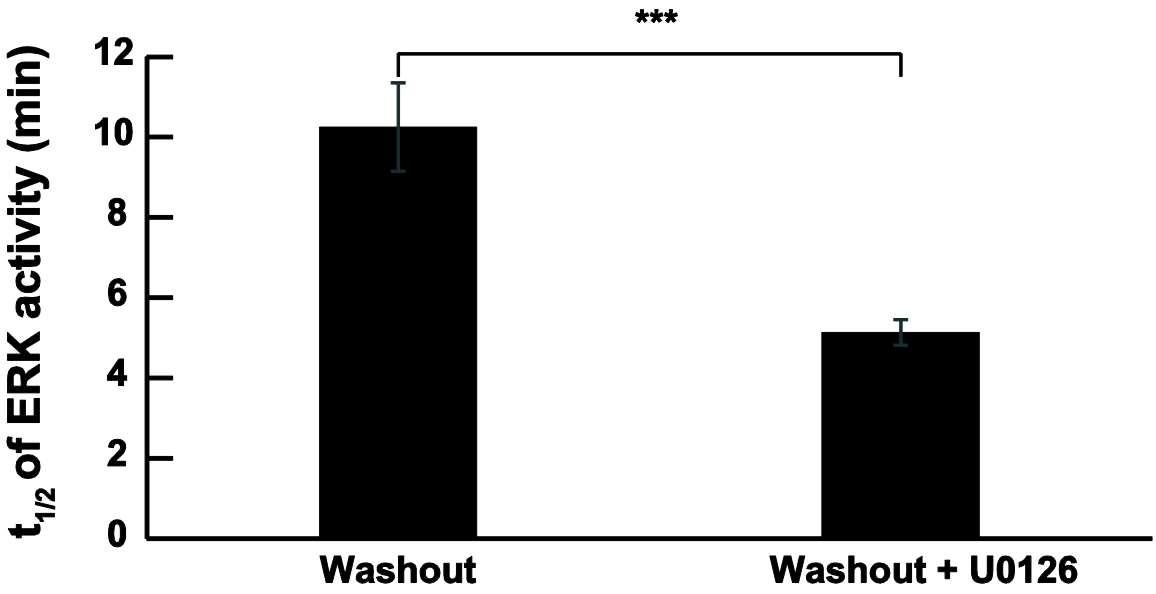

*Figure 3.5: Accelerated deactivation of EKAR through combined washout and MEK inhibition. Deactivation kinetics of ERK activity in response to washout of KCl (n=8) compared to combination of washout and MEK inhibition through U0126 (n=19). **, P<0.05*

First, we quantified the apparent activation and deactivation kinetic parameters of the signaling cascade by measuring the maximal steady state ERK response at different doses of external calcium (Figure 3.6A). We then built a representative mathematical model of this signaling cascade incorporating the estimated parameters (See methods for details). The model was then validated by simulating the system with a series of calcium pulses with temporal features similar to those experimentally observed in response to TEA stimulation. As expected, integrated ERK activity increase was observed in accordance with our experimental observations (Figure 3.6B).

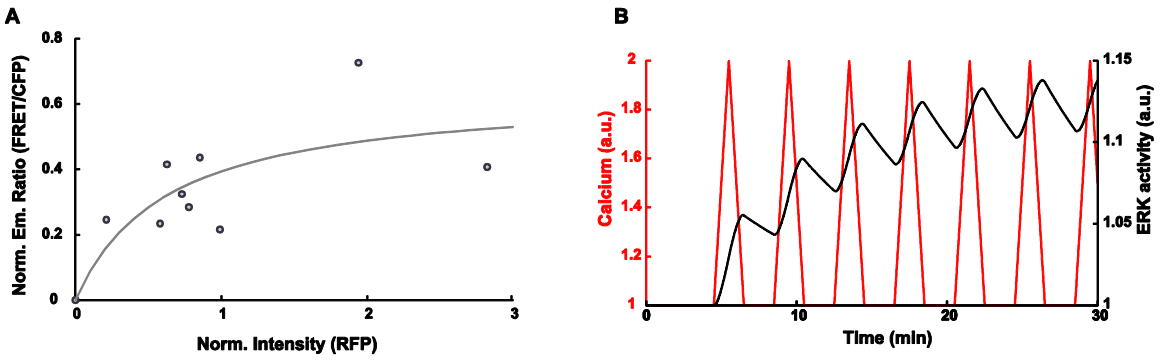

Figure 3.6: Calcium-ERK model development. A. Dose response of ERK activity increase (measured by EKAR$_{cyto}$) in response to calcium increase (measured by RCaMP). B. Simulation of model in response to oscillatory membrane depolarization.

A clear advantage of a computational model is the ability to rapidly and inexpensively test hypotheses. Processing of the signals due to mismatches in deactivation kinetics implies a clear frequency-dependent effect. Under high frequency conditions, the output signal would be expected to integrate the input oscillatory signal. However when presented with a low frequency stimulus, i.e. given sufficient time between successive pulses of stimuli, the output ERK activity decrease following the first pulse may be able to reach its basal level before responding to the next pulse resulting in oscillatory instead of integrated ERK activity patterns. We used the model to test this hypothesis by running simulations of ERK activation at different frequencies of input stimuli. ERK activity was found to integrate (Figure 3.7A) at high frequency (1.67 milliHz) of input signal but oscillatory (Figure 3.7B) when the input signal frequency was low. Experimental validation confirmed that the ERK system discerns frequency-dependent information (Figure 3.7C-D) exhibiting different temporal dynamics at different frequencies.

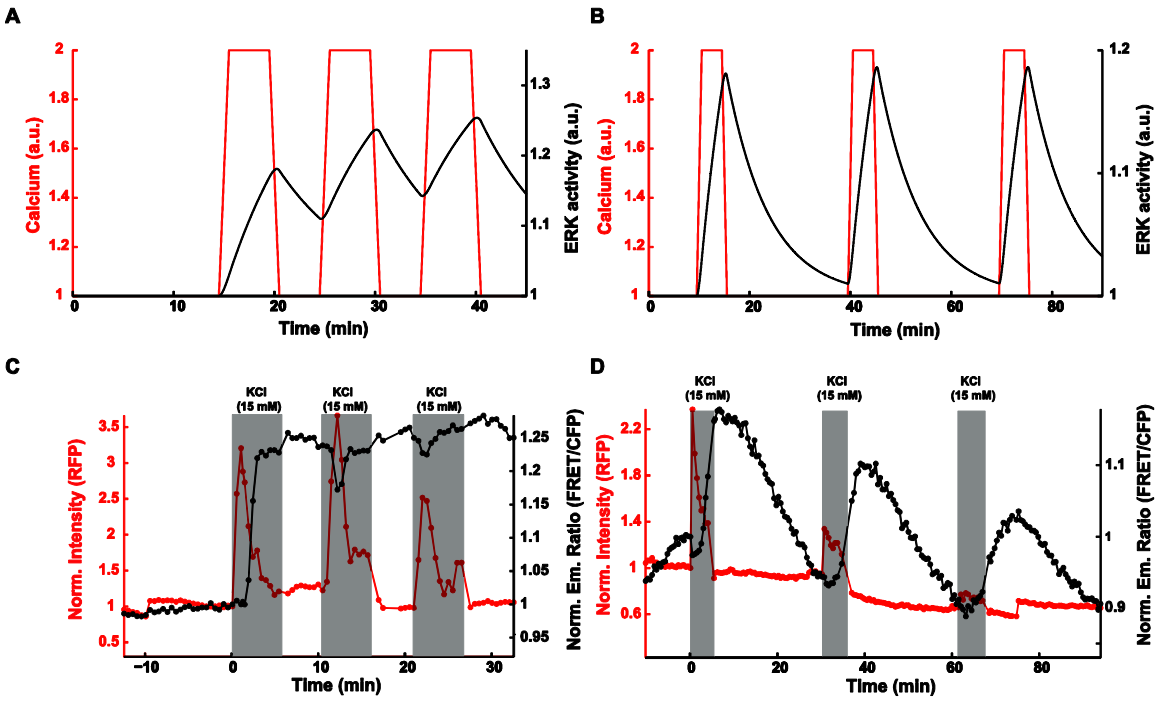

Figure 3.7: Frequency-dependence of temporal ERK activity dynamics. A. Model simulation of ERK activity (black) in response to high frequency calcium oscillations (red). B. Model simulation of ERK activity (black) in response to low frequency calcium oscillations (red). C. Representative time course of ERK activity (black, monitored by EKAR$_{cyto}$) of high frequency calcium oscillations (red, monitored by RCaMP) evoked by pulses of KCl stimulation (shaded in grey) (n=7). D. Representative time course of ERK activity (black, monitored by EKAR$_{cyto}$) of low frequency calcium oscillations (red, monitored by RCaMP) evoked by pulses of KCl stimulation (shaded in grey) (n=9). Norm. Em. Ratio, Normalized Emission Ratio; Norm. Intensity, Normalized Intensity.

Increasing the frequency of calcium oscillations to a value higher than the physiological frequency through inhibition of phosphodiesterases (*77*) did not change the ERK activity levels suggesting that ERK is maximally activated at the physiological frequency (Figure 3.8). Therefore, the ERK signaling cascade in MIN6 cells appears to act as a 'low-pass filter' for processing the input signal, similar to homologous pathways in worms (*143*) and NIH 3T3 cells (*144*). Furthermore, the filtering of high frequency signals enables ERK to be robustly activated at the physiological frequency. We then investigated

how upstream components of the cascade process the oscillatory calcium signals given their widely different deactivation kinetic parameters.

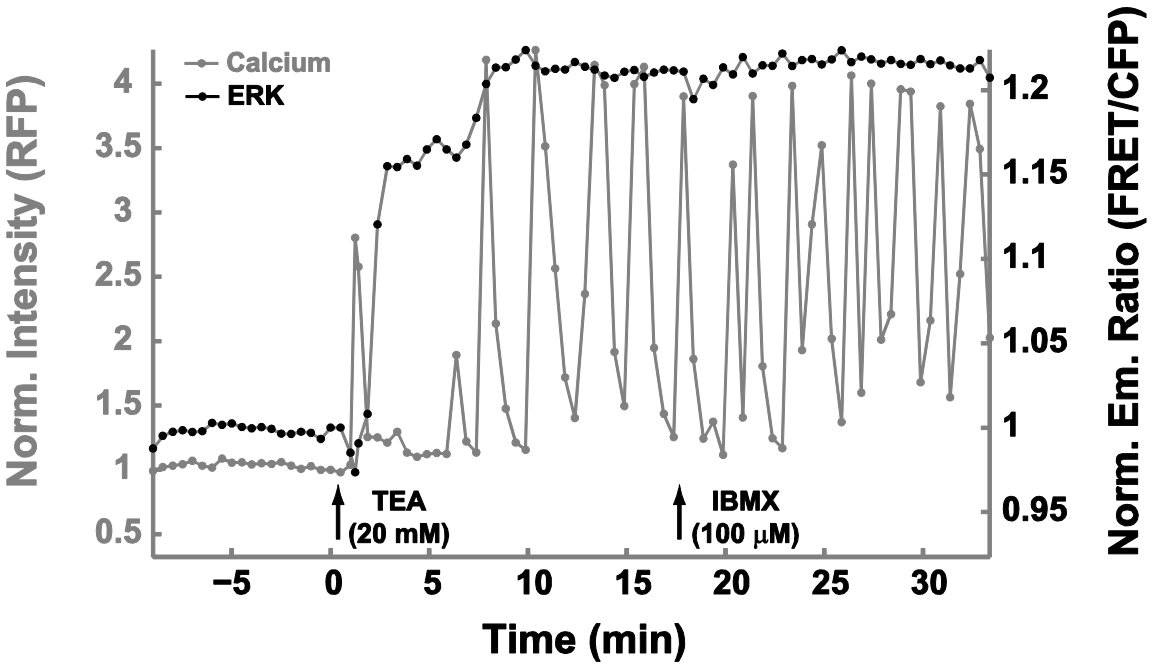

Figure 3.8: Effect of high frequency calcium oscillations on ERK activity dynamics. Representative time course of ERK activity (black, monitored by $EKAR_{cyto}$) and calcium (grey, monitored by RCaMP) in response to PDE inhibition through IBMX (n=6).

As in the case of ERK, we observed oscillatory Ras activity at low input frequencies but integrated Ras activity at high frequencies (Figure 3.9A-B). In contrast, RasGRF2 which has faster deactivation kinetics compared to Ras and ERK (Figure 3.4D) was found to be oscillatory in the range of frequencies that we tested (Figure 3.9C-D), confirming that the deactivation kinetics is critical in the processing of the oscillatory calcium signals in the ERK cascade. Significantly, the gradual increase in kinetics and the resultant gradual processing of the calcium signals at each step in the cascade suggested to us that the capacity to filter out high frequency signals will also differ at different levels of the cascade. To quantitatively test this hypothesis, we measured the "Gain," defined as the ratio of

amplitudes of output to input signals at each step of the cascade. Accordingly, when the output module faithfully reproduces an input oscillatory signal, the system has a high gain. In contrast, a low gain scenario indicates processing of an oscillatory signal to a sustained output.

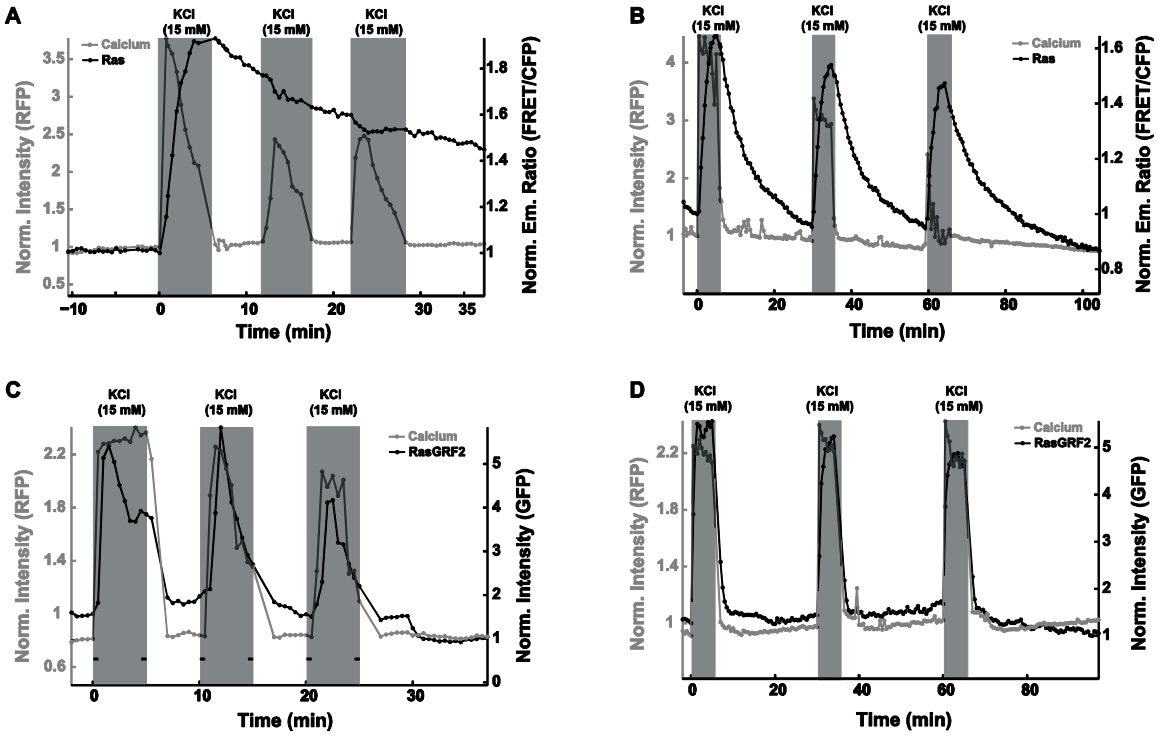

Figure 3.9: Frequency-dependence of Ras and RasGRF2 temporal dynamics. A. Representative time course of Ras activity (black, monitored by Raichu-Ras) of high frequency calcium oscillations (red, monitored by RCaMP) evoked by pulses of KCl stimulation (shaded in grey) (n=5). B. Representative time course of ERK activity (black, monitored by Raichu-Ras) of low frequency calcium oscillations (red, monitored by RCaMP) evoked by pulses of KCl stimulation (shaded in grey) (n=6). C. Representative time course of RasGRF2 activation (black, monitored by RasGRF2-mCherry) of high frequency calcium oscillations (red, monitored by GCaMP-Kras) evoked by pulses of KCl stimulation (shaded in grey) (n=6). D. Representative time course of Ras activation (black, monitored by RasGRF2-mCherry) of low frequency calcium oscillations (red, monitored by RCaMP) evoked by pulses of KCl stimulation (shaded in grey) (n=6). Norm. Em. Ratio, Normalized Emission Ratio; Norm. Intensity, Normalized Intensity.

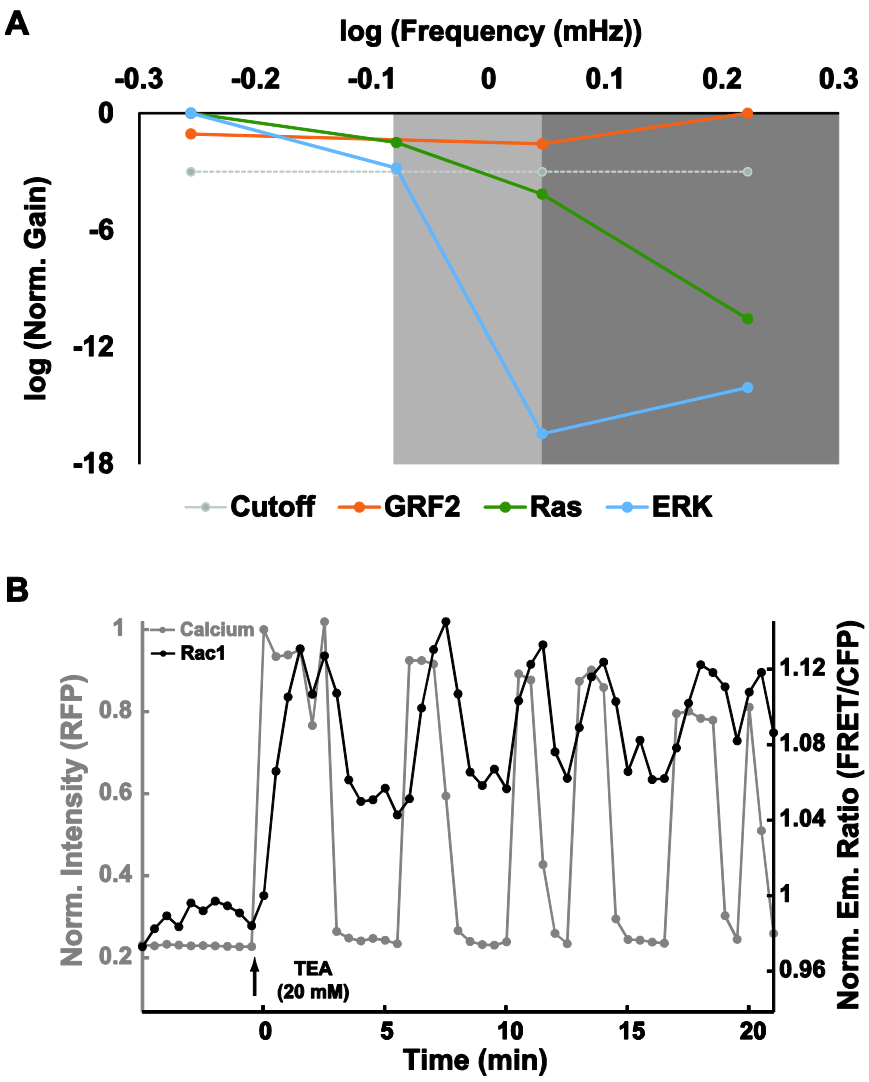

Figure 3.10: Sequential filtering of calcium signals. A. Change in gain as a function of frequency at different steps of the cascade, RasGRF2 (orange), Ras (green) and ERK (cyan) and the sequential filtering of high frequency signals represented by grey shaded areas, determined by an arbitrary threshold (grey, dashed). B. Representative time course of Rac1 activity response (black, monitored by Raichu-Rac1) and calcium oscillations (grey, monitored by RCaMP) in response to TEA (n=10). Norm. Em. Ratio, Normalized Emission Ratio; Norm. Intensity, Normalized Intensity.

In response to different frequencies of stimulation, ranging from 0.55 milliHz to 1.67 milliHz, RasGRF2 was found to have a consistently high gain thanks to its ability to faithfully reproduce the calcium oscillations (Figure 3.10A). On the other hand, the effector of RasGRF2, Ras which has slower deactivation kinetics compared to RasGRF2 exhibits

high gain at low frequencies but gradually filters out high frequency signals resulting in low gain at high frequencies. Strikingly, ERK, which has slower deactivation kinetics has a much stronger filtering capacity. As a result of this filtering process, ERK is activated in a robust manner. However, at the same time, the gradual filtering of high frequency signals through the cascade could still endow the signaling pathway with the ability to use the dynamical information, especially at the level of upstream signaling components of the cascade through activation of other signaling molecules. For instance, RasGRF2 is an activator of not only Ras but also another small GTPase, Rac1 which regulates insulin secretion through actin remodeling (*145*). We therefore set out to monitor the signaling dynamics of Rac1 activity changes in response to membrane depolarization, using the FRET-based biosensor, Raichu-Rac1. In response to TEA stimulation, we observed that Rac1 activity oscillates in tandem with calcium (Figure 3.10B) in a majority of the cells (60%, n=10) indicating that the dynamical information at the level of RasGRF2 is still retained in the Rac1 branch while the same signal is processed to produce a robust and sustained ERK response.

3.3 Discussion

In this study, we investigated how ERK interfaces with calcium in pancreatic beta-cells. Calcium and ERK regulate each other in a complex fashion. ERK is necessary but not sufficient for maintaining the oscillatory nature of calcium in response to glucose-mimicking agents like TEA. The mechanisms by which ERK may modulate calcium are not clear. Previously, we showed that PKA is also necessary for maintaining calcium oscillations (*77*). PKA is activated by cAMP which in turn is degraded by

phosphodiesterases. One such phosphodiesterase, PDE4 is known to be inhibited by ERK (*146*). Therefore, ERK may positively regulate PKA activity. It is conceivable that inhibition of ERK attenuates PKA activity and thus modulates calcium. Future experiments aimed at identifying PDE4-ERK interactions, if any, in beta-cells will help address this question. Calcium, on the other hand, is necessary and sufficient to activate ERK in response to membrane-depolarizing agents. Calcium-dependent ERK activity increase is necessarily mediated by Ras. Ras, in turn, is likely activated through the actions of the calcium-sensitive RasGRF2 whose role in mediating calcium-dependent ERK activation has been previously documented in neurons (*138*) and fibroblasts (*147*). Here, we demonstrated for the first time that RasGRF2 mediates calcium-dependent ERK activation in pancreatic beta-cells.

The intricate calcium-ERK crosstalk in MIN6 beta-cells also provides insight into general signaling mechanisms on multiple fronts. First, the presence of a calcium-ERK feedback ensures proper calcium signaling in beta-cells. Persistent oscillations require a combination of positive and negative feedback loops (*30*). In this study, we demonstrate that the ERK-calcium positive feedback loop is necessary for sustaining these oscillations with the result that inhibition of ERK leads to disruption of the oscillations. The calcium-ERK feedback loop is therefore a crucial component of the signaling mechanisms that govern beta-cell function like insulin secretion through robust calcium oscillations.

Second, the calcium-dependent changes in the dynamics of ERK activity highlight how ERK decodes calcium signals in beta-cells. TEA-induced calcium oscillations result in sustained and thus high time-averaged ERK activity. However, lower frequency calcium

oscillations elicit oscillatory ERK activity changes with lower time-averaged ERK activity as in the case of HeLa cells (*148*) and worm neurons (*143*) suggesting that frequency-dependent decoding of calcium by ERK may be a widespread phenomenon. Characterization of the frequency response of the ERK homolog protein, Hog-1 in yeast (*149, 150*) indicated that Hog-1 acts as a band-pass filter owing to a negative feedback loop in the Hog-1 signaling cascade. In the MIN6 system, however, we observe a low-pass filter-like response for ERK in the frequency range that we tested with the result that the cascade filters out high frequency signals to produce a robust and sustained ERK activity increase in response to TEA.

Finally, the decoding of calcium signals by the ERK signaling cascade sheds light on how cells may leverage temporal dynamics to transmit information. The differences in temporal dynamics of calcium and various signaling molecules in the ERK signaling cascade result in gradual and sequential processing of the signal down the cascade. While ERK and Ras filter out high frequency signals, upstream components like RasGRF2 retain the capacity to be oscillatory in the entire frequency range that we tested. As a result, RasGRF2 can make use of this dynamical information at the same time in other contexts. Specifically, in contrast to Ras, Rac1, another target of RasGRF2 oscillates in response to TEA likely affecting actin dynamics and hence insulin secretion (*151, 152*).

3.4 Methods

3.4.1 Construction of RasGRF2-mCherry

Murine RasGRF2 clone was obtained from the Ultimate™ ORF Collection. RasGRF2 was PCR amplified, digested and cloned into a pRSETB plasmid between

BamHI and *SacI* restriction sites. The red fluorescent protein mCherry was inserted between *SacI* and *EcoRI* sites. The RasGRF2-mCherry fusion was then subcloned into pCDNA3 (Invitrogen) between *BamHI* and *EcoRI* sites.

3.4.2 Cell Culture

MIN6 cells were seeded onto sterilized glass coverslips in 35-mm dishes and grown to 50–90% confluency in DMEM (10% FBS) at 37°C with 5% CO_2. Cells were transfected using Lipofectamine 2000 (Invitrogen) and grown for 48 h after transfection before the imaging.

3.4.3 Imaging

Cells were washed twice with HBSS (Hanks' balanced salt solution) buffer and maintained in the dark at room temperature.

3.4.4 Epifluorescence Microscopy

Cells were imaged on a Zeiss Axiovert 200M microscope with a cooled charge-coupled device camera (MicroMAX BFT512, Roper Scientific, Trenton, NJ) controlled by METAFLUOR 6.2 software (Universal Imaging, Downingtown, PA). Yellow/cyan emission ratio imaging used a 420DF20 excitation filter, a 450DRLP dichroic mirror and two emission filters (475DF40 for CFP and 535DF25 for YFP) alternated by a filter-changer Lambda 10-2 (Sutter Instruments, Novato, CA). RCaMP emission was monitored using 568DF55 excitation filter, 600DRLP dichroic mirror, and 653DF95 emission filter. Exposure time was 50–500 ms, and images were taken every 15-30s. Fluorescence images were background-corrected by subtracting the fluorescence intensity of background with no cells from the emission intensities of cells expressing fluorescent reporters. The ratios of yellow/cyan emissions were then

calculated at different time points. Both Yellow/Cyan ratio and RFP intensity of all time courses were normalized by dividing each value by the average basal value before stimulant/inhibitor addition.

3.4.5 TIRF microscopy

Cells were imaged on a Nikon Ti-Eclipse inverted microscope equipped with a 70-mW air-cooled argon ion laser and a 100-mW Coherent Sapphire 561-nm laser under a 100X oil-immersion objective from the same manufacturer. Total-internal-reflection excitation was achieved using manufacturer-installed TIRF setup on home-made glass-bottom dishes. Excitation was selected using preset dual band dichroic mirrors, while the fluorescent emissions were filtered using the following preset filter: GFP/RFP (Chroma number 89002). The filtered fluorescence was imaged using a PhotoMetrics Evolve 512 × 512 electron-multiplied CCD camera at 16-bit.

3.4.6 Calcium-ERK model

Steady state ERK activity was measured in response to different doses of external calcium (0.05 mM, 0.1 mM, 0.25 mM, 0.5 mM, 1.2 mM, 2 mM). The normalized EKAR response was quantified as a function of normalized RCaMP response and fit to a function of the form:

$$y_{ss} = \frac{V_m x_{ss}}{K_m + x_{ss}}$$

where 'y_{ss}' represents normalized steady state EKAR response and 'x_{ss}' represents normalized steady state RCaMP response. In order to predict the dynamical EKAR

response to changes in calcium, represented by RCaMP, we assumed a simple 1st order ODE to describe the rate of change of ERK activity as measured by EKAR as follows:

$$\frac{dy}{dt} = \frac{V_m x}{K_m + x} - k_r y$$

The parameters V_m and K_m were estimated as detailed above. Given that the analytical solution to this equation is of the form:

$$y = y_{ss}(1 - e^{-k_r t})$$

the parameter k_r can be estimated as:

$$k_r = \frac{ln2}{\tau_{\frac{1}{2}}}$$

where $\tau_{1/2}$ is the experimentally measured half-maximal deactivation kinetics.

Differential equations representing RCaMP and EKAR changes were written in custom MATLAB scripts and solved using the ode4 solver. Pulses of width 5 minutes and time periods ranging from 10 to 30 minutes were used to simulate high and low frequency conditions respectively.

Chapter 4 Spatial dynamics of ERK signaling in pheochromocytoma PC12 cells

4.1 Introduction

The prototypical ERK signaling cascade exemplifies the intricate regulatory mechanisms employed by cells to effect different functional responses using spatiotemporal dynamics. One of the first clues pointing to the role of ERK signaling dynamics in cellular decision making were uncovered when researchers observed that sustained ERK signaling in response to nerve growth factor (NGF) stimulus results in differentiation of PC12 cells. On the other hand, an EGF stimulus evokes a transient ERK activity response resulting in proliferation (*58*). These cell fates are determined by the differential expression of certain genes, which in turn are dependent on ERK signal duration. In fact, it has been shown that sustained ERK activity following NGF stimulus can phosphorylate and stabilize the transcription factor, Fos. On the other hand, an EGF-mediated transient increase in ERK activity is insufficient to stabilize any Fos proteins that may be produced (*153*). Differential regulation of the transcription factor activity can then influence cellular fate. Although the role of temporal ERK dynamics in influencing cellular processes have been well studied, very little is known about the spatial differences in ERK activity and how that affects cell functions.

One of the key challenges in the study of spatial signaling dynamics has been the lack of convenient tools that can probe biochemical activities at various locations inside the cell. Subcellular fractionation, the standard technique for doing this is a long and

complicated procedure also requiring the lysis of cells thereby losing crucial live-cell information in the process. Here, we harnessed the power of genetically encoded FRET-based biosensors by targeting them to different locations within the cells and obtained real-time, spatiotemporal changes in ERK activity in live cells. As a result, we were able to uncover interesting spatial differences in ERK activity patterns in PC12 cells. Investigations into the mechanisms of these differences led us to discover a complex location-dependent crosstalk between the cAMP-PKA and ERK pathways. The cells appear to use such spatial differences in signaling network topology to dictate biochemical activity and thus modulate cell functions, especially those that may be associated to specific subcellular locations. In PC12 cells, the distinct spatiotemporal dynamics of plasma membrane ERK activity are crucial for influencing plasma membrane-specific functions like cellular adhesion.

4.2 Results

4.2.1 Spatial differences in ERK activity dynamics

To monitor spatial dynamics of ERK activity in PC12 cells, we used the FRET-based reporter, EKAR whose power to provide temporal information was demonstrated in Chapter 3. The genetic encodability of this reporter is a major advantage endowing the user with the power to target this reporter to specific locations within the cell and obtain crucial spatial information. Targeted reporters however can suffer from losses in dynamic range and thus significant decrease in signal to noise ratio thereby affecting the ability to confidently measure activity changes. We therefore generated and used an improved version of EKAR (dubbed EKAR2.3 here) based on the optimized sensor, EKAR-EV

developed by Matsuda and colleagues (*154*). We then fused different targeting sequences to this sensor to direct it to specific organelles, generating an arsenal of organelle-specific ERK activity reporters: EKAR2.3-PM (non-lipid raft plasma membrane), LR-EKAR2.3 (lipid rafts), EKAR2.3-Cyto (cytosol), EKAR2.3-Nuc (nucleus), Mito-EKAR2.3 (outer mitochondrial membrane) and Golgi-EKAR2.3 (golgi apparatus).

These reporters were expressed in PC12 cells. The reporters were found to localize to their expected subcellular compartments ensuring that the information obtained from the targeted EKARs is in fact location-specific (Figure 4.1). We then monitored the FRET changes from the reporters in real time in response to growth factor stimulation. Upon stimulation with the Nerve Growth Factor (NGF) which drives the differentiation of PC12 cells into neurite-like cells (*155*), we observed robust and sustained ERK activity response in all the sub-cellular compartments (Figure 4.2). In contrast, when the cells were exposed to the Epidermal Growth Factor (EGF) which causes the PC12 cells to proliferate (*156*), we observed striking differences in ERK activity at different locations (Figure 4.3). The cytosolic and nuclear responses mirrored that of the documented whole cell transient ERK activity response (*157-159*). In stark contrast, the ERK activity in non-lipid raft plasma membrane, lipid rafts and golgi apparatus was sustained while the mitochondrial ERK activity appeared to be semi-sustained.

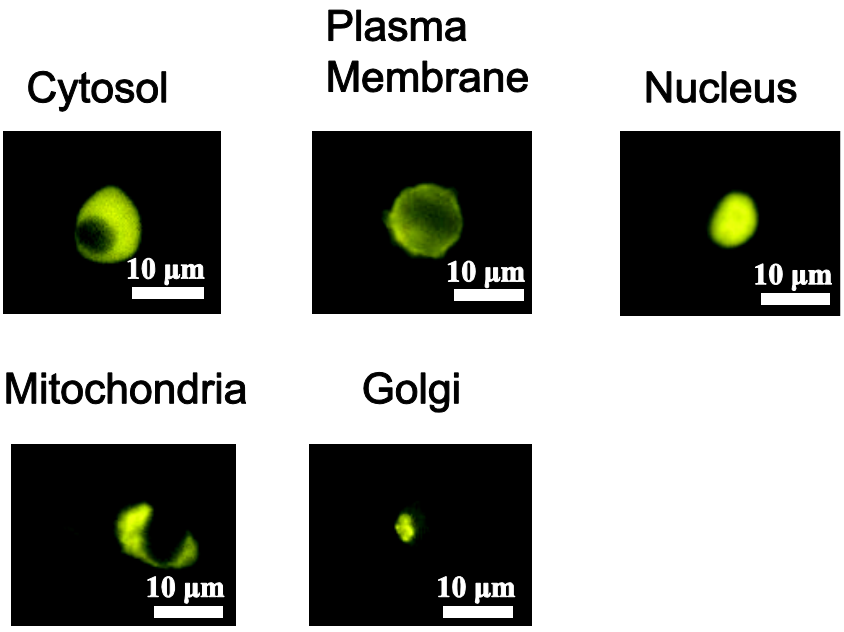

Figure 4.1: Localization patterns of targeted EKARs

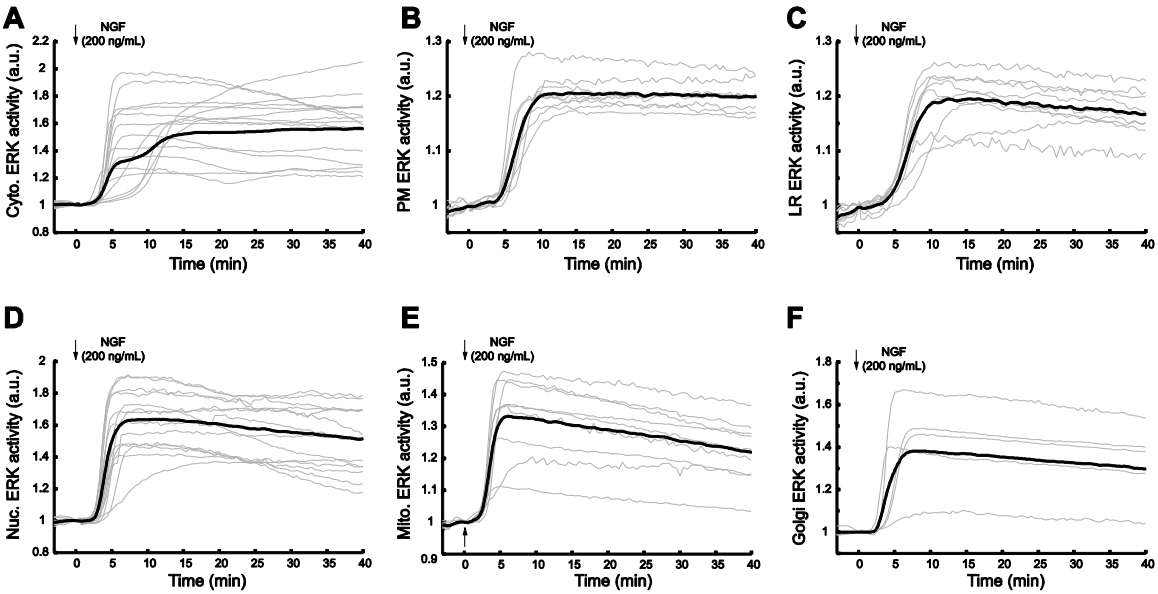

Figure 4.2: Time courses of ERK activity at different locations in response to NGF (individual responses in grey, mean in black). A. Cytosol (n=15). B. Plasma membrane (PM, n=10). C. Lipid rafts (LR, n=9). D. Nucleus (n=12). E. Mitochondria (n=9). F. Golgi apparatus (n=5).

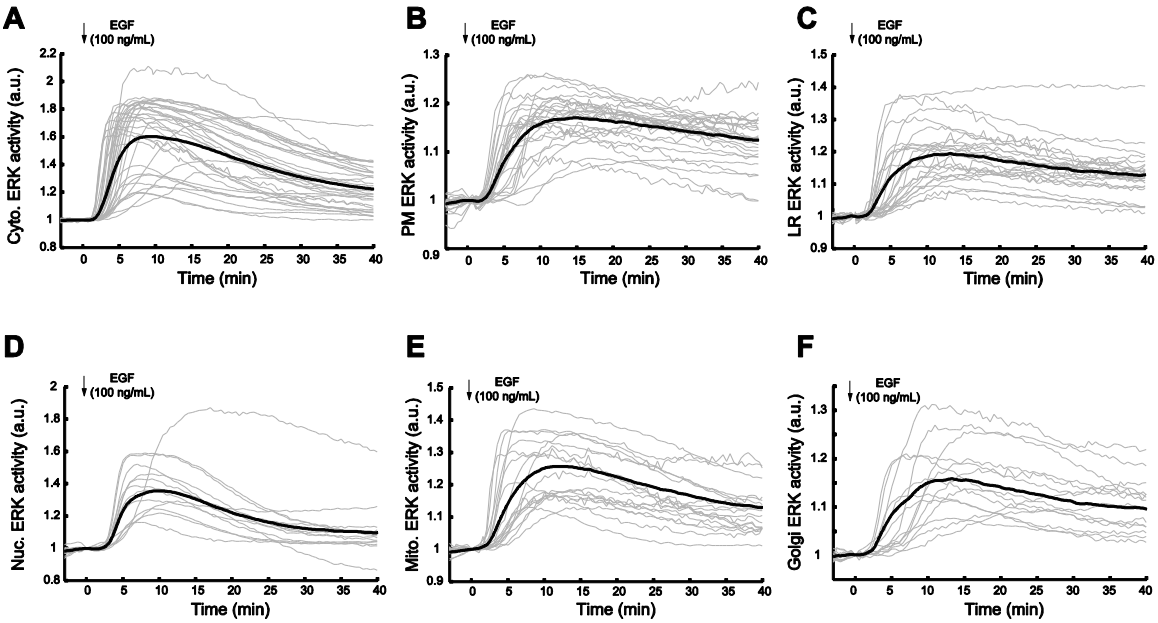

Figure 4.3: Time courses of ERK activity at different locations in response to EGF (individual responses in grey, mean in black). A. Cytosol (n=33). B. Plasma membrane (PM, n=26). C. Lipid rafts (LR, n=28) D. Nucleus (n=13). E. Mitochondria (n=18). F. Golgi apparatus (n=18).

In order to quantify these differences, we employed the Sustained Activity Metric (SAM), defined as follows:

$$SAM = \frac{R_{40} - R_0}{R_p - R_0}$$

where R_0 and R_{40} are the response amplitudes at 0 and 40 minutes respectively, and R_p is the maximum response measured between 0 and 40 minutes. The choice of 40 minutes as the window limit was based on the observation that ERK activity reaches steady state by that time. A SAM value of 1 thus indicates that the response is perfectly sustained while a SAM value of 0 corresponds to a perfectly adapted transient response. In general, comparing two responses, the one with higher SAM value is more sustained than the other. The SAM values for the different subcellular compartments in response to EGF and NGF

are shown in Figure 4.4 and Figure 4.5. Corroborating our earlier qualitative observations, the cytosolic SAM is nearly half of the plasma membrane SAM in response to EGF implying that the plasma membrane responses are much more sustained than that of the cytosol. On the other hand, in response to NGF, the SAMs were found to be consistently high in all compartments save the mitochondria with no significant difference between the plasma membrane and cytosolic ERK activity.

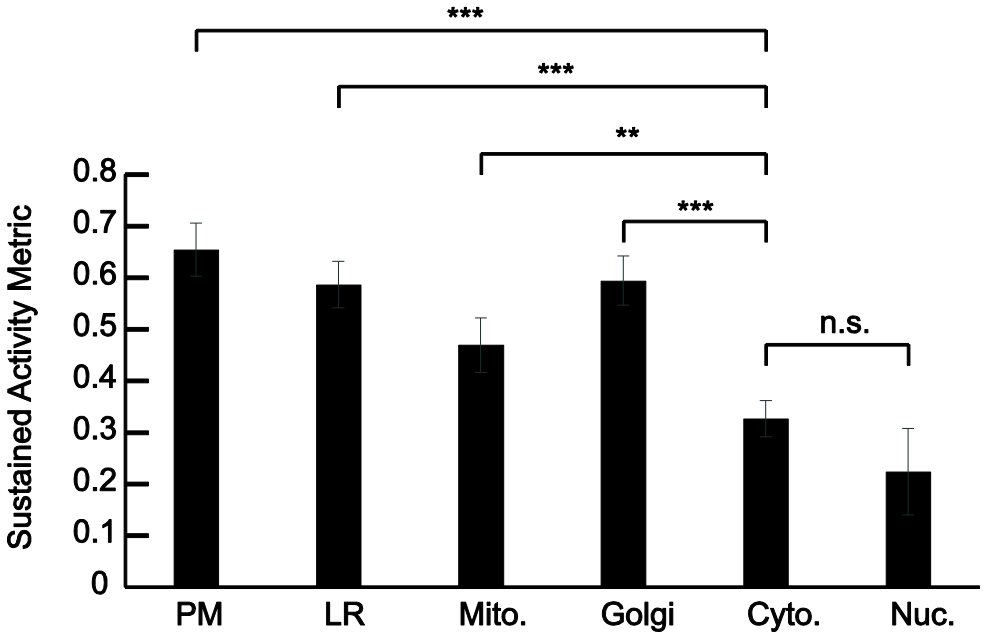

*Figure 4.4: Comparison of Sustained Activity Metric at different locations in response to EGF stimulation. PM, plasma membrane; LR, lipid rafts; Mito., mitochondria; Golgi, Golgi apparatus; Cyto., cytosol; Nuc., nucleus. ***, P<0.005. **, P<0.05. n.s. not significant*

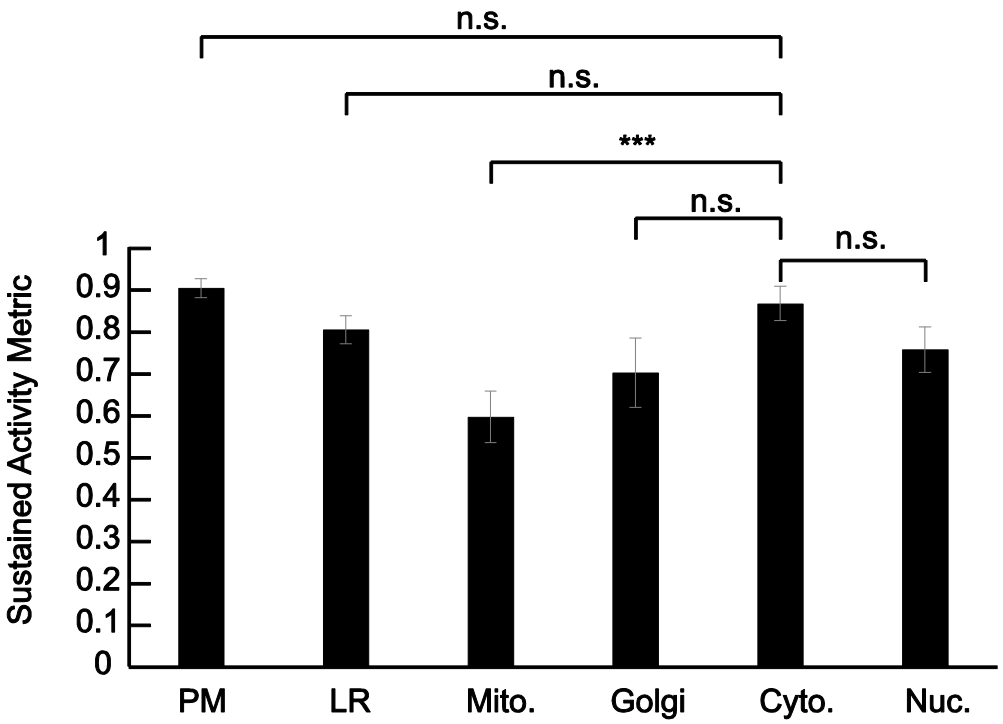

*Figure 4.5: Comparison of Sustained Activity Metric at different locations in response to NGF stimulation. PM, plasma membrane; LR, lipid rafts; Mito., mitochondria; Golgi, Golgi apparatus; Cyto., cytosol; Nuc., nucleus. ***, P<0.005. n.s. not significant*

4.2.2 Mechanisms

Having established clear and significant spatial differences in ERK activity in response to EGF, we investigated the mechanisms by which such differences may be established upon exposure to EGF. Specifically, we focused on the two 'extremes' that exemplify this pattern, namely the cytosol and the non-lipid raft plasma membrane (referred to as plasma membrane hereafter). The activity of ERK as measured by EKAR is indicative of the phosphorylation status of a typical ERK substrate. Phosphorylation of a signaling molecule is a dynamical process that is finely regulated not just by the kinase but also by the countering actions of phosphatases. It is therefore conceivable that the differences in ERK activation patterns in the plasma membrane and cytosol are the result of differences in the accessibility to phosphatases for an ERK substrate at these two

locations. In order to test this, we measured the ERK activity changes in cytosol and plasma membrane upon inhibition of the ERK signaling cascade following EGF stimulation. This exercise was motivated by the reasoning that the rate of change in ERK activity may be simply described as follows:

$$\frac{d[Sub_{active}]}{dt} = k_f[Input] - k_r[Phosphatases]$$

where [Sub_{active}] denotes the concentration of active substrate (and hence ERK activity) that is controlled by both the input kinase signaling pathway and phosphatases. Upon inhibition of the pathway, the rate of change in ERK activity reduces to just a simple function of the phosphatases. Hence, we monitored the slope (rate of change in ERK activity) in response to inhibition of the ERK pathway through U0126 after stimulation with EGF. The cytosolic slope was found to be significantly steeper than that of the plasma membrane suggesting that the phosphatases do play a role in this process (Figure 4.7).

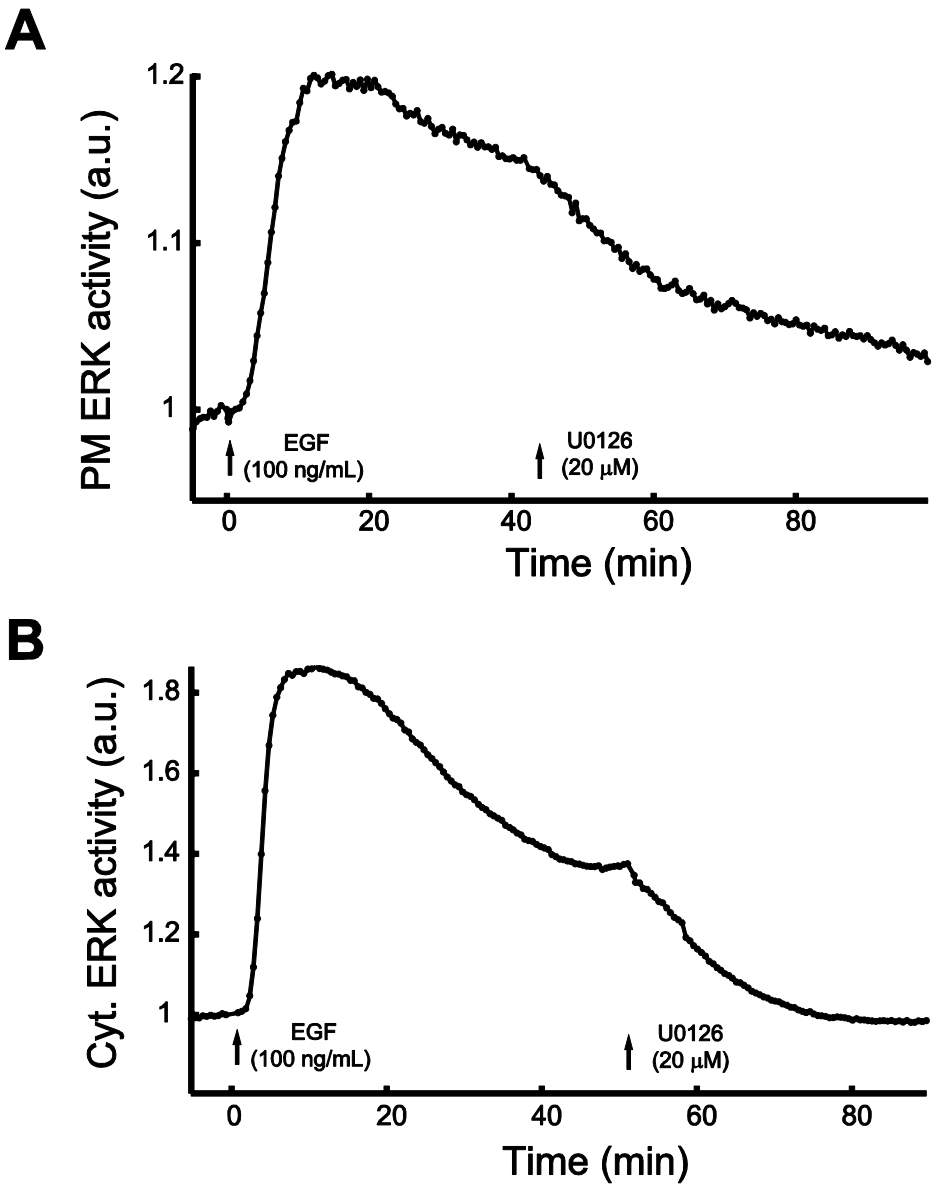

Figure 4.6: Subcellular differences in rate of change of ERK activity in response to MEK inhibition through U0126. A. Representative time course of plasma membrane ERK activity (n=17). B. Representative time course of cytosolic ERK activity (n=20).

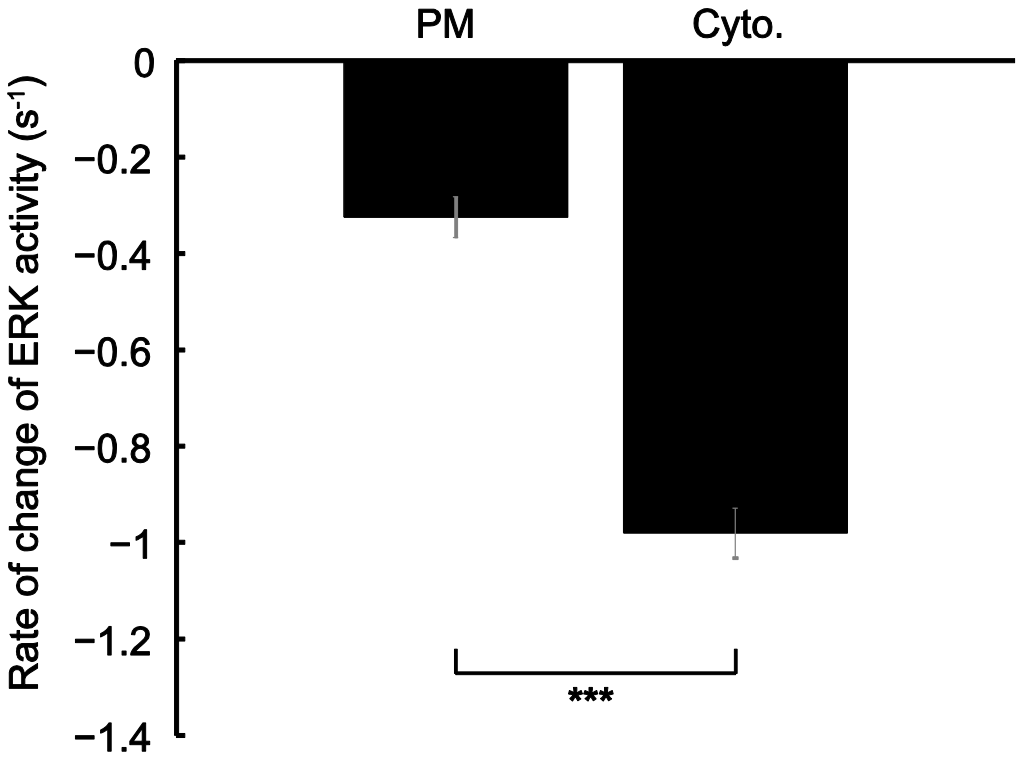

*Figure 4.7: EKAR slope measurements determine phosphatase contribution. Rate of change of EGF-mediated ERK activity following U0126 addition. PM, plasma membrane (n=17); Cyto., cytosol (n=20). ***, P<0.005.*

Spatiotemporal kinase activity dynamics is dependent not only on phosphatases but also the kinase itself. If ERK is regulated by other signaling molecules differently in different compartments, it could serve to explain these spatial differences. Previously, Herbst et al. showed that ERK is modulated by the cAMP-PKA signaling pathway (*25*). The cAMP-PKA pathway exhibits spatial dynamics affecting cellular function (*8, 22, 160*). We therefore wondered if ERK is regulated distinctly by the cAMP-PKA pathway in a location-specific manner resulting in the spatial differences of ERK activity.

We set out to investigate this hypothesis by measuring cytosolic and plasma membrane ERK activity in response to PKA inhibition. Accordingly, the cells were pre-treated with the PKA inhibitor, H89 (20 μM) for 20 minutes before stimulating with EGF.

We observed that the plasma membrane ERK response was drastically reduced indicating that PKA is necessary for regulating ERK in the plasma membrane (Figure 4.7A). The cytosolic ERK response was found to be strikingly different. PKA inhibition resulted in potentiation of ERK activity (Figure 4.8B) albeit with a slight delay in the induction of the activity indicating that the cytosolic pool of ERK is regulated by PKA in a complex fashion. We then confirmed these results by treating the cells with a peptide based inhibitor of PKA, myristoylated PKA (MyrPKI) prior to EGF stimulation. In order to quantify these results, the integrated ERK activity over 40 minutes was measured in response to PKA inhibition and control treatments (Figure 4.9). The resulting patterns indicate that the EGF-dependent spatiotemporal ERK activity dynamics appear to be modulated by compartment-specific regulation of ERK by PKA. The plasma membrane ERK activity is reduced upon treatment with MyrPKI while the cytosolic ERK activity is unaffected. The lack of significant potentiation of cytosolic ERK activity in response to MyrPKI is likely because MyrPKI may be weaker than H89 in its inhibition of PKA.

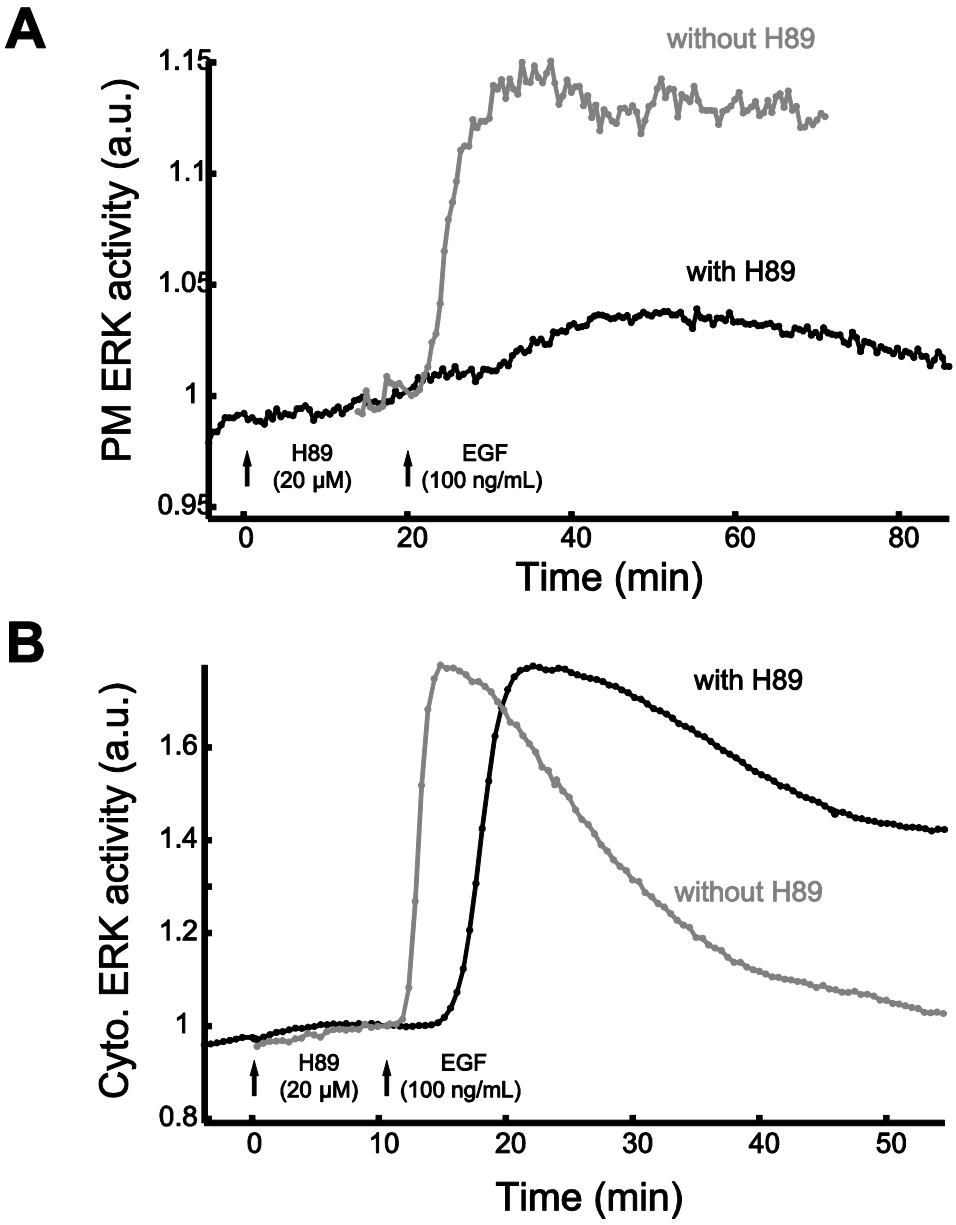

Figure 4.8: Subcellular differences in ERK activity following PKA inhibition. A. Representative time course of plasma membrane ERK activity in absence of (grey) and in response to (black) PKA inhibition (n=15). B. Representative time course of cytosolic ERK activity in absence of (grey) and in response to (black) PKA inhibition (n=14).

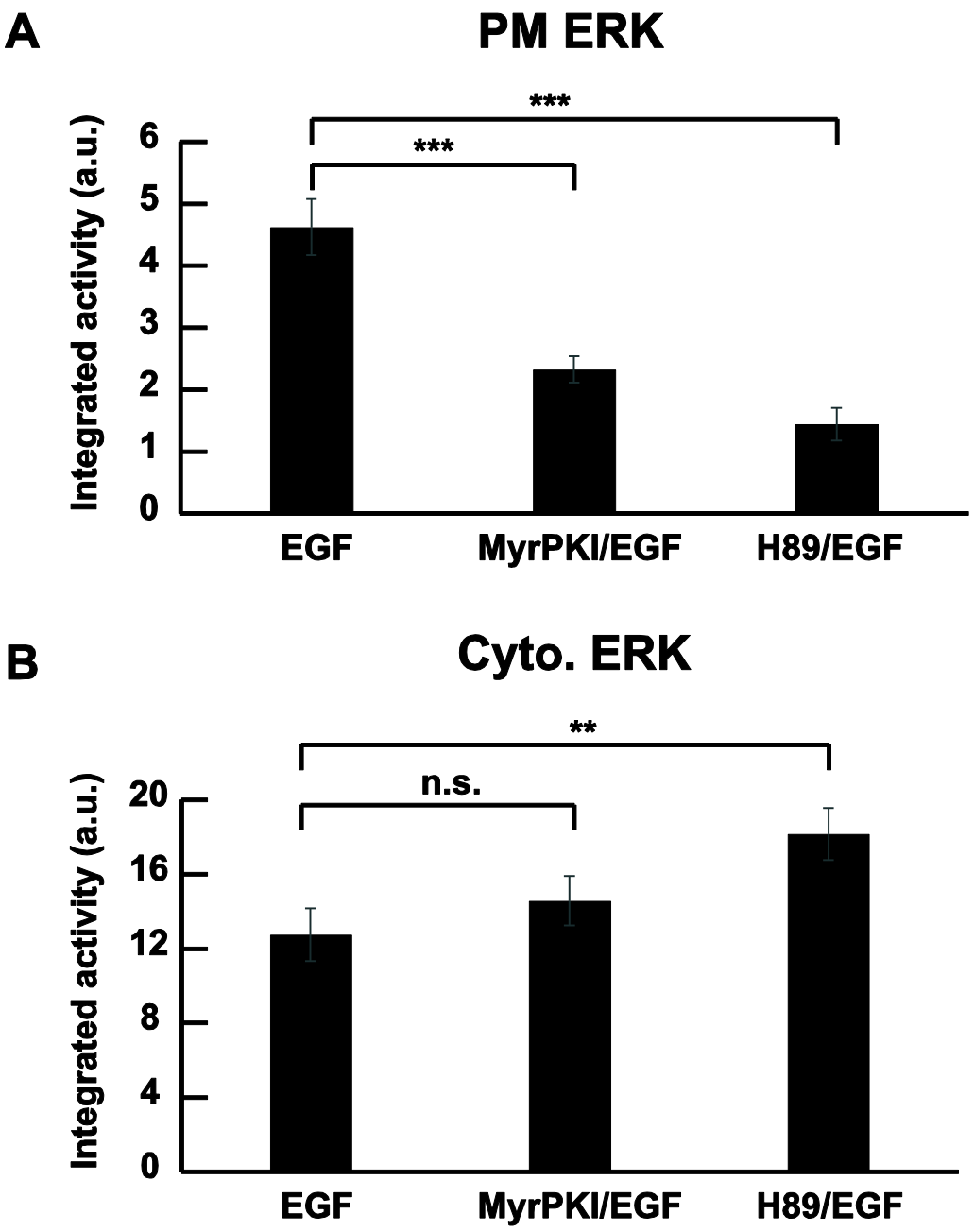

*Figure 4.9: Spatial differences in integrated ERK activity following PKA inhibition. A. Integrated plasma membrane ERK activity in response to PKA inhibition through H89 (n=15) or myristoylated PKI (MyrPKI, n=23). B. Integrated cytosolic ERK activity in response to PKA inhibition through H89 (n=14) or myristoylated PKI (MyrPKI, n=22). ***, P<0.005. **, P<0.05.*

We then set out to investigate if the EGF-dependent spatial differences in ERK activity can be modulated through elevation of PKA activity. Therefore, we exposed the cells to the generic phosphodiesterase inhibitor, IBMX which is expected to elevate the intracellular cAMP concentration and hence cause elevation of PKA activity. Contrary to expectations, we noticed decreased ERK activity in the plasma membrane and sustained activity in the cytosol in response to EGF stimulation following IBMX treatment (Figure 4.10).

Quantifying these results by integrating the ERK activity over the experimental time window of 40 minutes, we uncovered an interesting biphasic pattern of regulation of ERK by the cAMP-PKA pathway (Figure 4.11). In response to both PKA activity elevating and inhibiting agents, we observed decreased integrated ERK activity in the plasma membrane. In contrast, the integrated cytosolic ERK activity exhibited a reciprocal relationship with the plasma membrane activity. In response to both H89 and IBMX, the cytosolic ERK activity was increased compared to the control treatment with EGF alone. Therefore, in summary, the spatiotemporal differences in ERK activity are mediated by differential access to phosphatases at different locations and a complex control mechanism of the ERK signaling cascade through the cAMP-PKA signaling pathway. Having established these underlying mechanisms of spatiotemporal ERK dynamics, we investigated the functional roles of such spatiotemporal regulation. Specifically, we wondered if the potentiated ERK activity in the plasma membrane may be necessary for modulating cellular functions specific to the plasma membrane.

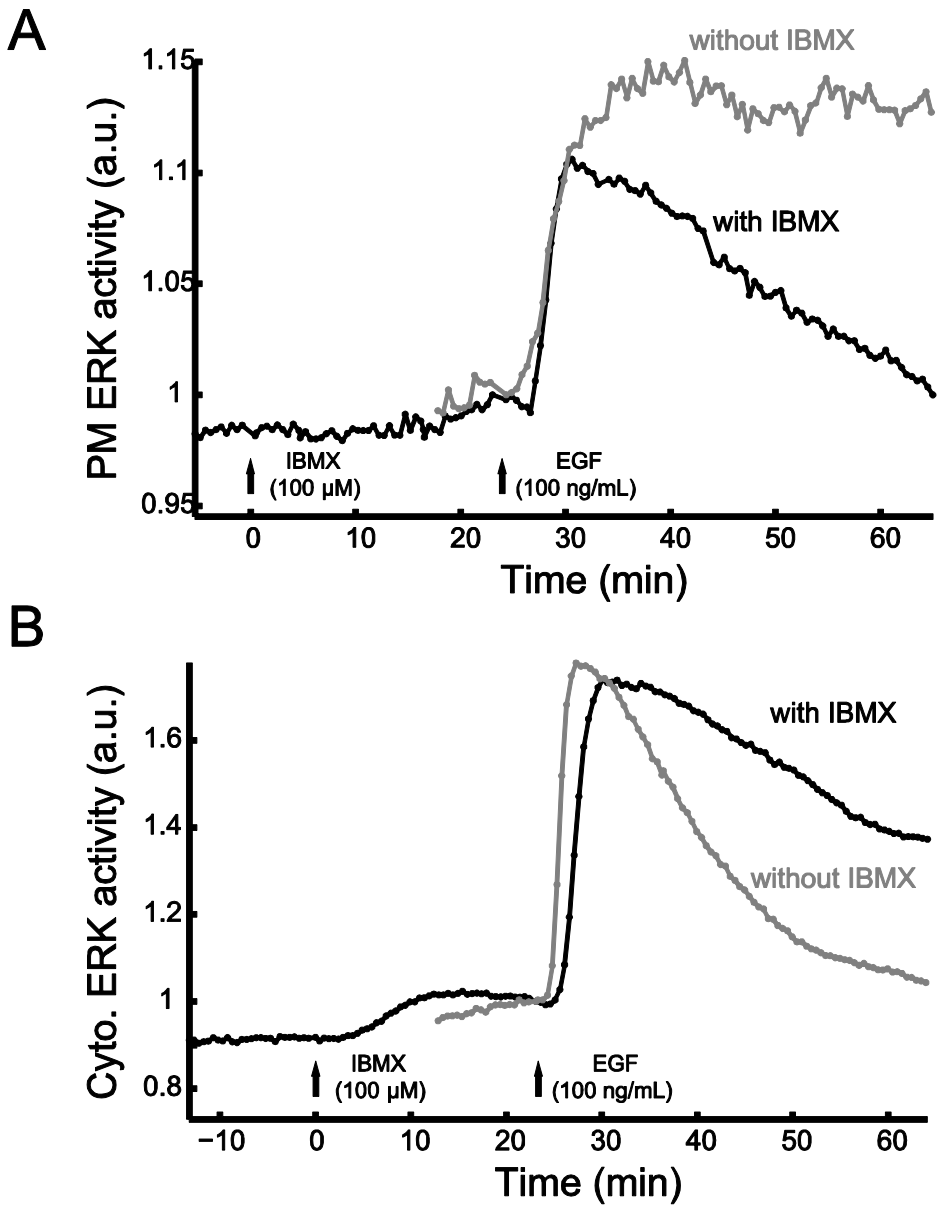

Figure 4.10: Subcellular differences in ERK activity mediated by activation of cAMP-PKA pathway. A. Representative time course of plasma membrane ERK activity in absence of (grey) and in response to (black) PDE inhibition through IBMX (n=12). B. Representative time course of cytosolic ERK activity in absence of (grey) and in response to (black) PDE inhibition through IBMX (n=16).

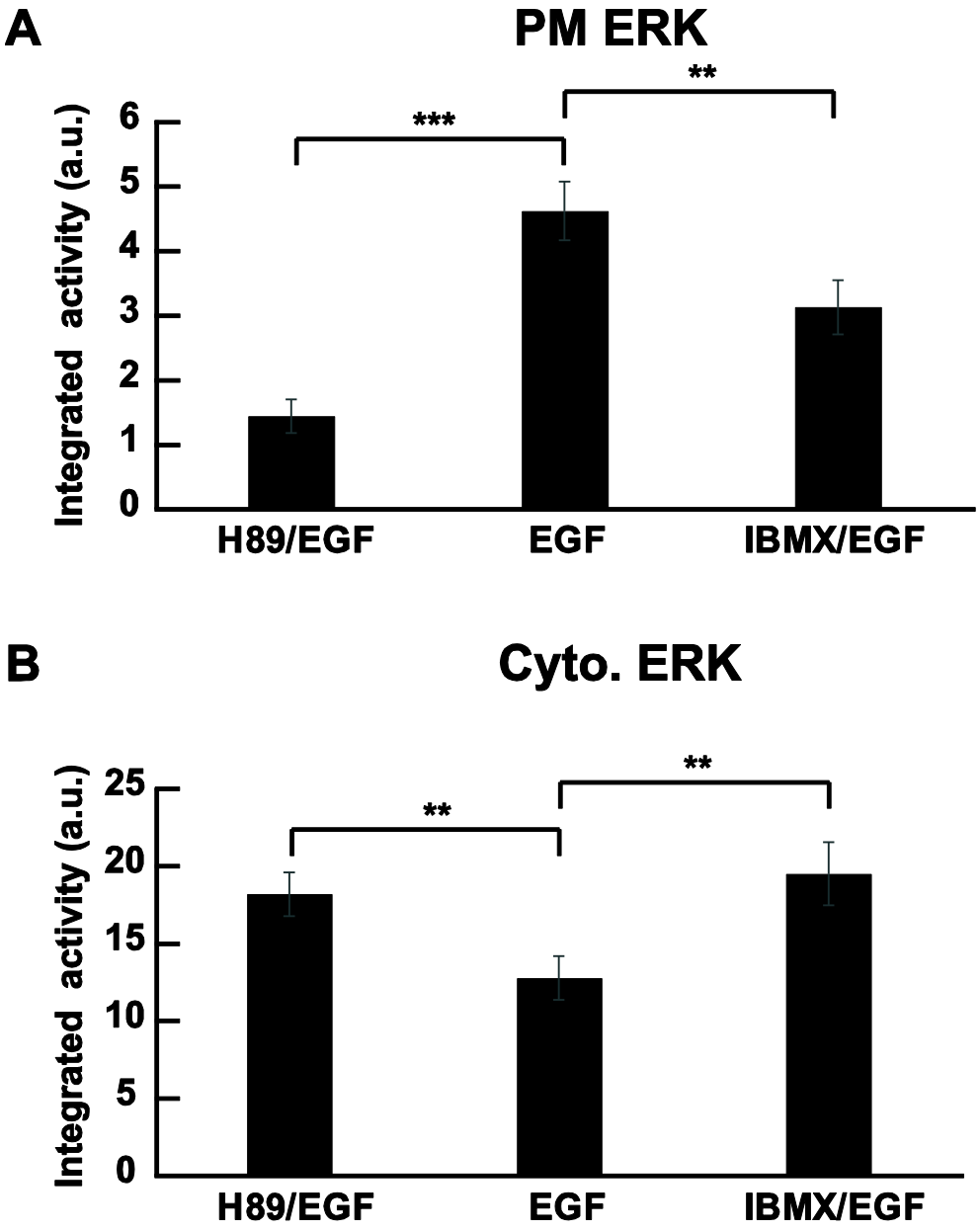

*Figure 4.11: Spatial differences in ERK activity response to modulation of cAMP-PKA pathway. A. Integrated plasma membrane ERK activity in response to PKA inhibition (through H89, n=15) and cAMP-PKA elevation (through IBMX, n=12). B. Integrated cytosolic ERK activity in response to PKA inhibition (through H89, n=15) and cAMP-PKA elevation (through IBMX, n=16). ***, P<0.005. **, P<0.05.*

4.2.3 Functional implications

The plasma membrane of a cell is the interface between cellular constituents and the environment and therefore dictates processes that require interactions with the surroundings such as cellular adhesion. Optimal adhesion of cells to surfaces is vital to overall cell function with implications ranging from maintaining integrity of epithelial tissues (*161*) to the diseased state of tumor metastasis (*162*). PC12 cells have been demonstrated to exhibit increased cellular adhesion when exposed to EGF compared to control cells (*163*) although the molecular events regulating such a process are unclear. In cancer cells, ERK has been implicated in the regulation of cellular adhesion to the extracellular matrix through the actions of its effector molecule, the Ribosomal S6 Kinase (RSK) (*164, 165*). We therefore wondered if the spatiotemporal dynamics of ERK activity following EGF treatment affects PC12 cell adhesion.

We observed that cells exposed to the ERK pathway inhibitor, U0126 increased the capacity of the PC12 cells to adhere to plastic (Figure 4.12, see Methods for details of the assay) suggesting that ERK may negatively regulate cell adhesion. Additionally, we confirmed this using ERK monobody binders (EMBers) that are known to inhibit ERK activity (*166*). We used two different binders dubbed EMBer7.1 and EMBer7.9 that are specifically targeted to the plasma membrane. As can be seen in Figure 4.13, the EMBer-mediated knock down of ERK activity resulted in greatly increased adhesion of cells to the substrate in response to EGF.

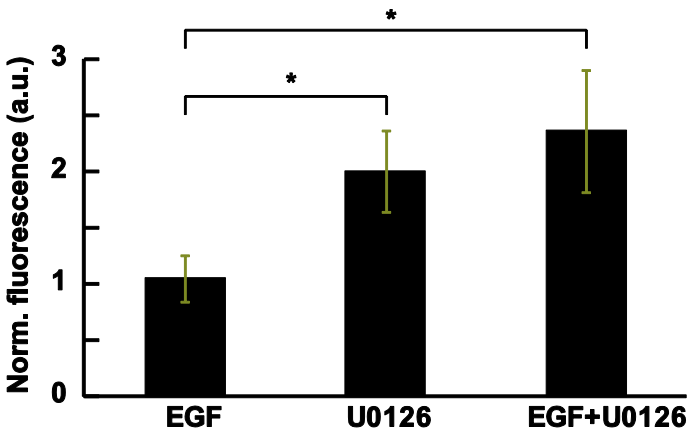

*Figure 4.12: Cell adhesion changes mediated by MEK inhibitor, U0126. Norm. fluorescence, Normalized fluorescence. *, P<0.1.*

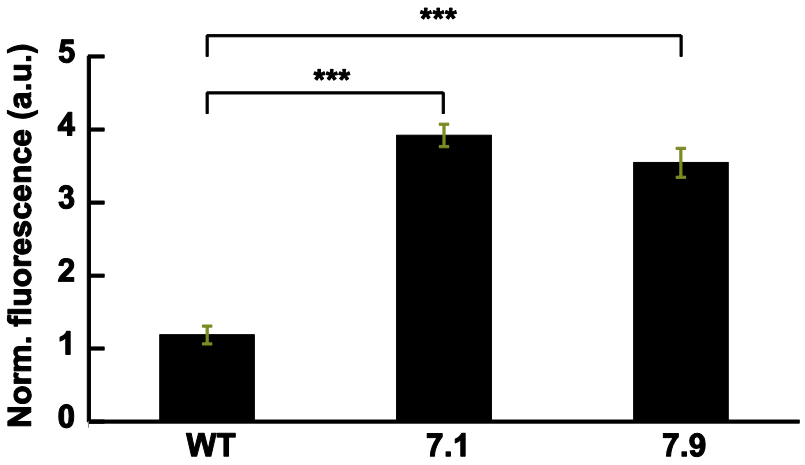

*Figure 4.13: Cell adhesion changes mediated by ERK binders. Norm. fluorescence, Normalized fluorescence. WT, wildtype cells. 7.1, EMBer-7.1. 7.9, EMBer-7.9. ***, P<0.005.*

We then investigated if the plasma membrane pool of ERK may be directly related to the modulation of cell adhesion. In order to test this, we made use of the spatial differences in ERK activity patterns that result following modulation of the cAMP-PKA pathway (Figure 4.11). The ERK pathway inhibitor, U0126 is expected to achieve global inhibition of ERK; hence increased cell adhesion could be theoretically attributed to either the plasma membrane pool or the cytosolic pool or both. However, by exposing the cells to H89 or IBMX, which specifically decrease the plasma membrane ERK activity while

retaining high cytosolic ERK activity we argued that any increases in cell adhesion may be specifically connected to the plasma membrane ERK pool. Strikingly, we observed significantly increased cellular adhesion in response to H89 and IBMX treatments (Figure 4.14) suggesting that the plasma membrane pool of ERK may be involved in modulating cell adhesion. In other words, the sustained plasma membrane ERK activity which results in higher integrated activity may be necessary to achieve optimal cell adhesion.

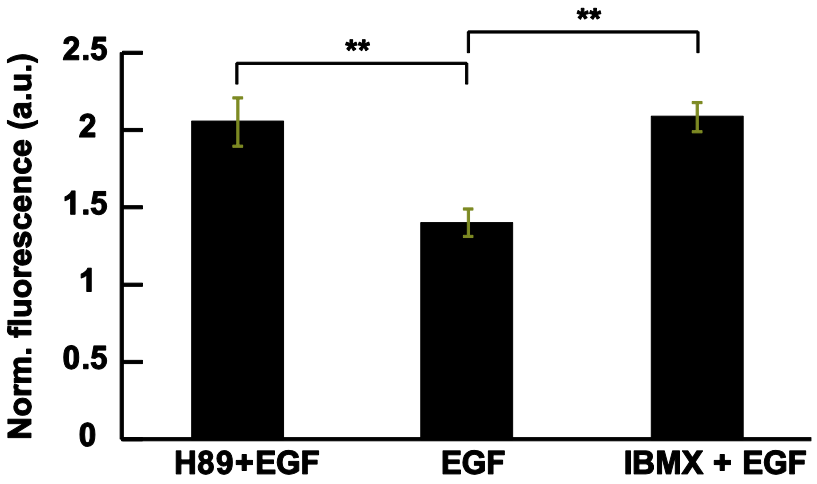

*Figure 4.14: Modulation of cell adhesion through cAMP-PKA pathway. Norm. fluorescence, Normalized fluorescence. **, P<0.05.*

4.3 Discussion

While temporal aspects of ERK signaling have been studied in detail, very little is known about the spatial dynamics of ERK signaling. It's well known that EGF and NGF cause widely different temporal ERK activity dynamics in PC12 cells. Here, we showed that these two stimuli result in completely different spatial patterns of signaling as well. NGF stimulation results in consistently sustained ERK activity in various sub-cellular organelles; however, EGF stimulation results in a range of ERK activity profiles – from transient profiles in the cytosol and nuclear to sustained profiles in plasma membrane and

other organelles – suggesting that these growth factors may have widely differing signaling mechanisms in different subcellular locations. These differences in subcellular phosphorylation patterns of ERK substrates may be caused by a variety of factors.

Phosphorylation is the result of a dynamic balance between the kinase and cognate phosphatase actions. Spatial gradients in phosphorylation have been predicted to occur through differences in the relative concentrations of kinase and phosphatase at different locations (*167*). In this study, we discovered that plasma membrane ERK cascade has low access to phosphatases leading to sustained phosphorylation levels while the cytosolic counterpart has higher access to phosphatases resulting in transient phosphorylation. Coincidentally, similar subcellular phosphatase differences in the ERK cascade have been noted in baby hamster kidney (BHK) cells as well (*168*). MEK, ERK and its substrates are regulated by a large number of phosphatases including PP2A and multiple dual-specificity phosphatases (*169*). Future investigations into the subcellular localization patterns of these phosphatases and their differential spatial signaling patterns, if any, will help us better understand the spatial ERK signaling mechanisms.

Aside from the phosphatase, the kinase ERK is also differentially regulated. The spatiotemporal ERK activity dynamics differences appear to be the result of dissimilar regulation of ERK cascade by the cAMP-PKA pathway. The cAMP-PKA pathway stimulates ERK in some cells and inhibits it in others through various targets including different Raf isoforms (*170*). In fact, B-Raf is deemed necessary for sustained ERK activation upon NGF stimulation in PC12 cells (*171*). It is likely therefore, subcellular differences in relative concentrations of the Raf isoforms within the same cell could

produce such distinct temporal ERK activity patterns. Alternatively, the effects of cAMP could be mediated through PKA-dependent and PKA-independent mechanisms simultaneously. Epac, another effector of cAMP has been previously demonstrated to switch PC12 cells from a proliferative state to differentiable state (*172*). The balance between PKA-dependent and Epac-dependent activation of ERK in different compartments could therefore likely determine ERK activity dynamics.

EGF-dependent ERK signaling in PC12 cells has largely been understood to be necessary for cell proliferation. However, spatial differences in EGF-dependent ERK signaling may be important for location-specific functions. For instance, ERK is involved in mitochondrial energetics (*173*) and apoptosis (*174, 175*) likely affecting brain function (*176*) and plays an important role in golgi fragmentation (*177*). It is therefore likely that differential kinetics of ERK activity at these locations compared to cytosolic and nuclear ERK responses are important for regulating local substrates involved in apoptosis and golgi fragmentation. However, very little is known about the role of ERK in the plasma membrane. Here, we showed that ERK signaling is critical for modulating cell adhesion. Specifically, the plasma membrane pool of ERK appears to be involved in regulating this process. As a result, cells can exploit spatial dynamics of the same signaling molecule to regulate different cellular processes simultaneously. The transient ERK activity output in the nucleus mediates cell proliferation processes; at the same time a sustained output in the plasma membrane likely ensures optimal adhesion of the cells to the matrix.

4.4 Methods

4.4.1 Generation of subcellular targeted EKARs

The EKAR-EV construct was kindly donated by the Matsuda Lab. The "core" of EKAR-EV comprising the phospho-amino acid binding WW domain, EV linker and substrate domain was PCR amplified, digested and subcloned into pRSETB plasmid between *SphI* and *SacI* restriction sites. The fluorescent proteins ECFP and YPet were inserted between *BamHI* and *SphI*, and *SacI* and *EcoRI* sites respectively. This construct was then subcloned into a pC3DNA (Invitrogen) plasmid between the *BamHI* and *EcoRI* sites and was dubbed EKAR2.3. In order to generate the targeted versions of EKARs, appropriate targeting sequences were inserted to the 5' or 3' of the sensor, as the case may be. The sub-cellular locations, position (N or C-terminal) and the amino acid targeting sequences are given below:

Table 4.1: Details of targeting sequences

Subcellular location	Position	Sequence
Non-lipid raft plasma membrane	C	K K K K K S K T K C V I M
Lipid rafts	N	G C I K S K R K D K D P
Nucleus	C	P K K K R K V E D A
Cytosol	C	E F L P P L E R L T L
Outer mitochondrial membrane	N	M A I Q L R S L F P L A L P G M L A L L G W W W F F S R K K

4.4.2 Cell culture

PC12 cells were seeded onto sterilized glass coverslips in 35-mm dishes and grown to 50–90% confluency in DMEM (10% FBS) at 37°C with 5% CO_2. Cells were transfected using Lipofectamine 2000 (Invitrogen) and grown for 48 h after transfection before the imaging.

4.4.3 Imaging

Cells were washed twice with HBSS (Hanks' balanced salt solution) buffer and maintained in the dark at room temperature.

4.4.4 Epifluorescence Microscopy

Cells were imaged on a Zeiss Axiovert 200M microscope with a cooled charge-coupled device camera (MicroMAX BFT512, Roper Scientific, Trenton, NJ) controlled by METAFLUOR 6.2 software (Universal Imaging, Downingtown, PA). Yellow/cyan emission ratio imaging used a 420DF20 excitation filter, a 450DRLP dichroic mirror and two emission filters (475DF40 for CFP and 535DF25 for YFP) alternated by a filter-changer Lambda 10-2 (Sutter Instruments, Novato, CA). Exposure time was 50–500 ms, and images were taken every 30s. Fluorescence images were background-corrected by subtracting the fluorescence intensity of background with no cells from the emission intensities of cells expressing fluorescent reporters. The ratios of yellow/cyan emissions were then calculated at different time points. Both Yellow/Cyan ratio and RFP intensity of all time courses were normalized by dividing each value by the average basal value before stimulant/inhibitor addition.

4.4.5 Cell adhesion assay

Cells were dissociated using 0.05 % trypsin and washed once with DPBS (Dulbecco Phosphate Buffered Saline). Cells were then resuspended in 1 mL of DPBS and cell count

measured. The cells were then centrifuged at 850g for 5 minutes and the DPBS aspirated. Cells were then resuspended in 2 mL of serum-free medium. At the same time, 20 μL of the green fluorescent dye, Calcein-AM was added to the cell suspension in order to label the cells and the suspension incubated at 37°C with 5% CO_2 for 30 minutes. The cells were then spun down and washed twice with DPBS to remove traces of non-labeled dye. The cells were then resuspended in serum-free medium and seeded in 96-well plates in quadruplicates for each condition at a density of $5x10^5$ cells/mL. Additionally, cells were also seeded in quadruplicates at different densities (0, $1x10^4$, $2x10^4$, $4x10^4$, $6x10^4$, $8x10^4$, $10x10^4$, $20x10^4$, $40x10^4$, $60x10^4$, $80x10^4$ and $100x10^4$ cells/mL) to calibrate cell adhesion as a function of the measured fluorescence. The plate was then incubated at 37°C with 5% CO_2 for 3 hours to reach steady-state. The fluorescence was then measured using a fluorescence plate reader. The fluorescence for each well was subtracted from the mean background fluorescence (no cells condition). The mean fluorescence obtained from the quadruplicates for each condition was then normalized to that of the control condition (untreated cells).

Chapter 5 Conclusions

The ability of cells to recognize, adapt and respond to a wide variety of external conditions is critical for regulating various cellular processes including survival. Typically, cells translate such extracellular cues into specific cellular responses through a diverse but finite set of signaling proteins. Given the limited repertoire of signaling molecules, it is common for many signaling molecules to be involved in the regulation of multiple cell processes. How cells achieve specificity of signaling using such shared sets of molecules is a long standing question. One particular manner in which specificity may be achieved is by exploiting the precise spatial localization and temporal dynamics of different signaling molecules.

In the insulin-secreting pancreatic beta cells, intracellular levels of calcium are known to oscillate in response to glucose-mediated membrane depolarization (*178*). Such oscillations are thought to regulate the pulsatility of insulin secretion which in turn is deemed to be important for glucose homeostasis (*80*). In essence, pancreatic beta-cells "encode" information in the versatile oscillatory calcium signal. The encoded information is however inadequate without the right set of tools to decode it and use it to regulate different processes including insulin secretion. We have shown that kinases are eminently suitable for this purpose – with a high capacity to "read" the information, process and reshape it and ultimately be able to use the decoded signal for various purposes.

The kinase, PKA not only decodes the calcium signal and oscillates in tandem with it but also actively modulates the frequency of the oscillations. Such complex behavior enables it to use information that may be embedded in frequency of the signal to carry out

a wide range of functions. Particularly, the frequency information is used to determine the spatial range of action of PKA. Another prominent kinase, ERK, on the other hand displays strikingly different behavior and means of decoding the calcium signal. While PKA faithfully follows the calcium signal, the ERK cascade processes the oscillatory input signal to produce an integrated response. This robust response is achieved via sequential processing of the calcium signal through a multi-step cascade. As a result, the ERK cascade can progressively filter out high frequency "noise" for sustained ERK activation while still retaining the dynamical information for use by other signaling molecules. *In toto*, we showed that two different kinases process the same input signal exhibiting varied temporal dynamics which in turn can be used to selectively and effectively modulate their respective targets.

Aside from temporal dynamics, kinases exhibit remarkable variation in the spatial dimension as well. In the neuroendocrine PC12 cells, we showed that these kinases, PKA and ERK talk to each other in a complex fashion to produce distinct behaviors in different locations. In response to EGF, ERK activity shows a transient increase in the cytosol and nucleus, which is known to be necessary for cell proliferation (*58*). Strikingly, however, in response to the same stimulus, the same signaling molecule, ERK displays a sustained response in the plasma membrane which is important for modulating cell adhesion to the matrix. Such spatial variations are brought about by different factors including the manner of crosstalk of PKA and ERK in these locations. In essence, the cells appear to enhance their "computation" power through spatial compartmentation. The same signaling network (the PKA-ERK network in this case) may have different topologies in different locations

through the use of regulatory molecules, ensuring different system outputs in different locations.

Spatiotemporal dynamics manifests as a result of complex non-linear interactions in signaling networks. Monitoring and understanding the spatiotemporal kinase activity dynamics detailed above posed a unique set of challenges which we addressed using a combination of modeling and experimental approaches. Non-linear systems are intuitively difficult to predict. Using mathematical modeling therefore, we were able to predict the system responses and generate hypotheses that could be tested on the bench. In order to monitor the dynamical aspects of signaling, we extensively used genetically encoded fluorescent biosensors. Live-cell imaging using such biosensors enabled us to capture the behavior of different signaling molecules in their native milieu. Multiplex imaging, in particular, helped us observe not one but two signaling entities at the same time with the result that we could directly correlate the system output to its input within the same cell. Improvement and widespread use of such techniques will help us expand our capability to study spatiotemporal signaling dynamics in future.

In conclusion, cells employ and use spatial and temporal dynamics of kinase signaling to process external information and regulate a variety of processes. Understanding the nature and mechanisms of dynamical aspects of signaling not only furthers our comprehension of how cells make decisions but could also serve as viable therapeutic targets. Targeting specific dynamical features through regulatory molecules instead of central hubs of signaling networks may provide selectivity for drugs (*179*).

References

1. D. A. Lovejoy. (John Wiley & Sons, 2005), pp. 42-54.
2. J. Higgins, A Chemical Mechanism for Oscillation of Glycolytic Intermediates in Yeast Cells. *Proceedings of the National Academy of Sciences of the United States of America* **51**, 989 (Jun, 1964).
3. B. Hess, The glycolytic oscillator. *The Journal of experimental biology* **81**, 7 (Aug, 1979).
4. M. T. Laub, L. Shapiro, H. H. McAdams, Systems biology of Caulobacter. *Annual review of genetics* **41**, 429 (2007).
5. J. J. Tyson, C. I. Hong, C. D. Thron, B. Novak, A simple model of circadian rhythms based on dimerization and proteolysis of PER and TIM. *Biophysical journal* **77**, 2411 (Nov, 1999).
6. A. Goldbeter, A model for circadian oscillations in the Drosophila period protein (PER). *Proceedings* **261**, 319 (Sep 22, 1995).
7. V. A. Maltsev, E. G. Lakatta, Normal heart rhythm is initiated and regulated by an intracellular calcium clock within pacemaker cells. *Heart, lung & circulation* **16**, 335 (Oct, 2007).
8. J. J. Saucerman *et al.*, Systems analysis of PKA-mediated phosphorylation gradients in live cardiac myocytes. *Proceedings of the National Academy of Sciences of the United States of America* **103**, 12923 (Aug 22, 2006).
9. M. Machacek *et al.*, Coordination of Rho GTPase activities during cell protrusion. *Nature* **461**, 99 (Sep 3, 2009).
10. F. C. Liu, A. M. Graybiel, Spatiotemporal dynamics of CREB phosphorylation: transient versus sustained phosphorylation in the developing striatum. *Neuron* **17**, 1133 (Dec, 1996).
11. S. Kostin, S. Hein, E. P. Bauer, J. Schaper, Spatiotemporal development and distribution of intercellular junctions in adult rat cardiomyocytes in culture. *Circulation research* **85**, 154 (Jul 23, 1999).
12. D. S. Chao *et al.*, SNARE membrane trafficking dynamics in vivo. *The Journal of cell biology* **144**, 869 (Mar 8, 1999).
13. J. S. Ehrlich, M. D. Hansen, W. J. Nelson, Spatio-temporal regulation of Rac1 localization and lamellipodia dynamics during epithelial cell-cell adhesion. *Developmental cell* **3**, 259 (Aug, 2002).
14. J. J. Bravo-Cordero *et al.*, A novel spatiotemporal RhoC activation pathway locally regulates cofilin activity at invadopodia. *Curr Biol* **21**, 635 (Apr 26, 2011).
15. J. Nakai, M. Ohkura, K. Imoto, A high signal-to-noise Ca(2+) probe composed of a single green fluorescent protein. *Nature biotechnology* **19**, 137 (Feb, 2001).
16. J. Akerboom *et al.*, Crystal structures of the GCaMP calcium sensor reveal the mechanism of fluorescence signal change and aid rational design. *The Journal of biological chemistry* **284**, 6455 (Mar 6, 2009).
17. K. J. Herbst, Q. Ni, J. Zhang, Dynamic visualization of signal transduction in living cells: from second messengers to kinases. *IUBMB life* **61**, 902 (Sep, 2009).

18. J. Zhang, Y. Ma, S. S. Taylor, R. Y. Tsien, Genetically encoded reporters of protein kinase A activity reveal impact of substrate tethering. *Proceedings of the National Academy of Sciences of the United States of America* **98**, 14997 (Dec 18, 2001).
19. X. Gao, J. Zhang, Spatiotemporal analysis of differential Akt regulation in plasma membrane microdomains. *Molecular biology of the cell* **19**, 4366 (Oct, 2008).
20. C. D. Harvey *et al.*, A genetically encoded fluorescent sensor of ERK activity. *Proceedings of the National Academy of Sciences of the United States of America* **105**, 19264 (Dec 9, 2008).
21. J. D. Violin, J. Zhang, R. Y. Tsien, A. C. Newton, A genetically encoded fluorescent reporter reveals oscillatory phosphorylation by protein kinase C. *The Journal of cell biology* **161**, 899 (Jun 9, 2003).
22. E. Tkachenko *et al.*, Protein kinase A governs a RhoA-RhoGDI protrusion-retraction pacemaker in migrating cells. *Nature cell biology* **13**, 660 (Jun, 2011).
23. L. R. V. Castro, E. Guiot, M. Polito, D. Paupardin-Tritsch, P. Vincent, Decoding spatial and temporal features of neuronal cAMP/PKA signaling with FRET biosensors. *Biotechnology Journal* **9**, 192 (Feb, 2014).
24. S. Zhai, E. D. Ark, P. Parra-Bueno, R. Yasuda, Long-Distance Integration of Nuclear ERK Signaling Triggered by Activation of a Few Dendritic Spines. *Science (New York, N.Y* **342**, 1107 (Nov 29, 2013).
25. K. J. Herbst, M. D. Allen, J. Zhang, Spatiotemporally regulated protein kinase A activity is a critical regulator of growth factor-stimulated extracellular signal-regulated kinase signaling in PC12 cells. *Molecular and cellular biology* **31**, 4063 (Oct, 2011).
26. J. G. Albeck, G. B. Mills, J. S. Brugge, Frequency-Modulated Pulses of ERK Activity Transmit Quantitative Proliferation Signals. *Molecular Cell* **49**, 249 (Jan 24, 2013).
27. O. Decroly, A. Goldbeter, Birhythmicity, chaos, and other patterns of temporal self-organization in a multiply regulated biochemical system. *Proceedings of the National Academy of Sciences of the United States of America* **79**, 6917 (Nov, 1982).
28. O. Kapuy, D. Barik, M. R. Sananes, J. J. Tyson, B. Novak, Bistability by multiple phosphorylation of regulatory proteins. *Progress in biophysics and molecular biology* **100**, 47 (Sep-Oct, 2009).
29. W. Ma, A. Trusina, H. El-Samad, W. A. Lim, C. Tang, Defining network topologies that can achieve biochemical adaptation. *Cell* **138**, 760 (Aug 21, 2009).
30. B. Novak, J. J. Tyson, Design principles of biochemical oscillators. *Nature reviews* **9**, 981 (Dec, 2008).
31. W. A. Lim, Designing customized cell signalling circuits. *Nature reviews* **11**, 393 (Jun, 2010).
32. J. E. Toettcher, C. Mock, E. Batchelor, A. Loewer, G. Lahav, A synthetic-natural hybrid oscillator in human cells. *Proceedings of the National Academy of Sciences of the United States of America* **107**, 17047 (Sep 28, 2010).
33. A. B. Parekh, Decoding cytosolic Ca2+ oscillations. *Trends in biochemical sciences* **36**, 78 (Feb, 2011).

34. R. Cheong, A. Levchenko, Oscillatory signaling processes: the how, the why and the where. *Current opinion in genetics & development* **20**, 665 (Dec, 2010).
35. S. J. Lee, Y. Escobedo-Lozoya, E. M. Szatmari, R. Yasuda, Activation of CaMKII in single dendritic spines during long-term potentiation. *Nature* **458**, 299 (Mar 19, 2009).
36. R. M. Mulkey, S. Endo, S. Shenolikar, R. C. Malenka, Involvement of a calcineurin/inhibitor-1 phosphatase cascade in hippocampal long-term depression. *Nature* **369**, 486 (Jun 9, 1994).
37. D. J. Michael, W. Xiong, X. Geng, P. Drain, R. H. Chow, Human insulin vesicle dynamics during pulsatile secretion. *Diabetes* **56**, 1277 (May, 2007).
38. B. Hellman *et al.*, Glucose induces oscillatory Ca2+ signalling and insulin release in human pancreatic beta cells. *Diabetologia* **37 Suppl 2**, S11 (Sep, 1994).
39. D. M. Bers, Cardiac excitation-contraction coupling. *Nature* **415**, 198 (Jan 10, 2002).
40. A. Hoffmann, A. Levchenko, M. L. Scott, D. Baltimore, The IkappaB-NF-kappaB signaling module: temporal control and selective gene activation. *Science (New York, N.Y* **298**, 1241 (Nov 8, 2002).
41. V. O. Nikolaev, M. Bunemann, L. Hein, A. Hannawacker, M. J. Lohse, Novel single chain cAMP sensors for receptor-induced signal propagation. *The Journal of biological chemistry* **279**, 37215 (Sep 3, 2004).
42. H. Cheng, W. J. Lederer, M. B. Cannell, Calcium sparks: elementary events underlying excitation-contraction coupling in heart muscle. *Science (New York, N.Y* **262**, 740 (Oct 29, 1993).
43. B. J. Bacskai *et al.*, Spatially resolved dynamics of cAMP and protein kinase A subunits in Aplysia sensory neurons. *Science (New York, N.Y* **260**, 222 (Apr 9, 1993).
44. S. R. Neves *et al.*, Cell shape and negative links in regulatory motifs together control spatial information flow in signaling networks. *Cell* **133**, 666 (May 16, 2008).
45. G. Di Benedetto *et al.*, Protein kinase A type I and type II define distinct intracellular signaling compartments. *Circulation research* **103**, 836 (Oct 10, 2008).
46. G. Manning, Genomic overview of protein kinases. *WormBook : the online review of C. elegans biology*, 1 (2005, 2005).
47. M. M. Petrovic, K. Vales, B. Putnikovic, V. Djulejic, D. M. Mitrovic, Ryanodine receptors, voltage-gated calcium channels and their relationship with protein kinase A in the myocardium. *Physiol Res* **57**, 141 (2008).
48. C. B. Neylon, C. J. Fowler, J. B. Furness, Regulation of the slow afterhyperpolarization in enteric neurons by protein kinase A. *Auton Neurosci* **126-127**, 258 (Jun 30, 2006).
49. Y. Mebratu, Y. Tesfaigzi, How ERK1/2 activation controls cell proliferation and cell death: Is subcellular localization the answer? *Cell Cycle* **8**, 1168 (Apr 15, 2009).
50. M. C. Lawrence *et al.*, The roles of MAPKs in disease. *Cell Res* **18**, 436 (Apr, 2008).

51. S. Khoo *et al.*, Regulation of insulin gene transcription by ERK1 and ERK2 in pancreatic beta cells. *The Journal of biological chemistry* **278**, 32969 (Aug 29, 2003).
52. C. Benes *et al.*, Mode of regulation of the extracellular signal-regulated kinases in the pancreatic beta-cell line MIN6 and their implication in the regulation of insulin gene transcription. *Biochem J* **340 (Pt 1)**, 219 (May 15, 1999).
53. M. C. Lawrence, K. McGlynn, B. Naziruddin, M. F. Levy, M. H. Cobb, Differential regulation of CHOP-10/GADD153 gene expression by MAPK signaling in pancreatic beta-cells. *Proceedings of the National Academy of Sciences of the United States of America* **104**, 11518 (Jul 10, 2007).
54. G. Manning, D. B. Whyte, R. Martinez, T. Hunter, S. Sudarsanam, The protein kinase complement of the human genome. *Science (New York, N.Y* **298**, 1912 (2002).
55. J. A. Ubersax, J. E. Ferrell, Mechanisms of specificity in protein phosphorylation. *Nat. Rev. Mol. Cell Biol.* **8**, 530 (2007).
56. M. D. Brown, D. B. Sacks, Protein scaffolds in MAP kinase signalling. *Cell. Signal.* **21**, 462 (2009).
57. G. K. Carnegie, C. K. Means, J. D. Scott, A-kinase anchoring proteins: from protein complexes to physiology and disease. *IUBMB life* **61**, 394 (2009).
58. C. J. Marshall, Specificity of receptor tyrosine kinase signaling: transient versus sustained extracellular signal-regulated kinase activation. *Cell* **80**, 179 (1995).
59. S. S. Taylor, Signaling through cAMP and cAMP-dependent protein kinase: diverse strategies for drug design. *Biochim. Biophys. Acta* **1784**, 16 (2008).
60. S. Seino, T. Shibasaki, PKA-dependent and PKA-independent pathways for cAMP-regulated exocytosis. *Physiol. Rev.* **85**, 1303 (2005).
61. R. Bertram, A. Sherman, L. S. Satin, Metabolic and electrical oscillations: partners in controlling pulsatile insulin secretion. *Am. J. Physiol. Endocrinol. Metab.* **293**, E890 (2007).
62. J. Gromada, B. Brock, O. Schmitz, P. Rorsman, Glucagon-like peptide-1: regulation of insulin secretion and therapeutic potential. *Basic Clin. Pharmacol. Toxicol.* **95**, 252 (2004).
63. D. Delmeire, Type VIII adenylyl cyclase in rat beta cells: coincidence signal detector/generator for glucose and GLP-1. *Diabetologia* **46**, 1383 (2003).
64. C. Ammälä, F. M. Ashcroft, P. Rorsman, Calcium-independent potentiation of insulin release by cyclic AMP in single beta-cells. *Nature* **363**, 356 (1993).
65. J. C. Henquin, H. P. Meissner, The ionic, electrical, and secretory effects of endogenous cyclic adenosine monophosphate in mouse pancreatic B cells: studies with forskolin. *Endocrinology* **115**, 1125 (1984).
66. H. Hatakeyama, T. Kishimoto, T. Nemoto, H. Kasai, N. Takahashi, Rapid glucose sensing by protein kinase A for insulin exocytosis in mouse pancreatic islets. *J. Physiol. (Lond.)* **570**, 271 (2006).
67. A. Vaag, J. E. Henriksen, S. Madsbad, N. Holm, H. Beck-Nielsen, Insulin secretion, insulin action, and hepatic glucose production in identical twins discordant for non-insulin-dependent diabetes mellitus. *J. Clin. Invest.* **95**, 690 (1995).

68. L. R. Landa, Interplay of Ca2+ and cAMP signaling in the insulin-secreting MIN6 beta-cell line. *J. Biol. Chem.* **280**, 31294 (2005).
69. J. Zhang, C. J. Hupfeld, S. S. Taylor, J. M. Olefsky, R. Y. Tsien, Insulin disrupts beta-adrenergic signalling to protein kinase A in adipocytes. *Nature* **437**, 569 (2005).
70. J. Zhang, Y. Ma, S. S. Taylor, R. Y. Tsien, Genetically encoded reporters of protein kinase A activity reveal impact of substrate tethering. *Proc. Natl. Acad. Sci. USA* **98**, 14997 (2001).
71. G. Grynkiewicz, M. Poenie, R. Y. Tsien, A new generation of Ca2+ indicators with greatly improved fluorescence properties. *J. Biol. Chem.* **260**, 3440 (1985).
72. A. E. Bugrim, Regulation of Ca2+ release by cAMP-dependent protein kinase. A mechanism for agonist-specific calcium signaling? *Cell calcium* **25**, 219 (1999).
73. M. Leiser, N. Fleischer, cAMP-dependent phosphorylation of the cardiac-type alpha 1 subunit of the voltage-dependent Ca2+ channel in a murine pancreatic beta-cell line. *Diabetes* **45**, 1412 (1996).
74. M. D. Allen, J. Zhang, Subcellular dynamics of protein kinase A activity visualized by FRET-based reporters. *Biochem. Biophys. Res. Commun.* **348**, 716 (2006).
75. L. M. DiPilato, X. Cheng, J. Zhang, Fluorescent indicators of cAMP and Epac activation reveal differential dynamics of cAMP signaling within discrete subcellular compartments. *Proc. Natl. Acad. Sci. USA* **101**, 16513 (2004).
76. J. D. Violin, beta2-adrenergic receptor signaling and desensitization elucidated by quantitative modeling of real time cAMP dynamics. *J. Biol. Chem.* **283**, 2949 (2008).
77. Q. Ni *et al.*, Signaling diversity of PKA achieved via a Ca2+-cAMP-PKA oscillatory circuit. *Nature chemical biology* **7**, 34 (Jan, 2011).
78. T. R. Chay, J. Keizer, Minimal model for membrane oscillations in the pancreatic beta-cell. *Biophys. J.* **42**, 181 (1983).
79. S. F. Oliveria, M. L. Dell'Acqua, W. A. Sather, AKAP79/150 anchoring of calcineurin controls neuronal L-type Ca2+ channel activity and nuclear signaling. *Neuron* **55**, 261 (2007).
80. P. Bergsten, E. Grapengiesser, E. Gylfe, A. Tengholm, B. Hellman, Synchronous oscillations of cytoplasmic Ca2+ and insulin release in glucose-stimulated pancreatic islets. *J. Biol. Chem.* **269**, 8749 (1994).
81. O. Dyachok, Y. Isakov, J. Sagetorp, A. Tengholm, Oscillations of cyclic AMP in hormone-stimulated insulin-secreting beta-cells. *Nature* **439**, 349 (2006).
82. L. B. Lester, M. C. Faux, J. B. Nauert, J. D. Scott, Targeted protein kinase A and PP-2B regulate insulin secretion through reversible phosphorylation. *Endocrinology* **142**, 1218 (2001).
83. M. J. Berridge, A. Galione, Cytosolic calcium oscillators. *FASEB J.* **2**, 3074 (1988).
84. J. W. Putney, G. S. Bird, Cytoplasmic calcium oscillations and store-operated calcium influx. *J. Physiol. (Lond.)* **586**, 3055 (2008).

85. N. M. Woods, K. S. R. Cuthbertson, P. H. Cobbold, Repetitive transient rises in cytoplasmic free calcium in hormone-stimulated hepatocytes. *Nature* **319**, 600 (1986).
86. R. E. Dolmetsch, K. Xu, R. S. Lewis, Calcium oscillations increase the efficiency and specificity of gene expression. *Nature* **392**, 933 (Apr 30, 1998).
87. W. Li, J. Llopis, M. Whitney, G. Zlokarnik, R. Y. Tsien, Cell-permeant caged InsP3 ester shows that Ca2+ spike frequency can optimize gene expression. *Nature* **392**, 936 (1998).
88. T. A. Dunn, Imaging of cAMP levels and protein kinase A activity reveals that retinal waves drive oscillations in second-messenger cascades. *J. Neurosci.* **26**, 12807 (2006).
89. Z. Hilioti, Oscillatory phosphorylation of yeast Fus3 MAP kinase controls periodic gene expression and morphogenesis. *Curr. Biol.* **18**, 1700 (2008).
90. H. Shankaran, Rapid and sustained nuclear-cytoplasmic ERK oscillations induced by epidermal growth factor. *Mol. Syst. Biol.* **5**, 332 (2009).
91. S. Markoulaki, S. Matson, T. Ducibella, Fertilization stimulates long-lasting oscillations of CaMKII activity in mouse eggs. *Dev. Biol.* **272**, 15 (2004).
92. L. N. Borodinsky, N. C. Spitzer, Second messenger pas de deux: the coordinated dance between calcium and cAMP. *Sci. STKE* **2006**, pe22 (2006).
93. M. Zaccolo, T. Pozzan, CAMP and Ca2+ interplay: a matter of oscillation patterns. *Trends Neurosci.* **26**, 53 (2003).
94. R. Nesher *et al.*, Beta-cell protein kinases and the dynamics of the insulin response to glucose. *Diabetes* **51 Suppl 1**, S68 (Feb, 2002).
95. L. E. Fridlyand, M. C. Harbeck, M. W. Roe, L. H. Philipson, Regulation of cAMP dynamics by Ca2+ and G protein-coupled receptors in the pancreatic beta-cell: a computational approach. *Am J Physiol Cell Physiol* **293**, C1924 (Dec, 2007).
96. O. Dyachok, E. Gylfe, Ca(2+)-induced Ca(2+) release via inositol 1,4,5-trisphosphate receptors is amplified by protein kinase A and triggers exocytosis in pancreatic beta-cells. *The Journal of biological chemistry* **279**, 45455 (Oct 29, 2004).
97. T. Kanno, S. Suga, J. Wu, M. Kimura, M. Wakui, Intracellular cAMP potentiates voltage-dependent activation of L-type Ca2+ channels in rat islet beta-cells. *Pflugers Archiv : European journal of physiology* **435**, 578 (Mar, 1998).
98. Y. V. Gorbunova, N. C. Spitzer, Dynamic interactions of cyclic AMP transients and spontaneous Ca(2+) spikes. *Nature* **418**, 93 (Jul 4, 2002).
99. Y. Tang, H. G. Othmer, Frequency encoding in excitable systems with applications to calcium oscillations. *Proceedings of the National Academy of Sciences of the United States of America* **92**, 7869 (Aug 15, 1995).
100. T. R. Chay, J. Keizer, Minimal model for membrane oscillations in the pancreatic beta-cell. *Biophys J* **42**, 181 (May, 1983).
101. A. S. Sherman, Y.-X. Li, and J.E. Keizer, in *Computational Cell Biology,* C. P. Fall, Ed. (Springer-Verlag, New York, 2002).
102. R. Bertram, J. Previte, A. Sherman, T. A. Kinard, L. S. Satin, The phantom burster model for pancreatic beta-cells. *Biophysical journal* **79**, 2880 (Dec, 2000).

103. B. Lee, J. C. Jonas, G. C. Weir, S. G. Laychock, Glucose regulates expression of inositol 1,4,5-trisphosphate receptor isoforms in isolated rat pancreatic islets. *Endocrinology* **140**, 2173 (May, 1999).
104. I. Bezprozvanny, J. Watras, B. E. Ehrlich, Bell-shaped calcium-response curves of Ins(1,4,5)P3- and calcium-gated channels from endoplasmic reticulum of cerebellum. *Nature* **351**, 751 (Jun 27, 1991).
105. G. W. De Young, J. Keizer, A single-pool inositol 1,4,5-trisphosphate-receptor-based model for agonist-stimulated oscillations in Ca2+ concentration. *Proceedings of the National Academy of Sciences of the United States of America* **89**, 9895 (Oct 15, 1992).
106. R. E. Hagar, B. E. Ehrlich, Regulation of the type III InsP3 receptor and its role in beta cell function. *Cellular and molecular life sciences : CMLS* **57**, 1938 (Dec, 2000).
107. C. D. Ferris, R. L. Huganir, D. S. Bredt, A. M. Cameron, S. H. Snyder, Inositol trisphosphate receptor: phosphorylation by protein kinase C and calcium calmodulin-dependent protein kinases in reconstituted lipid vesicles. *Proceedings of the National Academy of Sciences of the United States of America* **88**, 2232 (Mar 15, 1991).
108. S. Supattapone *et al.*, Cyclic AMP-dependent phosphorylation of a brain inositol trisphosphate receptor decreases its release of calcium. *Proceedings of the National Academy of Sciences of the United States of America* **85**, 8747 (Nov, 1988).
109. C. A. Leech, M. A. Castonguay, J. F. Habener, Expression of adenylyl cyclase subtypes in pancreatic beta-cells. *Biochemical and biophysical research communications* **254**, 703 (Jan 27, 1999).
110. L. R. Landa, Jr. *et al.*, Interplay of Ca2+ and cAMP signaling in the insulin-secreting MIN6 beta-cell line. *The Journal of biological chemistry* **280**, 31294 (Sep 2, 2005).
111. D. M. Cooper, N. Mons, J. W. Karpen, Adenylyl cyclases and the interaction between calcium and cAMP signalling. *Nature* **374**, 421 (Mar 30, 1995).
112. R. K. Sunahara, C. W. Dessauer, A. G. Gilman, Complexity and diversity of mammalian adenylyl cyclases. *Annual review of pharmacology and toxicology* **36**, 461 (1996).
113. J. L. Guillou, H. Nakata, D. M. Cooper, Inhibition by calcium of mammalian adenylyl cyclases. *The Journal of biological chemistry* **274**, 35539 (Dec 10, 1999).
114. U. S. Bhalla, R. Iyengar, Emergent properties of networks of biological signaling pathways. *Science (New York, N.Y* **283**, 381 (Jan 15, 1999).
115. C. Y. Huang, V. Chau, P. B. Chock, J. H. Wang, R. K. Sharma, Mechanism of activation of cyclic nucleotide phosphodiesterase: requirement of the binding of four Ca2+ to calmodulin for activation. *Proceedings of the National Academy of Sciences of the United States of America* **78**, 871 (Feb, 1981).
116. X. Yu, J. H. Byrne, D. A. Baxter, Modeling interactions between electrical activity and second-messenger cascades in Aplysia neuron R15. *Journal of neurophysiology* **91**, 2297 (May, 2004).

117. R. Roskoski, Jr., ERK1/2 MAP kinases: Structure, function, and regulation. *Pharmacological Research* **66**, 105 (Aug, 2012).
118. V. Cestari, C. Rossi-Arnaud, D. Saraulli, M. Costanzi, The MAP(K) of fear: From memory consolidation to memory extinction. *Brain Research Bulletin* **105**, 8 (Jun, 2014).
119. K. Lorenz, J. P. Schmitt, M. Vidal, M. J. Lohse, Cardiac hypertrophy: Targeting Raf/MEK/ERK1/2-signaling. *International Journal of Biochemistry & Cell Biology* **41**, 2351 (Dec, 2009).
120. E. M. Dioum, J. W. Schneider, M. H. Cobb, Contribution of MAP Kinases ERK1/2 in Beta Cell Function. *Faseb Journal* **24**, (Apr, 2010).
121. M. C. Lawrence *et al.*, The robes of MAPKs in disease. *Cell Research* **18**, 436 (Apr, 2008).
122. M. Frodin *et al.*, Glucose, other secretagogues, and nerve growth factor stimulate mitogen-activated protein kinase in the insulin-secreting beta-cell line, INS-1. *The Journal of biological chemistry* **270**, 7882 (Apr 7, 1995).
123. E. Gomez, C. Pritchard, T. P. Herbert, cAMP-dependent protein kinase and Ca2+ influx through L-type voltage-gated calcium channels mediate Raf-independent activation of extracellular regulated kinase in response to glucagon-like peptide-1 in pancreatic beta-cells. *Journal of Biological Chemistry* **277**, 48146 (Dec 13, 2002).
124. D. Arnette *et al.*, Regulation of ERK1 and ERK2 by glucose and peptide hormones in pancreatic beta cells. *Journal of Biological Chemistry* **278**, 32517 (Aug 29, 2003).
125. L. Duan, M. H. Cobb, Calcineurin increases glucose activation of ERK1/2 by reversing negative feedback. *Proceedings of the National Academy of Sciences of the United States of America* **107**, 22314 (Dec 21, 2010).
126. K. Nakayama, T. Satoh, A. Igari, R. Kageyama, E. Nishida, FGF induces oscillations of Hes1 expression and Ras/ERK activation. *Current Biology* **18**, R332 (Apr 22, 2008).
127. S.-Y. Shin *et al.*, Positive- and negative-feedback regulations coordinate the dynamic behavior of the Ras-Raf-MEK-ERK signal transduction pathway. *Journal of Cell Science* **122**, 425 (Feb 1, 2009).
128. H. Wang *et al.*, EGF regulates survivin stability through the Raf-1/ERK pathway in insulin-secreting pancreatic beta-cells. *Bmc Molecular Biology* **11**, (Aug 31, 2010).
129. M. F. Favata *et al.*, Identification of a novel inhibitor of mitogen-activated protein kinase kinase. *Journal of Biological Chemistry* **273**, 18623 (Jul, 1998).
130. D. T. Dudley, L. Pang, S. J. Decker, A. J. Bridges, A. R. Saltiel, A Synthetic inhibitor of the mitogen-activated protein-kinase cascade. *Proceedings of the National Academy of Sciences of the United States of America* **92**, 7686 (Aug, 1995).
131. J. Akerboom *et al.*, Genetically encoded calcium indicators for multi-color neural activity imaging and combination with optogenetics. *Frontiers in molecular neuroscience* **6**, 2 (2013, 2013).

132. K. Aoki *et al.*, Stochastic ERK Activation Induced by Noise and Cell-to-Cell Propagation Regulates Cell Density-Dependent Proliferation. *Molecular Cell* **52**, 529 (Nov 21, 2013).
133. L. A. Feig, G. M. Cooper, Inhibition of NIH-3T3 cell-proliferation by a mutant ras protein with preferential affinity for GDP. *Molecular and cellular biology* **8**, 3235 (Aug, 1988).
134. N. Mochizuki *et al.*, Spatio-temporal images of growth-factor-induced activation of Ras and Rap1. *Nature* **411**, 1065 (Jun 28, 2001).
135. P. J. Lockyer, S. Kupzig, P. J. Cullen, CAPRI regulates Ca2+-dependent inactivation of the Ras-MAPK pathway. *Current Biology* **11**, 981 (Jun 26, 2001).
136. S. A. Walker *et al.*, Identification of a Ras GTPase-activating protein regulated by receptor-mediated Ca2+ oscillations. *Embo J* **23**, 1749 (Apr 21, 2004).
137. J. F. de Mora *et al.*, Ras-GRF1 signaling is required for normal beta-cell development and glucose homeostasis. *Embo Journal* **22**, 3039 (Jun 16, 2003).
138. S.-x. Jin, L. A. Feig, Long-Term Potentiation in the CA1 Hippocampus Induced by NR2A Subunit-Containing NMDA Glutamate Receptors Is Mediated by Ras-GRF2/Erk Map Kinase Signaling. *Plos One* **5**, (Jul 22, 2010).
139. C. L. de Hoog, W. T. Fan, M. D. Goldstein, M. F. Moran, C. A. Koch, Calmodulin-independent coordination of Ras and extracellular signal-regulated kinase activation by Ras-GRF2. *Molecular and cellular biology* **20**, 2727 (Apr, 2000).
140. B. Schwechter, C. Rosenmund, K. F. Tolias, RasGRF2 Rac-GEF activity couples NMDA receptor calcium flux to enhanced synaptic transmission. *Proceedings of the National Academy of Sciences of the United States of America* **110**, 14462 (Aug 27, 2013).
141. N. P. Fam *et al.*, Cloning and characterization of Ras-GRF2, a novel guanine nucleotide exchange factor for Ras. *Molecular and cellular biology* **17**, 1396 (Mar, 1997).
142. S. Mehta *et al.*, Calmodulin-controlled spatial decoding of oscillatory Ca2+ signals by calcineurin. *eLife* **3**, e03765 (2014).
143. T. Tomida, S. Oda, M. Takekawa, Y. Iino, H. Saito, The Temporal Pattern of Stimulation Determines the Extent and Duration of MAPK Activation in a Caenorhabditis elegans Sensory Neuron. *Science Signaling* **5**, (Oct 16, 2012).
144. J. E. Toettcher, O. D. Weiner, W. A. Lim, Using Optogenetics to Interrogate the Dynamic Control of Signal Transmission by the Ras/Erk Module. *Cell* **155**, 1422 (Dec 5, 2013).
145. S. Asahara *et al.*, Ras-related C3 botulinum toxin substrate 1 (RAC1) regulates glucose-stimulated insulin secretion via modulation of F-actin. *Diabetologia* **56**, 1088 (May, 2013).
146. R. Hoffmann, G. S. Baillie, S. J. MacKenzie, S. J. Yarwood, M. D. Houslay, The MAP kinase ERK2 inhibits the cyclic AMP-specific phosphodiesterase HSPDE4D3 by phosphorylating it at Ser579. *Embo Journal* **18**, 893 (Feb 15, 1999).
147. Q. Wang, K. A. Siminovitch, G. P. Downey, C. A. McCulloch, Ras-guanine-nucleotide-releasing factors 1 and 2 interact with PLC gamma at focal adhesions

to enable IL-1-induced Ca2+ signalling, ERK activation and MMP-3 expression. *Biochemical Journal* **449**, 771 (Feb 1, 2013).
148. S. Kupzig, S. A. Walker, P. J. Cullen, The frequencies of calcium oscillations are optimized for efficient calcium-mediated activation of Ras and the ERK/MAPK cascade. *Proceedings of the National Academy of Sciences of the United States of America* **102**, 7577 (May 24, 2005).
149. J. T. Mettetal, D. Muzzey, C. Gomez-Uribe, A. van Oudenaarden, The frequency dependence of osmo-adaptation in Saccharomyces cerevisiae. *Science (New York, N.Y* **319**, 482 (Jan 25, 2008).
150. P. Hersen, M. N. McClean, L. Mahadevan, S. Ramanathan, Signal processing by the HOG MAP kinase pathway. *Proceedings of the National Academy of Sciences of the United States of America* **105**, 7165 (May 20, 2008).
151. M. A. Kalwat, D. C. Thurmond, Signaling mechanisms of glucose-induced F-actin remodeling in pancreatic islet beta cells. *Experimental and Molecular Medicine* **45**, (Aug, 2013).
152. A. Tomas, B. Yermen, L. Min, J. E. Pessin, P. A. Halban, Regulation of pancreatic beta-cell insulin secretion by actin cytoskeleton remodelling: role of gelsolin and cooperation with the MAPK signalling pathway. *Journal of Cell Science* **119**, 2156 (May 15, 2006).
153. M. J. Pellegrino, P. J. S. Stork, Sustained activation of extracellular signal-regulated kinase by nerve growth factor regulates c-fos protein stabilization and transactivation in PC12 cells. *Journal of Neurochemistry* **99**, 1480 (Dec, 2006).
154. N. Komatsu *et al.*, Development of an optimized backbone of FRET biosensors for kinases and GTPases. *Molecular biology of the cell* **22**, 4647 (Dec 1, 2011).
155. L. A. Greene, A. S. Tischler, Establishment of a noradrenergic clonal line of rat adrenal pheochromocytoma cells which respond to nerve growth-factor. *Proceedings of the National Academy of Sciences of the United States of America* **73**, 2424 (1976, 1976).
156. K. Huff, D. End, G. Guroff, Nerve growth factor-induced alteration in the response of PC12 pheochromocytoma cells to epidermal growth-factor. *Journal of Cell Biology* **88**, 189 (1981, 1981).
157. L. E. Heasley, G. L. Johnson, The beta-PDGF receptor induces neuronal differentiation of PC12 cells. *Molecular biology of the cell* **3**, 545 (May, 1992).
158. T. T. Nguyen *et al.*, Coregulation of the mitogen-activated protein-kinase, extracellular signal-regulated kinase-1, and the 90-kda ribosomal s6 kinase in pc12 cells - distinct effects of the neurotrophic factor, nerve growth-factor, and the mitogenic factor, epidermal growth-factor. *Journal of Biological Chemistry* **268**, 9803 (May 5, 1993).
159. S. Traverse, N. Gomez, H. Paterson, C. Marshall, P. Cohen, Sustained activation of the mitogen-activated protein (map) kinase cascade may be required for differentiation of PC12 cells - comparison of the effects of nerve growth-factor and epidermal growth-factor. *Biochemical Journal* **288**, 351 (Dec 1, 1992).
160. M. Zaccolo, T. Pozzan, Discrete microdomains with high concentration of cAMP in stimulated rat neonatal cardiac myocytes. *Science (New York, N.Y* **295**, 1711 (Mar 1, 2002).

161. N. Sachs, A. Sonnenberg, Cell-matrix adhesion of podocytes in physiology and disease. *Nature Reviews Nephrology* **9**, 200 (Apr, 2013).
162. F. Perlikos, K. J. Harrington, K. N. Syrigos, Key molecular mechanisms in lung cancer invasion and metastasis: A comprehensive review. *Critical Reviews in Oncology Hematology* **87**, 1 (Jul, 2013).
163. C. E. Chandler, H. R. Herschman, Tumor promoter modulation of epidermal growth factor-induced and nerve growth factor-induced adhesion and growth-factor binding of pc-12 pheochromocytoma cells. *Journal of Cellular Physiology* **105**, 275 (1980, 1980).
164. J. E. Gawecka *et al.*, RSK2 Protein Suppresses Integrin Activation and Fibronectin Matrix Assembly and Promotes Cell Migration. *Journal of Biological Chemistry* **287**, 43424 (Dec 21, 2012).
165. D. Vial, P. J. McKeown-Longo, Epidermal Growth Factor (EGF) Regulates alpha 5 beta 1 Integrin Activation State in Human Cancer Cell Lines through the p90RSK-dependent Phosphorylation of Filamin A. *Journal of Biological Chemistry* **287**, 40371 (Nov 23, 2012).
166. J. K. Mann *et al.*, Epitope-Guided Engineering of Monobody Binders for in Vivo Inhibition of Erk-2 Signaling. *Acs Chemical Biology* **8**, 608 (Mar, 2013).
167. G. C. Brown, B. N. Kholodenko, Spatial gradients of cellular phospho-proteins. *Febs Letters* **457**, 452 (Sep 3, 1999).
168. A. Harding, T. H. Tian, E. Westbury, E. Frische, J. F. Hancock, Subcellular localization determines MAP kinase signal output. *Current Biology* **15**, 869 (May 10, 2005).
169. L. K. Nguyen, D. Matallanas, D. R. Croucher, A. von Kriegsheim, B. N. Kholodenko, Signalling by protein phosphatases and drug development: a systems-centred view. *Febs Journal* **280**, 751 (Jan, 2013).
170. N. Gerits, S. Kostenko, A. Shiryaev, M. Johannessen, U. Moens, Relations between the mitogen-activated protein kinase and the cAMP-dependent protein kinase pathways: Comradeship and hostility. *Cellular Signalling* **20**, 1592 (Sep, 2008).
171. V. Wixler, U. Smola, M. Schuler, U. Rapp, Differential regulation of Raf isozymes by growth versus differentiation inducing factors in PC12 pheochromocytoma cells. *Febs Letters* **385**, 131 (May 6, 1996).
172. S. Kiermayer *et al.*, Epac activation converts cAMP from a proliferative into a differentiation signal in PC12 Cells. *Molecular biology of the cell* **16**, 5639 (Dec, 2005).
173. G. Nowak, Protein kinase C-alpha and ERK1/2 mediate mitochondrial dysfunction, decreases in active Na+ transport, and cisplatin-induced apoptosis in renal cells. *Journal of Biological Chemistry* **277**, 43377 (Nov 8, 2002).
174. Y. Ishikawa, E. Kusaka, Y. Enokido, T. Ikeuchi, H. Hatanaka, Regulation of Bax translocation through phosphorylation at Ser-70 of Bcl-2 by MAP kinase in NO-induced neuronal apoptosis. *Molecular and Cellular Neuroscience* **24**, 451 (Oct, 2003).

175. H. J. Lee *et al.*, Mitogen-activated protein kinase/extracellular signal-regulated kinase attenuates 3-hydroxykynurenine-induced neuronal cell death. *Journal of Neurochemistry* **88**, 647 (Feb, 2004).
176. J. H. Zhu, F. L. Guo, J. Shelburne, S. Watkins, C. T. Chu, Localization of phosphorylated ERK/MAP kinases to mitochondria and autophagosomes in Lewy body diseases. *Brain Pathology* **13**, 473 (Oct, 2003).
177. Y. D. Shaul, R. Seger, ERK1c regulates Golgi fragmentation during mitosis. *Journal of Cell Biology* **172**, 885 (Mar 13, 2006).
178. M. S. Islam, Calcium Signaling in the Islets. *Islets of Langerhans* **654**, 235 (2010, 2010).
179. M. Behar, D. Barken, S. L. Werner, A. Hoffmann, The Dynamics of Signaling as a Pharmacological Target. *Cell* **155**, 448 (Oct 10, 2013).

Curriculum Vitae

AMBHIGHAINATH GANESAN

Department of Biomedical Engineering
The Johns Hopkins University
School of Medicine
ambhi@jhmi.edu
Baltimore, MD 21205

Mobile: 443-604-2197
Email:

EDUCATION

Ph. D., 2014 (expected)

Biomedical Engineering, The Johns Hopkins University School of Medicine, USA
PIs: Dr. Andre Levchenko and Dr. Jin Zhang

B. Tech., 2007

Biotechnology, Indian Institute of Technology Madras, India
Minors: Biomedical Engineering & Chemical Engineering
GPA: 9.27/10 (First in class)

RESEARCH EXPERIENCE

Johns Hopkins University School of Medicine (2008-present)

PIs: Prof. Andre Levchenko and Prof. Jin Zhang

- Generated and improved fluorescent biosensors to monitor signaling activities in single live cells
- Investigated kinase signaling mechanisms in pancreatic beta-cells using live-cell imaging and pharmacological approaches
- Built computational models of Diabetes-related signaling pathways using non-linear Ordinary Differential Equations
- Discovered and studied spatial signaling dynamics of proto-oncogenic targets in neuroendocrine cells
- Investigated signaling dynamics of PKA in cardiovascular systems

Indian Institute of Technology Madras (2006-2007)

PI: Prof. S. N. Gummadi

- Purified and characterized pectin and pectate lyases from *Debaromyces nepalensis*.
- Discovered unique sequence motifs to distinguish pectin lyases from pectate lyases using bioinformatics approaches

Max Planck Institute for Terrestrial Microbiology (2006)

PI: Dr. Lotte Søgaard-Andersen

- Constructed in-frame deletion mutants of Histidine Protein Kinases in *M. Xanthus*
- Studied development phenotypes of the deletion mutants

PUBLICATIONS

- Q. Ni*, **A. Ganesan***, N.-N. Aye-Han*, X. Gao, M.D. Allen, A. Levchenko and J. Zhang. Signalling Diversity of PKA via a Ca^{2+}-cAMP-PKA Oscillatory Circuit. 2011. *Nature Chemical Biology*. 7(1): 34-40.
  (Recommended by Faculty of 1000, Featured in Chemical & Engineering News)
- **A. Ganesan** and A. Levchenko. Principles of model building: an experimentation-aided approach to development of models for signaling networks. 2012. *Methods Cell Biol*. 110: 1-17
- **A. Ganesan** and J. Zhang. How cells process information: quantification of spatiotemporal signaling dynamics. 2012. *Protein Sci*. 21(7): 918-928.
- S. Mehta, N.-N. Aye-Han, **A. Ganesan**, L. Oldach, K. Gorshkov and J. Zhang. Calmodulin-controlled spatial decoding of oscillatory calcium signals by calcineuin. *eLife (July 2014)*.
- Y. Yaniv*, **A. Ganesan***, D. Yang, B.D. Ziman, A. Levchenko, J. Zhang, E.G. Lakatta. Experimental and in silico studies of the kinetics and magnitude of PKA activation in live sinoatrial node pacemaker cells. *Manuscript in preparation.*
- **A. Ganesan**, A. Levchenko and J. Zhang. ERK-mediated decoding of calcium signals in pancreatic beta-cells. *Manuscript in preparation*.
- N.-N. Aye-Han, **A. Ganesan**, G.C. Mo, I.E. Dick, S. Mehta, Q. Ni, D.T. Yue, A. Levchenko and J. Zhang. Spatial control of a PKA-mediated oscillatory circuit. *Manuscript in preparation*.
  *Equal contribution

TALKS

- **A. Ganesan**, A. Levchenko and J. Zhang. (**Invited talk**). Phosphodiesterase-mediated control of spatial ERK activity dynamics in pancreatic beta-cells. Gordon Research Seminar on Cyclic Nucleotide Phosphodiesterases. May 2014.
- **A. Ganesan**, A. Levchenko and J. Zhang. **(Invited talk)**. A tale of two kinases: Decoding calcium oscillations in pancreatic beta-cells. Anna University (SVCE). Chennai, India. January 2013.
- **A. Ganesan***, Q. Ni*, N.N. Aye-Han*, X. Gao, M.D. Allen, J. Zhang and A. Levchenko. PKA is a control node in a Ca^{2+}-cAMP-PKA Oscillatory Circuit. The 55th Annual Biophysical Society Meeting, Baltimore, MD. March 2011.
- **A. Ganesan***, H.K. Prabhala*, T. Yu, A. Groisman and A. Levchenko. Using microfluidic device based experimentation to unravel the topology of a maltose sub-regulon. The third annual q-bio Conference on Cellular Information Processing. Santa Fe, NM. August 2009.
  *Equal contribution

POSTER PRESENTATIONS

- **A. Ganesan**, A. Levchenko and J. Zhang. ERK-mediated decoding of Ca^{2+} oscillations in pancreatic beta cells. The 56th Annual Biophysical Society Meeting, San Diego, CA. February 2012.
- **A. Ganesan**[*], Q. Ni[*], N.N. Aye-Han[*], X. Gao, M.D. Allen, A. Levchenko and J. Zhang. PKA is a control node in a Ca^{2+}-cAMP-PKA Oscillatory Circuit. The fourth annual q-bio Conference on Cellular Information Processing, Santa Fe, NM. August 2010.
- X.Shi, B. Clement, **A. Ganesan** and L. Søgaard-Andersen. A systems biology approach in the analysis of developmentally regulated orphan histidine protein kinases in *Myxococcus xanthus*. The 33rd International Conference on the Biology of the Myxobacteria. Michigan. July 2006.

[*]Equal contribution.

FUNDING, AWARDS AND HONORS

2013 – James S. McDonnell Foundation fellowship (PI, $250,000)

2011 – Predoctoral fellowship, American Heart Association (PI, $46,000)

2007 – Institute Merit Prize, IIT Madras (for topping the Biotechnology Class of 2007)

2006 – Innovative Students Project Grant, IIT Madras (INR170,000)

2006 – VSRP Fellowship, Tata Institute of Fundamental Research

2006 – Summer Research Fellowship, Indian Academy of Sciences

2003 – All India Rank 1106 in IIT-JEE (Placed in the top 0.6 % of 170,000 candidates)

2001-2007 – National Talent Search Scholarship, Government of India

LEADERSHIP EXPERIENCE

Vice President, Graduate Students Association, JHU School of Medicine (2009-2010)

- Managed annual budget of $ 28,000 as the ex-officio chair of Finance Committee
- Presided over Travel Grant Selection Committee to award travel grants to graduate students
- Organized several lectures by eminent researchers to help disseminate new scientific thoughts

Vice President, Indian Graduate Students Association, JHU (2008-2009)

- Developed grants to obtain funding for the Association
- Organized several cultural events to promote cultural diversity on campus
- Spearheaded and coordinated publicity campaigns for different events